


January 2018

Assessing the Impacts of Climate Change on Streamflow and Reservoir Operation in Central Florida

Toni Panaou

University of South Florida, apanaou@mail.usf.edu

Follow this and additional works at: <http://scholarcommons.usf.edu/etd>

 Part of the [Civil Engineering Commons](#), [Climate Commons](#), and the [Water Resource Management Commons](#)

Scholar Commons Citation

Panaou, Toni, "Assessing the Impacts of Climate Change on Streamflow and Reservoir Operation in Central Florida" (2018). *Graduate Theses and Dissertations*.

<http://scholarcommons.usf.edu/etd/7211>

This Dissertation is brought to you for free and open access by the Graduate School at Scholar Commons. It has been accepted for inclusion in Graduate Theses and Dissertations by an authorized administrator of Scholar Commons. For more information, please contact scholarcommons@usf.edu.

Assessing the Impacts of Climate Change on Streamflow and Reservoir Operation in Central Florida

by

Toni Panaou

A dissertation submitted in partial fulfillment
of the requirements for the degree of
Doctor of Philosophy in Civil Engineering
Department of Civil and Environmental Engineering
College of Engineering
University of South Florida

Major Professor: Mahmood Nachabe, Ph.D.
Tirusew Asefa, Ph.D.
Philip van Beynen, Ph.D.
Benjamin Jacob, Ph.D.
Rangachar Kasturi, Ph.D.
Kenneth Trout, Ph.D.

Date of Approval:
December 4, 2017

Keywords: Water Supply, GCM, El Nino Southern Oscillation, Markov Chain, Performance Metrics

Copyright © 2018, Toni Panaou

ACKNOWLEDGMENTS

I would like to thank my major professor, Dr. Mahmood Nachabe in guiding and supporting me throughout this dissertation process. His knowledge and advice helped me accomplish this goal and I could not have completed it without his mentoring. He continuously challenged me to critically think outside the box and encouraged me to keep moving forward.

I would also like to thank Tampa Bay Water for providing valuable financial support to make this research possible. I would especially like to thank Dr. Tirusew Asefa from this organization for assisting with the modeling simulation software and giving valuable advice. Without all of this support and expert advice, none of this would have been possible.

I would also like to thank my committee members, Drs. Philip van Beynen, Rangachar Kasturi, and Kenneth Trout for their insightful comments. Their feedback significantly and substantially improved the quality of my dissertation. I also owe a special thanks to Dr. Benjamin Jacob who continuously inspired and supported me. He saw unlimited potential in my work, even when at times I had doubts. He taught me to dream beyond what I thought I was capable of achieving.

I especially want to thank my parents, Maria and Frank Panaou, for always being there for me. They continuously encourage me even at times when I thought I might not succeed. They were my rock when I needed it and I truly appreciate it. And lastly my wonderful cats, Bowtie and Gizmo, for their purrs that calmed me down when super stressed. They always knew how to relax me when pressures were high.

TABLE OF CONTENTS

LIST OF TABLES	iii
LIST OF FIGURES	v
ABSTRACT.....	vii
CHAPTER 1: INTRODUCTION	1
1.1 Overview.....	1
1.2 Research Objectives.....	1
CHAPTER 2: EXAMINING CLIMATE STATES AND TRANSITION PROBABILITIES OF PRECIPITATION PROJECTIONS IN GENERAL CIRCULATION MODELS	3
2.1 Introduction.....	3
2.2 Materials and Methods.....	6
2.3 Results.....	8
2.3.1 Raw GCM Precipitation from CMIP3 and CMIP5.....	8
2.3.2 Comparison of Downscaled GCM Products to the Gauge	11
2.3.3 Comparison of Downscaled Products to the GCMs	13
2.3.4 ENSO Influence on Precipitation.....	14
2.4 Conclusion	15
2.5 Tables.....	17
2.6 Figures	24
CHAPTER 3: ASCERTAINING IF GENERAL CIRCULATION MODELS REPLICATE HISTORIC PERFORMANCE METRICS FOR HYDROLOGIC AND SYSTEMS SIMULATIONS	29
3.1 Introduction.....	29
3.2 Materials and Methods.....	32
3.2.1 Rainfall-Runoff Model.....	32
3.2.2 Daily Flow Generations	33
3.2.3 Performance Metrics	34
3.3 Results and Discussion	36
3.3.1 Reliability, Resilience, Vulnerability and Sustainability Metrics.....	36
3.3.2 Statistical Analytics	39
3.3.3 Autocorrelation	40
3.4 Conclusion	40
3.5 Tables.....	41
3.6 Figures	45
CHAPTER 4: PERFORMANCE EVALUATION OF A WATER SUPPLY SYSTEM UNDER A CHANGING CLIMATE	54
4.1 Introduction.....	54

4.2 Results.....	57
4.2.1 Reliability, Resilience, Vulnerability and Sustainability Metrics.....	57
4.2.2 Statistical Analytics	61
4.2.3 Precipitation.....	64
4.3 Discussion.....	64
4.4 Conclusion	65
4.5 Tables.....	67
4.6 Figures	73
CHAPTER 5: CONCLUSION.....	78
REFERENCES	79
APPENDIX A: LIST OF ACRONYMS.....	87
APPENDIX B: COPYRIGHT PERMISSIONS	89

LIST OF TABLES

Table 1: ENSO cycle years (DJF).....	17
Table 2: Mean and standard deviation for CCSM-Raw, NOAA_Leo, CCSM-D_Leo, NOAA_Plant, and CCSM-D_Plant.....	17
Table 3: Mean and standard deviation for BCCR3-Raw, NOAA_Leo, BCCR3-D_Leo, NOAA_Plant, and BCCR3- D_Plant	17
Table 4: Average and standard deviation for BCCR5-Raw, NOAA_Leo, BCCR5-D_Leo, NOAA_Plant, and BCCR5-D_Plant	18
Table 5: Compared Dry Period transition probabilities for BCCR3-Raw, BCCR5-Raw and CCSM-Raw to gauges.....	18
Table 6: Compared Dry Period transition probabilities for BCCR3-D, BCCR5-D and CCSM-D to gauges.....	19
Table 7: Compared Dry Period transition probabilities for BCCR3-D, BCCR5-D and CCSM-D to their respective Raw GCMs.	20
Table 8: Compared Wet Period transition probabilities BCCR3-Raw, BCCR5-Raw and CCSM-Raw compared to gauges.....	21
Table 9: Compared Wet Period transition probabilities for BCCR3-D, BCCR5-D and CCSM-D to gauges.....	22
Table 10: Compared Wet Period for BCCR3-D, BCCR5-D and CCSM-D to their respective Raw GCMs.	23
Table 11: GCM models.....	41
Table 12: Surface water source flows targets	42
Table 13: Tampa Bay Water permits	42
Table 14: Average number of days to rebound out of an unsatisfactory event (1982-2005).....	42
Table 15: Reservoir unsatisfactory events (1982-2005)	43
Table 16: Daily reservoir elevation level (m) (1982-2005)	44
Table 17: Streamflow statistics for Alafia and Morris Bridge (mgd) (1982-2005)	44

Table 18: Approximate CDF values of Morris Bridge daily flow (1982-2005)	44
Table 19: Approximate CDF values of Alafia daily flow (1982-2005).....	45
Table 20: GCM models and RCPs of each utilized in the future scenario research	67
Table 21: Average number of days the system remained in an unsatisfactory state based on an average of GFDL-ESM2G, MIROC and NorESM	68
Table 22: Unsatisfactory events for RCP 8.5 for timeframes 2030-2039	68
Table 23: Unsatisfactory events for RCP 8.5 for timeframes 2090-2100	69
Table 24: Streamflow statistics for Alafia and Morris Bridge for RCP 8.5 by GCM simulation and average for all GCMs (mgd)	70
Table 25: Daily reservoir level for gauge and average of GFDL-ESM2G, MIROC and NorESM.....	70
Table 26: Unsatisfactory reservoir events for average of GFDL-ESM2G, MIROC and NorESM	71
Table 27: CDF values for Morris Bridge daily flow for average of GFDL-ESM2G, MIROC and NorESM	71
Table 28: CDF values for Alafia daily flow for average of GFDL-ESM2G, MIROC and NorESM	71
Table 29: CDF values for Morris Bridge daily flow for RCP 8.5 for individual GCM simulations	72
Table 30: Annual autocorrelation in days by RCP for Morris Bridge daily flow for average of GFDL-ESM2G, MIROC and NorESM.....	72
Table 31: Summer (July-October) autocorrelation in days by RCP for Morris Bridge daily flow for average of GFDL-ESM2G, MIROC and NorESM	72

LIST OF FIGURES

Figure 1: CMIP3 and CMIP5 GCM locations and rain gauge locations for Tampa Bay, FL region	24
Figure 2: January PDF for NOAA_Plant, CCSM-Raw, and CCSM-D_Plant.....	24
Figure 3: August PDF for NOAA_Plant, BCCR3-Raw, and BCCR3-D_Plant.....	25
Figure 4: August PDF for NOAA_Plant, CCSM-Raw, and CCSM-D_Plant.....	25
Figure 5: August PDF for NOAA_Plant, BCCR5-Raw, and BCCR5-D_Plant.....	26
Figure 6: BCCR3-Plant City average precipitation for ENSO cycle.....	26
Figure 7: BCCR5-St. Leo average precipitation for ENSO cycle.....	27
Figure 8: BCCR3-St. Leo - Dry Period (sum of December, January and February) showing ENSO cycles in Gauge, BCCR3-Raw and BCCR3-D_Leo	27
Figure 9: BCCR5-Plant City - Dry Period (sum of December, January and February) showing ENSO cycles in Gauge, BCCR5-Raw and BCCR5-D_Plant	28
Figure 10: Site map of Greater Tampa Bay, Florida region	45
Figure 11: Water supply system including rain gauge and stream gauge locations, river tributaries and reservoir.....	46
Figure 12: Reservoir system depicting failure events and unsatisfactory states	47
Figure 13: Historical reservoir performance metrics utilizing Maximum Vulnerability Metric	47
Figure 14: Historical reservoir performance metrics utilizing Average Vulnerability Metric.....	48
Figure 15: Historical CDF plots of Morris Bridge daily flow	48
Figure 16: Historical CDF plots of Alafia daily flow	49
Figure 17: Historical August PDF for Plant City at gauge (NOAA_Plant) and GCM (CCSM-D_Plant)	49
Figure 18: Historical monthly box-and-whisker plots for Morris Bridge daily flow.....	50
Figure 19: Historical monthly box-and-whisker plots for Alafia daily flow	51

Figure 20: Daily auto correlation for simulated Historical and GCMs at Morris Bridge for summer months (June, July, Aug & Sept).....	52
Figure 21: Daily auto correlation for simulated Historical and GCMs at Alafia for summer months (June, July, Aug & Sept).....	53
Figure 22: Emission scenarios with RCP 2.6 being the lowest and RCP 8.5 the highest.....	73
Figure 23: Reliability Metric by GCM	73
Figure 24: Metrics using the average of three GCMs Metrics (GFDL-ESM2G, MIROC and NorESM) by RCP and Max Vulnerability	74
Figure 25: Resiliency Metric by GCM	74
Figure 26: Examining the Unsatisfactory Events with the Vulnerability Maximum Metric by GCM	75
Figure 27: Examining all the Unsatisfactory Events to calculate the Vulnerability Average by GCM.....	75
Figure 28: Sustainability Metric by GCM utilizing the Vulnerability Maximum Metric.....	76
Figure 29: Sustainability Metric by GCM utilizing the Vulnerability Average Metric.....	76
Figure 30: Alafia and Morris Bridge streamflow and water withdrawal at Alafia and TBC examined by RPC and time period.....	77
Figure 31: Average annual precipitation at Plant City gauge by time period and RCP for GFDL-ESM2G, MIROC, NorESM and average of all three.....	77

ABSTRACT

Climate change is a global concern as it may affect many aspects of life, including water supply. A tool used to model climate change's impacts is called a General Circulation Model (GCM). GCMs project future scenarios including temperature and precipitation, but these are designed at a coarse resolution and require downscaling for employment for regional hydrologic modeling. There is a vast amount of research on downscaling and bias-correcting GCMs data, but it is unknown whether these techniques alter precipitation signals embedded in these models or reproduce climate states that are viable for water resource planning and management. Using the Tampa, Florida region for the case study, the first part of the research investigated 1) whether GCM and the downscaled, bias-corrected data were able to replicate important historical climate states; and 2) if climate state and/or transition probabilities in raw GCMs were preserved or lost in translation in the corrected downscaled data. This has an important implication in understanding the limitations of bias-correction methods and shortcomings of future projection scenarios. Results showed that the GCM, and downscaled and bias-corrected data did a poor job in capturing historical climate states for wet or dry states as well as the variability in precipitation including some extremes associated with El Niño events. Additionally, the corrected products ended up creating different cycles compared to the original GCMs. Since the corrected products did not preserve GCMs historical transition probabilities, more than likely similar types of deviations will occur for "future" predictions and therefore another correction could be applied if desired to reproduce the degree of spatial persistence of atmospheric features and climatic states that are hydrologically important.

Furthermore, understanding the sustainability of water supply systems in a changing climate is required for undertaking adaptation measures. Many water suppliers employ GCMs to examine climate change's effect on hydrologic variables such as precipitation, but little is known on the propagation of

mismatch errors in downscaled products through cascade of hydrologic and systems models. The second study examined how deviations in downscaled GCMs precipitation propagated into streamflow and reservoir simulation models by using key performance metrics. Findings exhibited that simulations better reproduced the resilience metric, but failed to capture reliability, vulnerability and sustainability metrics. Discrepancies were attributed to multiple factors including variances in GCMs precipitation and streamflow cumulative distribution functions, and divergences in serial correlation and system memory.

Finally, the last study examined multiple models, emission scenarios and an ensemble to obtain a range of possible implications on reservation operations for time periods 2030-2053, 2054-2077 and 2077-2100 since the future emission trajectory is uncertain. Currently there are four Representative Concentration Pathways (RCPs) as defined by the IPCC's fifth Assessment Report which provides time-dependent projections based on different forecasted greenhouse gas emission and land use changes. For this research Representative Concentration Pathways (RCPs) 4.0, 6.0 and 8.5 were examined. Scenarios were evaluated utilizing reliability, resilience, vulnerability and sustainability performance metrics and compared to a historical baseline. Findings exhibited that RCP 4.5, the lower end of emission scenario, improved reservoir reliability and resilience over time. Conversely, RCP 8.5, highest emissions, resulted in a steady decline of all metrics by 2100. Although vulnerability increased by 2100 for all emission scenarios, on average RCP 4.5 was less vulnerable. Investigation of permits and adjustments to capture extreme flows might be necessary to combat climate changes and precipitation inputs along with improvements to atmospheric emissions, which correlated with system recuperation with time.

CHAPTER 1: INTRODUCTION

1.1 Overview

Climate change is a global concern but how will this impact water supply? This is a major question that water managers are trying to answer using General Circulation Models (GCMs). A GCM is a numerical model that simulates how oceans, atmosphere, land surface and cryosphere will respond to increasing greenhouse gas concentrations. There are multiple GCMs and runs, each taking into account different forcing scenarios. These scenarios include varied amounts of greenhouse gas emissions by certain time periods, changes in temperature, population growth and more. GCMs are created at a coarse resolution, around 250 and 600 kilometers (km) to simulate the entire earth. To support the spatial resolution of regional hydrologic simulations required for water supply, hydrologists have developed dynamical and statistical techniques to downscale a GCM to a regional scale (~1 to 10 km) (Ahmed et al. 2012, Daniels et al. 2012, and Sharma et al. 2013); however, these techniques cause biases such as variances in mean precipitation, underestimation of high precipitation, or differences in number of drizzle days (Grillakis et al. 2013; IPCC 2013). It is unknown if these techniques alter precipitation signals embedded in these models or if they reproduce climate states that are viable for water resource planning and management. Replicating important historical climate states such as wet or dry season or El Niño Southern Oscillation (ENSO) is vital for water supply; therefore it is critical to understand GCM shortcomings prior to implementation for future projection scenarios.

1.2 Research Objectives

This research had three objectives. Firstly, historical GCMs were examined to determine (1) If the original raw GCMs data or their statistically downscaled products captured the persistence of climate cycles observed in historical data; and (2) If the bias-correction process altered the original GCM time series and

climate states embedded in these cycles. The second objective studied whether downscaled GCM errors propagated into the simulated streamflow and reservoir models. These were compared to baseline flows and evaluated via reservoir performance metrics. Finally, the last section simulated future streamflow using GCMs precipitation as a driver and examined the system's resilience, reliability, vulnerability and sustainability for multiple emission scenarios. 1982-2005 data from the GCMs were employed as the benchmark to determine future deviations.

CHAPTER 2: EXAMINING CLIMATE STATES AND TRANSITION PROBABILITIES OF PRECIPITATION PROJECTIONS IN GENERAL CIRCULATION MODELS

2.1 Introduction

Climate change is a major concern for many water suppliers in the United States (U.S.) and worldwide. To develop a long-term resilient water management and supply plan, General Circulation Models (GCMs) are employed to project future scenarios of climate including temperature and precipitation. Data from these GCMs, however, are produced at a coarse resolution, typically between 250 and 600 kilometers (km), which causes biases such as underestimation of high precipitation, differences in number of drizzle days, or variances in mean precipitation (Grillakis et al. 2013; IPCC 2013). Hydrologists have used statistical methods to downscale GCM precipitation to a regional scale, ~1 to 10 km, to support the spatial resolution of hydrologic simulations required for water supply and management (Panaou et al. 2016; Hwang and Graham 2013; Asefa and Adams 2013; Ahmed et al. 2012; Daniels et al. 2012; and Sharma et al. 2011). Commonly used statistical downscaling techniques include bias-correction and spatial disaggregation (BCSD), bias-correction and constructed analog (BCCA), or bias-correction and stochastic analog method (BCSA) (Gutmann et al. 2014; Hwang and Graham 2013; Daniels et al. 2012). The goal of bias-correction is to account for regional scale processes that may not be represented by large scale GCM simulation data (Bruyère et al. 2013; Tryhorn and DeGaetano 2011). This is achieved by either (1) applying a correction factor which has been used by Inter-Sectoral Impact Model Intercomparison Project (ISI-MIP) to preserve the relative and absolute trends in the simulated data (Yin et al. 2015; Hempel et al. 2013); (2) employing the delta method, a statistical bias-correction, which adds the difference between the means of the simulated and historical data to the simulated (Hempel et al. 2013; Wetterhall et al. 2012; Watanabe

This chapter has previously been published in *Journal of Water Resources Planning and Management*. Permission is included in Appendix B.

2012); or (3) correcting using the empirical distribution or quantile mapping method where the monthly frequency distribution of the simulated GCM is corrected to match historical data such as rain gauge data (Wood et al. 2004; Argüeso et al. 2013; Ehret et al. 2012; Lafon et al. 2013).

Although these downscaling techniques can match the statistics and probability distribution of historical precipitation, they do not eliminate all errors (Maraun 2016; Eden and Widmann 2014; Grillakis et al. 2013). For instance, quantile mapping automatically modifies the number of wet days in order to match the probability distribution function (PDF) (Maraun 2016). Further, when sampling noise is extremely high, nonparametric quantile mapping basically employs random corrections which generates very noisy solutions (Maraun 2016). van Pelt et al. (2009) study examines two bias-correction methods. They conclude that although the first method amends the average, numerous consecutive precipitation days were incorrectly removed. The second method adjusted the coefficient of variance and mean, but the average underperformed while the temporal precipitation pattern improved. This leads to the hypothesis of this paper that bias-correction may alter the precipitation transition states of climate cycles embedded in the GCMs, which are hydrologically detrimental. For example, monthly and sometimes annual scale climate states that drive precipitation variability are important for water supply planning. At these temporal scales, persistence of certain states, such as multiple months or years of less-than-average precipitation during the wet season can have severe consequences on water management. Multiple consecutive months with below average precipitation could affect streamflow and the availability of surface water (Clark et al. 2014). Additionally, multiple wet months would increase the availability of surface water, which could be captured and stored for future use. It is important to simulate the transition between these climate states to create a more robust model that can facilitate informed decisions. Although annual budgets are important and was considered, this research focuses on winter and summer months.

Tampa Bay, Florida (FL) provides a great example where two nested scales of variability influence precipitation. The first scale is associated with the intra-annual transition from Dry-to-Wet season. About two-thirds of precipitation in the region occurs in only four months, June through September, creating a “wet season” easily distinguishable from the “dry season” that persists the rest of the year. Superimposed

on this seasonal cycle is the El Niño Southern Oscillation (ENSO), which creates an inter-annual variability with a time scale ranging from two to seven years (NOAA 2015; Schmidt et al. 2001; Zorn and Waylen 1997). ENSO significantly affects both temperature and precipitation during the winter months. For the Tampa region, El Niño typically produces above average monthly precipitation whereas La Niña produces below average monthly precipitation for these same months (Schmidt et al. 2001). The persistence of these dry and wet climate states have significant implication for water supply management, affecting both supply and demand. There is a vast amount of research regarding how to downscale and bias-correct GCM data, but no attention is given to assessment of whether these efforts alter signals embedded in global climate models and/or, whether these projections reproduce climate states such as ENSO that are important for making management decisions. The lack of such investigation makes it difficult for water supply managers to be prepared for the impact of potential climate change in their region.

In this study, experimental first order Markov Chain models were employed to evaluate empirical aggregation of data to attain the historical variability of the precipitation patterns and climate states. By applying the technique, dry or wet weather patterns and the transition and persistence in climate states of a system over time were ascertained. To achieve this, the states of a system, e.g. “wet” or “dry”, were defined, and a transition probability matrix was then developed. Markov Chains was selected as it has been successfully utilized in many water resources applications for precipitation states, weather cycles and hydrological evaluations, i.e. Gabriel and Neumann (1962), Todorovic and Woolhiser (1975), Mishra et al. (2013), Akyuz et al (2012), Smith and Marshall (2008), Moon et al. (2006), among others, therefore was selected for this research. Gabriel and Neumann (1962) is noted as one of the first to model the Markov Chains process for precipitation. Results deduced this a suitable model to account for weather cycles and distributions of dry and of wet events. Akyuz et al. (2012) successfully reproduced the stochastic structure of hydrological droughts in annual streamflow using first- and second-order Markov Chain models. Recently, Avilés et al. (2016) compared Markov chain and Bayesian network based models to characterize droughts. Their results showed that Markov Chains better predicted transition between wet and dry states.

Utilizing Markov Chains and graphical tools, this study evaluated GCMs and their downscaled and bias-corrected products and compared the results to National Oceanic and Atmospheric Administration (NOAA) gauge data. The objective was to investigate (1) whether the raw GCM and their downscaled, bias-corrected counterpart capture the persistence of climate states observed in historical data, and (2) if climate states and/or transition probabilities in raw GCMs are preserved or lost in translation. This is important because if key climate state signals are lost in translation in historical runs, one could possibly expect similar loss of information in future scenario projections. Note that usually future projection scenarios are developed by propagating a mismatch between historical observed data and a retrospective GCM run during a quantile mapping (see for examples, Li et al. 2009; Asefa et al., 2013).

2.2 Materials and Methods

The GCMs Bjerknes Centre for Climate Research (BCCR) model BCCR3-BCM2.0 (BCCR3) and model bcc-csm1-1 (BCCR5), and Community Climate System Model (CCSM) model CGCM3.1 were selected. The spatial resolutions for BCCR and CCSM are $2.8^\circ \times 2.8^\circ$ and $1.4^\circ \times 1.4^\circ$, respectively. BCCR was chosen because results are available for both the third phase, BCCR3, and a more recent fifth phase, BCCR5, from the World Climate Research Programmer's Coupled Model Intercomparison Projects (CMIP5 and CMIP3 Lawrence Livermore National Laboratory of the U.S. Department of Energy, <http://www-pcmdi.llnl.gov/projects/pcmdi/>). Hwang and Graham (2013) compared various statistical downscaling methods of GCMs and recommended that BCSA provided a better fit of historical data in the Tampa Bay area. Therefore, these GCMs were downscaled and bias-corrected using the BCSA technique of Hwang and Graham (2013) and Maurer's nationally available precipitation data that is gridded at 1/8 degree spatial resolution (about 12 km) (Maurer et al. 2002; http://hydro.engr.scu.edu/files/gridded_obs/daily/ncfiles/). Maurer's gridded precipitation dataset is widely known and has been used in many statistical downscaling techniques in the U.S. (Ning et al. 2015; Notaro et al. 2015; Hwang 2012). For CMIP5, BCCR5 was downscaled using the same BCSA technique for consistency. For this case study, the raw GCM datasets are denoted BCCR3-Raw, BCCR5-Raw, and CCSM-Raw, whereas the downscaled precipitation datasets are BCCR3-D, BCCR5-D, and CCSM-D. For

comparison, the GCMs were downscaled to the locations of two rainfall gauges in the Tampa region, namely Plant City and St. Leo, FL rain gauges (Figure 1). These locations were selected because both gauges are maintained by NOAA and have complete records that started in 1900.

For each dataset, the monthly precipitation, and basic statistics of monthly precipitation such as mean, median, standard deviation and skewness were calculated. In addition, the empirical frequency distribution function of precipitation for each month was developed. Due to the limitation of the data size, two states were selected for examination in the transition probability. The probability of a state was defined with respect to being above the median (wet) or below the median (dry), therefore being either wet or dry, for the Markov Chains transition probability matrix. Using Markov Chains and quantiles, transition probabilities are simulated between states. Markov Chain is a discrete-time stochastic model that describes the probable sequence of events. The probability of a precipitation event depends only on the current state and not on a previous event. For a set of states where $S = \{s_1, s_2, s_3, \dots, s_r\}$, transition probabilities can be represented by the following Markov Chain equation if it has ‘r’ states:

$$P_{ij} = \sum_{k=1}^r P_{ik}P_{kj} \quad (1)$$

The process begins at one state and then moves on to the next state successively. For example, if the state is currently s_i in the chain, then it will have a probability p_{ij} of transitioning to state s_j in the following period. Thus, elements in the transition probability matrix represent probabilities of shifting between states. Persistence in a certain state, e.g. “wet” month followed by more “wet” months in the sequence, is reflected by high values of P_{ii} , the diagonal elements of the transition probability matrix (Moon et al. 2006; Grinstead and Snell 1997).

$$M = \frac{D}{W} \begin{bmatrix} D & W \\ p_{11} & p_{12} \\ p_{21} & p_{22} \end{bmatrix} \quad (2)$$

Weiss (1964) described the probability model as a Markov Chain with two conditional probabilities parameters p_0 and $(1-p_1)$, where p_0 is the probability of a wet state if the preceding day was dry, and $(1-p_1)$ is the probability of a dry state if the preceding day was wet.

$$p_1 = \Pr\{W/W\}; \quad (1-p_1) = \Pr\{D/W\} \quad (3)$$

$$p_0 = \Pr\{W/D\}; \quad (1-p_0) = \Pr\{D/D\} \quad (4)$$

To assess the impact of ENSO, this research uses ‘dry period’, which is the sum of December, January and February, by year. These winter months are assessed as it eliminates potential impacts of hurricane season that ends in November. Furthermore, this is when some of the highest impacts are observed (FCC 2017; NWSCPC 2003). Since majority of precipitation is received in the summer months, ‘wet period’, July, August and September summed by year is examined. This ensures capturing entire months that are affected by high precipitation. After calculating the transition probabilities, any difference greater than 10% was noted.

ENSO is defined by measuring the Oceanic Niño Index (ONI). This is a three month running mean of sea surface temperatures in the east-central tropical Pacific Ocean in a region known as Niño 3.4 (5°N-5°S, 120°-170°W). La Niña occurs when the ONI is below 0.5°C normal for at least five consecutive overlapping months, and an El Niño period is when the ONI is above 0.5°C for the same five minimum criteria. Normal is the period in-between with an ONI value ranging between -0.5 and 0.5 (Peña et al. 2015; Gergis and Fowler 2005). These can be further broken down. For example, El Niño is classified as Very Strong (≥ 2.0), Strong (1.5 to 1.9), Moderate (1.0 to 1.4) and Weak (with a 0.5 to 0.9 SST anomaly) events, based on the ONI (Null 2016; Wang and Kumar 2015). This research is based on the ONI Index for the 1950-2015 period. (NOAA NWSCPC 2015) shown in Table 1.

2.3 Results

2.3.1 Raw GCM Precipitation from CMIP3 and CMIP5

As expected, the PDF of the raw GCM and gauge data did not match, supporting the need for downscaling and bias-correction. The disparities were not consistent and varied by GCM and by month. For example, Figure 2 showed how in January, CCSM-Raw underestimated the frequency of below average precipitation and overestimated frequency at high values. Figure 3 depicted an over estimated precipitation for CMIP3’s BCCR3-Raw for August. At a cumulative frequency of around 0.5, the NOAA_Plant gage experiences around 22 centimeters (cm) of precipitation whereas BCCR3-Raw estimated around 32 cm. Furthermore, the GCM estimated the maximum at 51.68 cm whereas the gauge was 35.68 cm. For August,

one of the months with the highest precipitation for this region, all simulation output from GCMs deviated drastically from the Plant City gauge. Both CCSM-Raw (Figure 4) and BCCR5-Raw (Figure 5) under predicted precipitation, generating values less than half the amount of what is experienced for this region. Therefore, neither CMIP3 nor CMIP5 raw data replicated precipitation statistics for the region.

This finding is supported by the summary statistics (Table 2) which amplifies differences between GCMs predictions and historical records, further supporting the need for downscaling and bias-correction in order to encapsulate natural climate variability. With the exception of January and February, Table 2 demonstrated how CCSM-Raw deviated throughout most of the year, inaccurately depicting March, April and May with the highest precipitation. Since these are typically dry months with the least precipitation, the GCM predictions failed to capture the precipitation seasonality of this region. Similarly, BCCR3-Raw (Table 3) and BCCR5-Raw (Table 4) showed greatest variations from gauge data during the region's wet season, which consists of June, July, August and September. For instance, BCCR3-Raw over predicted precipitation and was more than double NOAA_Leo in June with a mean of 38.87 cm of precipitation, whereas the gauge was 18.03 cm (Table 3). Conversely, in June BCCR5-Raw was four times smaller with mean of 4.97 cm whereas NOAA_Leo was 20.84 cm (Table 4). Comparing CMIP3 to CMIP5, CMIP5 over corrected the previous errors of CMIP3. The reductions were so drastic that most months had similar means, thus missing rainfall seasonality that is a pronounced and important aspect of climate in this region. It is also important to note that there are minor variances in geographic locations displayed by the differences in the month mean. For instance in June, the mean for St. Leo gauge is 17.99 cm but Plant City gauge is 19.83 cm (Table 2).

Although an El Niño year typically produces above average precipitation for this region, there are months that might not achieve this. To account for this, dry period was created, which is the sum of three dry season months, December, January and February, which smooths out the values should a month have low precipitation during an El Niño year, or alternatively high value during La Niña. The combination of multiple months provided a better representation of the cycle by accounting for any irregularities. Since transition probabilities only take into account the current state and prior state without regard for actual date

of occurrence, the probability value encapsulates the ENSO cycle as well as its length in the calculated values. This technique allows the GCM and gauges to be compared by only exposing persistence of cycles for the entire record and not zooming in on one actual event at a specific time. Since ENSO oscillates between La Niña, Normal and El Niño without staying in one state for many consecutive years, the probability will never be close to one. Furthermore, since the actual date of occurrence is not a factor and only the current state and prior state, the GCM and gauges are comparable as transition probabilities expose the statistical probability of precipitation cycles. One instance where the cycle appeared to have been represented is BCCR3-Raw (Table 5b), which had similar transition probabilities to the St. Leo gauge. All other instances CMIP3 GCMs dry period transition probabilities deviated. For example, if CCSM-Raw was in a current dry state there was an equal likelihood of next dry period being dry or wet since calculated transition probabilities was 0.5; however, the Plant City gauge data had a slight trend to transition from a dry state to a wet state indicative of a cycle (Table 5a).

CMIP5 BCCR5-Raw findings (Table 5c and Table 5d) were inferior to CMIP3 since none of the results captured the transition probabilities of the gauges. For instance, there was 100% difference between BCCR5-Raw and NOAA_Leo for Current Wet-to-Wet (Table 5d). BCCR5-Raw also had more of a trend to want to switch to the alternate state, exhibiting minimal persistence. For instance, if in a currently wet state there was an 81.8% chance of switching to a dry state. This incorrectly stated that there was not a likely chance of remaining in an El Niño state for multiple years. Additionally, it showed a 72.7% chance of switching from a dry state to a wet state, once again incorrectly stating that there was not a likely chance of remaining in a La Niña state for multiple years. Although the GCMs are a valuable product for climate change predictions and planning, it has limitations such as the inability to capture transition probabilities and the embedded ENSO cycles and large frontal storms experienced in this region.

Similarly, wet period results demonstrated that both CMIP3 and CMIP5 GCMs did not exhibit the transition probabilities for the respective gauges. For instance, BCCR3-Raw exemplified that if in a current dry state it was equally likely to shift to a dry or wet state since the transition probabilities were 0.5 (Table 8b). Conversely, the gauge was more likely to transition to a wet state with a probability of 0.667 for Current

Dry-to-Wet. Similarly, CCSM-Raw data indicated that there was no state preference and if in a current wet state as there was an equal likelihood of next wet period being dry or wet, whereas the gauges were more likely to transition to a dry state (Table 8a).

CMIP5's BCCR5-Raw also diverged from both gauges for wet period. For instance, BCCR5-Raw's transition probability for Current Dry-to-Dry was 0.417 whereas NOAA_Plant was 0.273 (Table 8c), with a 34.5% difference. Moreover, BCCR5-Raw reduced Current Dry-to-Wet persistence compared to both gauges, decreasing the amount of precipitation. Although CMIP3 did a slightly better job than CMIP5, neither captured all historical transitions of the gauges for wet periods.

2.3.2 Comparison of Downscaled GCM Products to the Gauge

Bias-correction generally improved the mean precipitation for all GCMs' corrected products, such as BCCR5-D_Leo and CCSM-D_Leo, thus better capturing rainfall characteristics such as seasonality (Table 2, Table 3, and Table 4). For instance, downscaling using the BCSA approach generated a new dataset, CCSM-D_Plant, which more closely matched the historical PDF versus CCSM-Raw as shown in Figure 2. For August, BCCR3-D_Plant (Figure 3) corrected an over predicted raw GCM resulting in similar PDF curves compared to the gauge. Although both CCSM-D_Plant (Figure 4) and BCCR5-D_Plant (Figure 5) improved the original raw GCMs, the maximum monthly precipitation in August was still underestimated, not eliminating all biases. This might result in the corrected GCMs missing some extreme events, such as tropical storms, that characterize this region. Although not perfect, e.g.: at a low cumulative frequency between 0.05 to 0.3 on NOAA_Plant displayed lower precipitation than CCSM-D_Plant (Figure 4), or the mean for BCCR3-D_Plant (Table 3) in January was 2.99 cm greater than the gauge, bias-corrected data which substantially resolved biases of the raw GCMs.

Although basic statistics matched reasonably well, downscaled and bias-corrected GCMs have limitations evident by the distorted transition probabilities in dry periods. As shown in Table 6, BCCR3-D_Plant increased the chance of the occurrence of a dry period following another dry period, possibly accentuating multiple La Niña years by 24% compared to the gauge. Additionally, BCCR3-D_Plant increased precipitation in dry period followed by another wet year, potentially implying a 30% escalation

in persistence of El Niño. CCSM-D_Plant closely matched the gauge, whereas CCSM-D_Leo reduced the resolution of the wet state and the embedded effect of multiple La Niña years, with a probability of 0.438 compared to 0.529 of the St. Leo gauge (Table 6b). Overall, the downscaled and bias-corrected transition probabilities deviated by more than 10% in 75% of the climate states.

Assessing CMIP5 dry period results to CMIP3, CMIP5 digressed. For instance, there was a 100% difference compared to the gauge for BCCR5-D_Leo Current Wet-to-Wet (Table 6f), whereas there was a -21.4% for BCCR3-D_Leo (Table 6d). There was not one instance where BCCR5-D was similar to any of the gauges with deviation ranging from -100% to 25%. Furthermore, BCCR5-D_Plant and BCCR5-D_Leo reduced the chance of the occurrence of a wet period followed by another wet period by 25% and 66.7%, compared to respective gauges. Furthermore, BCCR5-D_Plant and BCCR5-D_Leo diminished the possibility of sequential dry periods with transition probabilities of 0.364 and 0.273, respectively, whereas both gauges were 0.455 (Table 6e and Table 6f). These corrected products decreased the chance of persistence in the cycles or having extremes since the transition probabilities of the diagonals were reduced which is not surprising since the raw GCM also did not show persistence of a climate state.

CMIP3 wet period results revealed that downscaling and bias-correcting did not fix errors and in some cases made things worse. BCCR3-D_Leo, CCSM-D_Plant, and CCSM-D_Leo did not reproduce any of the transition probabilities of the gauges. In fact, they over predicted remaining in a dry state if already in a dry state as well as if already in a wet state they had a higher chance of remaining in a wet state. For instance, BCCR3-D_Leo had a 0.526 transition probability whereas NOAA_Leo was 0.368 for Current Wet-to-Wet (Table 9d). This over estimation of multiple sequential wet states could impact water resource planning resulting in water shortages. Moreover, BCCR3-D_Leo had an equal likelihood of a wet or dry state following a dry state with 0.50 transition probabilities (Table 9d), making it difficult to predict precipitation conditions. The only instance where the corrected product resembled the gauge was BCCR3-D_Plant (Table 9c). Ultimately, the bias-corrected products only captured wet period transition probabilities 25% of the time, failing to replicate historical precipitation patterns for the most critical time for this region, wet season, when the region receives the majority of their rainfall. CMIP5 downscaled and bias-corrected

wet period products declined in accuracy for Plant City (Table 9e) but improved for St. Leo (Table 9f) compared to CMIP3 (Table 9c and Table 9d). BCCR5-D_Plant had a 38.9% increase of Current Wet-to-Wet state versus the gauge, overstating the availability of water. This same product also increased the chance of remaining in a dry state for consecutive periods by 53.2%, with 0.583 probability versus gauges 0.273. Although the correct precipitation products, e.g. BCCR3-D_Leo and CCSM-D_Plant, matched the PDF, the correction process failed to resolve all biases by failing to capture how climate states transition.

2.3.3 Comparison of Downscaled Products to the GCMs

After downscaling and bias-correction of the CMIP3 GCMs, the signals embedded in the GCMs became distorted. For instance, for dry period, BCCR3-D_Plant was altered by -28.6% for Current Wet-to-Dry state and by 20% from Current Wet-to-Wet state (Table 7c), over estimating the amount of precipitation received during dry period. Since BCCR3-Raw transition probabilities were similar to the St. Leo gauge (Table 5d) but corrected product BCCR3-D_Leo did not match (Table 6d), the sequencing of states in the raw GCM were altered which could be translated into potential distortion in future predictions. CCSM-D was also affected; however, in reverse. CCSM-D_Plant (Table 7a) and CCSM-D_Leo (Table 7b) transition probabilities decreased by 14.3% for Current Wet-to-Wet and increased by 11.1% for Current Wet-to-Dry compared to the GCM, predicting the dry period has less precipitation. These errors could also be interpreted as the reduction in the probability of the occurrence of multiple, consecutive wet or potentially sequential El Niño years while increasing the chance of drier years. CMIP5 dry period performance were just as unreliable as CMIP3 as there was a 50/50 chance of either matching or not matching the transition probabilities of the GCM since BCCR5-D_Plant (Table 7e) varied greatly but BCCR5-D_Leo 100% matched (Table 7f). Overall, both CMIP3 and CMIP5 signals were altered compared to the GCMs. Ultimately, the results illustrate that bias-correction changed the transition states that were modeled in the GCM by either over or under estimation of wet and dry states. If the correction techniques alter the transition probabilities of GCMs compared to historical, climate signals embedded in future predictions will also be misrepresented which could impact water supply planning.

Similarly, CMIP3 wet period downscaling and bias-correcting products also did not capture the raw GCMs' transition probabilities. CCSM-D_Plant over estimated precipitation for Current Wet-to-Wet, changing the number of consecutive wet periods whereas CCSM-D_Leo increased the transition probability by 15.3% for Current Dry-to-Wet, inaccurately amplifying the wet-dry cycle (Table 10a). CMIP5 wet period corrected products, BCCR5-D_Plant (Table 10b) and BCCR5-D_Leo (Table 10c), produced even more disparities compared to the GCM than CMIP3. In fact, there were no instances where the transition probabilities of the corrected products preserved the cycles of the GCM. BCCR5-D_Plant diminished the chance of a wet-dry cycle with a 0.455 probability compared to BCCR5-Raw's 0.636 (Table 10b). BCCR5-D_Plant and BCCR5-D_Leo increased precipitation for Current Wet-to-Wet by 33.3% and 20%, respectively, while magnifying dry conditions with Current Dry-to-Dry increased by 28.6% and 16.7%, respectively (Table 10b and Table 10c). Furthermore, the changes in values along the diagonals exhibited an increased persistence of a wet or dry states compared to the raw GCM, conceivably resulting in more extremes. It is inconclusive when bias-correction will over or under predict precipitation transition probability compared to the GCM, but it is probable that similar errors will be transmitted to future GCM corrected products. Using these tools for planning, water supply operators might over estimate available water during the over predicted, multiple years of wet-to-wet periods and inadequately designing their climate change mitigation and adaptation plans.

2.3.4 ENSO Influence on Precipitation

To further examine the ENSO cycle, the dry period results for gauges, GCMs and corrected products were separated by either La Niña, Normal or El Niño, and the mean of each was calculated. The 'years,' sum of December, January and February, for La Niña, Normal or El Niño were defined by NOAA and are located in Table 1. Both the Plant City (Figure 6) and St. Leo gauge (Figure 7) data confirmed La Niña with below average precipitation, El Niño with above average precipitation and Normal in-between, accurately representing the cycle. As seen in Figure 7, the GCMs and downscaled and bias-corrected data did not capture the variability in precipitation from the ENSO cycle. If present, cycles were not occurring at the same years as defined by Table 1. Additional investigation, not performed in the research, to examine

sea surface temperature and calculate the ONI index for the GCMs would be required to confirm the timing of each phase of the cycle.

To further examine the errors in the transition probabilities for dry season and the ENSO cycle, Dry Period precipitation were graphed by year (Figure 8 and Figure 9). Although the products match the statistics of the gauges, the GCM and bias-corrected products do not match the timing of the typical high and low precipitation associated with the ENSO, justifying one reason why the results above (Figure 6 and Figure 7) did not have La Niña with below average precipitation, El Niño with above average precipitation and Normal in-between. Although GCMs were not designed to match the time series, these graphs demonstrate how bias-correction failed to capture the extremes of the gauges and that the data is skewed. For instance, in Figure 8 the gauge experiences three high peak precipitation events, 42.85 cm, 45.7 cm and 73.59 cm, during this timeframe; conversely, BCCR3-D_Leo never had precipitation above 42 cm. Similarly, BCCR5-Plant City graph (Figure 9) portrays the gauge with a precipitation of 67.8 cm whereas BCCR5-D_Plant never peaks above 47 cm. These numbers confirm that although the products were downscaled and bias-corrected to match the statistics of the gauges, they did not reproduce extremes, such as El Niño events.

These graphs also magnify how at times the bias-correction process also altered the timing of the events of the raw GCM compared to the corrected product. In 1970 and 1994 on the BCCR3-Leo graph (Figure 8), BCCR3-Raw had lower-than-average precipitation but BCCR3-D_Leo had above-average precipitation. In 1940 and 1996, BCCR3-Raw was close to average precipitation whereas BCCR3-D_Leo was once again higher than the average. These shifts in cycles are also evident in the BCCR5-Plant graph (Figure 9). In 1990, BCCR5-Raw simulated precipitation close-to-average whereas BCCR5-D_Plant was extremely low. Additionally, in 1998, BCCR5-Raw had above-average precipitation but BCCR5-D_Plant was below average. Once again, these errors might translate to skewing future prediction data.

2.4 Conclusion

Matching the transition of climate states in a GCM or downscaled product to historical data is crucial for future water supply planning. This study evaluated BCCR3, CCSM, and BCCR5 GCMs and

their downscaled and bias-corrected products for St. Leo and Plant City locations in Tampa Bay, FL. The following were concluded: (1) The raw GCMs required downscaling and bias-correction since BCCR3-Raw and BCCR5-Raw had large deviations in the means during the summer months, and CCSM-Raw deviated throughout the year. CCSM-Raw and BCCR5-Raw did not honor precipitation seasonality for the region; (2) The corrections of the raw data using the BCSA technique successfully reproduced the basic statistics of the observed gauge data; (3) The GCM and downscaled and bias-corrected products did not depict historical climate states for wet or dry periods when compared to gauge data. In some instances, the raw GCM did a better job capturing these states and in others, the downscaled and bias-corrected products outperformed the raw GCM; (4) The downscaled and bias-corrected products distorted the timing of the dry period cycles compared to the raw GCMs. For instance, for one time period, the GCM had above-average precipitation indicative of a possible El Niño event but the corrected product did not; (5) Extreme precipitation in the dry period from strong El Niño events was not simulated by the GCMs or corrected products; however, La Niña events were better captured; (6) Corrected products didn't preserve GCM historical transition probabilities. More than likely similar types of deviations will also be occurring for "future" predictions, potentially suggesting the need to carry forward biases in transition probabilities; and finally (7) If desiring to capture climatic cycles, a method that accounts for bias in transition probabilities is likely needed. It is important to note that coming up with sophisticated bias correction techniques cannot be the solution by itself as there is limitation on what downscaling and bias-correction can achieve. On the other hand, capturing all elements of climatic processes that are responsible for precipitation for all regions at GCM level might prove to be extremely difficult and exhibit limitations in their practical applications. A close working relationship between climate modelers and stakeholders those who are consuming the data to understand limitations of such products and provide feedback on where improvement may be needed should go a long way in producing actionable science. Understanding regional scale climatic processes that impact regional water resources management is an important step. Two such stakeholder-scientist partnership that are trying to do just that are the Water Utilities Climate Alliance (www.wucaonline.org) and Florida Water and Climate Alliance (www.floridawca.org). Such continued engagement between

scientist and stakeholders would result in understanding what's important for water resources management decision making and where improvement in climate modeling may need to be focused.

2.5 Tables

Table 1: ENSO cycle years (DJF) (NOAA NWSCPC 2015)

La Niña	1964, 1966, 1969, 1970, 1973, 1977, 1978, 1980, 1983, 1987, 1988, 1992, 1995, 1998
Normal	1962, 1963, 1967, 1979, 1981, 1982, 1984, 1986, 1990, 1991, 1993, 1994, 1997
El Niño	1965, 1968, 1971, 1972, 1974, 1975, 1976, 1985, 1989, 1996, 1999

Table 2: Mean and standard deviation for CCSM-Raw, NOAA_Leo, CCSM-D_Leo, NOAA_Plant, and CCSM-D_Plant

Units: $\times 10^{-2} m$	Jan	Feb	Mar	Apr	May	Jun	Jul	Aug	Sep	Oct	Nov	Dec
CCSM-RAW												
Mean	7.53	12.61	19.26	17.26	14.17	9.81	6.82	4.38	6.74	10.51	9.16	8.01
Standard Deviation	3.38	4.63	5.13	4.52	4.79	4.64	3.77	3.47	4.38	4.21	4.94	3.27
NOAA_Leo												
Mean	8.61	8.81	10.30	5.74	10.98	17.99	19.77	20.44	16.14	6.71	6.10	6.75
Standard Deviation	4.36	5.33	7.89	4.57	8.80	9.27	6.13	8.86	9.19	4.80	6.22	6.97
CCSM-D_Leo												
Mean	7.09	8.27	10.50	6.13	9.16	17.07	19.06	18.59	18.12	7.97	5.14	6.22
Standard Deviation	4.12	4.54	4.85	4.74	5.24	7.69	4.93	4.95	9.37	4.81	4.46	5.89
NOAA_Plant												
Mean	6.84	8.20	8.61	5.01	9.32	19.83	19.17	21.06	15.97	6.56	5.29	6.36
Standard Deviation	4.74	5.35	6.71	3.91	6.56	9.86	6.63	7.29	8.61	4.43	4.70	6.80
CCSM-D_Plant												
Mean	6.35	7.99	9.75	5.29	9.63	19.20	18.88	19.17	17.13	7.90	5.01	6.34
Standard Deviation	4.06	4.65	4.71	3.12	4.73	6.55	4.08	4.53	7.24	4.48	4.13	5.70

Table 3: Mean and standard deviation for BCCR3-Raw, NOAA_Leo, BCCR3-D_Leo, NOAA_Plant, and BCCR3-D_Plant

Units: $\times 10^{-2} m$	Jan	Feb	Mar	Apr	May	Jun	Jul	Aug	Sep	Oct	Nov	Dec
BCCR3-RAW												
Mean	5.81	5.85	5.04	5.49	10.51	38.87	35.19	31.31	22.68	8.28	3.34	4.54
Standard Deviation	4.48	6.26	4.75	6.41	9.19	14.38	10.77	9.36	6.78	4.48	3.32	4.54
NOAA_Leo												
Mean	8.66	9.10	10.22	5.50	10.59	18.03	19.66	20.29	16.22	6.90	5.99	6.56
Standard Deviation	4.25	6.22	7.81	4.55	8.73	9.99	6.19	8.65	9.30	4.75	6.08	6.82
BCCR3-D_Leo												
Mean	6.92	8.15	10.33	6.51	9.72	18.36	19.66	18.22	18.11	7.67	5.02	5.86
Standard Deviation	5.64	5.91	7.18	6.14	7.41	8.97	6.02	5.55	10.30	5.20	5.08	5.99
NOAA_Plant												
Mean	6.65	7.31	8.65	5.39	9.50	21.45	20.11	21.59	17.09	6.15	5.01	6.21
Standard Deviation	4.32	5.34	6.92	3.99	7.47	10.13	6.12	7.35	9.92	4.43	4.45	6.46
BCCR3-D_Plant												
Mean	9.63	8.39	9.74	6.01	9.30	18.52	19.34	19.33	17.24	7.29	4.91	6.38
Standard Deviation	4.68	6.22	7.23	4.70	7.22	8.53	5.59	6.08	7.30	4.65	4.89	6.33

Table 4: Average and standard deviation for BCCR5-Raw, NOAA_Leo, BCCR5-D_Leo, NOAA_Plant, and BCCR5-D_Plant

Units: $\times 10^{-2}$ m	Jan	Feb	Mar	Apr	May	Jun	Jul	Aug	Sep	Oct	Nov	Dec
BCCR5-Raw												
Mean	5.46	5.16	3.37	3.97	4.49	4.97	2.72	3.85	10.11	12.06	7.16	4.81
Standard Deviation	3.15	3.51	1.93	3.01	2.62	4.07	1.17	2.14	8.60	7.49	4.54	2.75
NOAA_Leo												
Mean	8.97	7.99	11.47	6.49	6.55	20.84	20.23	19.72	18.78	7.70	6.18	6.74
Standard Deviation	3.54	6.80	9.24	4.84	5.60	10.68	6.71	5.83	11.27	4.67	6.68	8.58
BCCR5-D_Leo												
Mean	7.50	7.97	11.27	6.02	6.48	21.09	18.70	18.95	18.09	6.92	5.70	5.74
Standard Deviation	6.29	6.01	7.32	2.45	3.71	10.16	7.61	6.74	9.68	5.25	3.67	3.78
NOAA_Plant												
Mean	7.39	7.04	9.91	6.68	7.94	22.06	19.41	21.14	18.83	6.55	5.09	6.82
Standard Deviation	3.71	5.97	8.19	4.10	6.43	10.44	6.22	8.48	11.73	3.94	4.07	8.63
BCCR5-D_Plant												
Mean	6.89	7.05	9.58	6.51	6.22	20.25	18.70	20.01	17.90	6.95	4.87	6.71
Standard Deviation	5.81	5.33	5.43	3.93	3.38	10.00	7.24	6.71	9.98	5.26	3.72	5.36

Table 5: Compared Dry Period transition probabilities for BCCR3-Raw, BCCR5-Raw and CCSM-Raw to gauges.

(a) Dry Period: CCSM-Raw & NOAA_Plant

NOAA_Plant	Dry	Wet	Units: $\times 10^{-2}$ m
Current Dry	0.467	0.533	Dry is < 18.4851
Current Wet	0.563	0.438	Wet is > 18.4852
CCSM-Raw			
Current Dry	0.500	0.500	Dry is < 28.5155
Current Wet	0.500	0.500	Wet is > 28.5156
Difference			
Current Dry	6.7%	-6.7%	
Current Wet	-12.5%	12.5%	

(b) Dry Period: BCCR3-RAW & NOAA_Leo

NOAA_Leo	Dry	Wet	Units: $\times 10^{-2}$ m
Current Dry	0.529	0.471	Dry is < 21.385
Current Wet	0.500	0.500	Wet is > 21.3851
BCCR3-RAW			
Current Dry	0.526	0.474	Dry is < 15.7429
Current Wet	0.529	0.471	Wet is > 15.743
Difference			
Current Dry	-0.6%	0.7%	
Current Wet	5.6%	-6.3%	

(c) Dry Period: BCCR5-Raw & NOAA_Plant

NOAA_Plant	Dry	Wet	Units: $\times 10^{-2}$ m
Current Dry	0.455	0.545	Dry is < 17.8399
Current Wet	0.636	0.364	Wet is > 17.840
BCCR5-Raw			
Current Dry	0.273	0.727	Dry is < 15.8422
Current Wet	0.818	0.182	Wet is > 15.8423
Difference			
Current Dry	-66.7%	25.0%	
Current Wet	22.2%	-100.0%	

(d) Dry Period: BCCR5-Raw & NOAA_Leo

NOAA_Leo	Dry	Wet	Units: $\times 10^{-2}$ m
Current Dry	0.455	0.545	Dry is < 19.050
Current Wet	0.636	0.364	Wet is > 19.0501
BCCR5-Raw			
Current Dry	0.273	0.727	Dry is < 15.8422
Current Wet	0.818	0.182	Wet is > 15.8423
Difference			
Current Dry	-66.7%	25.0%	
Current Wet	22.2%	-100.0%	

Table 6: Compared Dry Period transition probabilities for BCCR3-D, BCCR5-D and CCSM-D to gauges.

(a) Dry Period: CCSM-D_Plant & NOAA_Plant				(b) Dry Period: CCSM-D_Leo & NOAA_Leo			
NOAA_Plant	Dry	Wet	Units: x10⁻² m	NOAA_Leo	Dry	Wet	Units: x10⁻² m
Current Dry	0.467	0.533	Dry is < 18.4851	Current Dry	0.563	0.438	Dry is < 21.3850
Current Wet	0.563	0.438	Wet is > 18.4852	Current Wet	0.471	0.529	Wet is > 21.3851
CCSM-D_Plant	Dry	Wet		CCSM-D_Leo	Dry	Wet	
Current Dry	0.500	0.500	Dry is < 18.6862	Current Dry	0.500	0.500	Dry is < 19.2735
Current Wet	0.563	0.438	Wet is > 18.6863	Current Wet	0.563	0.438	Wet is > 19.2736
Difference	Dry	Wet		Difference	Dry	Wet	
Current Dry	6.7%	-6.7%		Current Dry	-12.5%	12.5%	
Current Wet	0.0%	0.0%		Current Wet	16.3%	-21.0%	

(c) Dry Period: BCCR3-D_Plant & NOAA_Plant				(d) Dry Period: BCCR3-D_Leo & NOAA_Leo			
NOAA_Plant	Dry	Wet	Units: x10⁻² m	NOAA_Leo	Dry	Wet	Units: x10⁻² m
Current Dry	0.438	0.563	Dry is < 18.4851	Current Dry	0.529	0.471	Dry is < 21.385
Current Wet	0.588	0.412	Wet is > 18.4852	Current Wet	0.500	0.500	Wet is > 21.3851
BCCR3-D_Plant	Dry	Wet		BCCR3-D_Leo	Dry	Wet	
Current Dry	0.579	0.421	Dry is < 23.1155	Current Dry	0.421	0.579	Dry is < 20.1284
Current Wet	0.412	0.588	Wet is > 23.1156	Current Wet	0.588	0.412	Wet is > 20.1285
Difference	Dry	Wet		Difference	Dry	Wet	
Current Dry	24.4%	-33.6%		Current Dry	-25.7%	18.7%	
Current Wet	-42.9%	30.0%		Current Wet	15.0%	-21.4%	

(e) Dry Period: BCCR5-D_Plant & NOAA_Plant				(f) Dry Period: BCCR5-D_Leo & NOAA_Leo			
NOAA_Plant	Dry	Wet	Units: x10⁻² m	NOAA_Leo	Dry	Wet	Units: x10⁻² m
Current Dry	0.455	0.545	Dry is < 17.8399	Current Dry	0.455	0.545	Dry is < 19.050
Current Wet	0.636	0.364	Wet is > 17.840	Current Wet	0.636	0.364	Wet is > 19.0501
BCCR5-D_Plant	Dry	Wet		BCCR5-D_Leo	Dry	Wet	
Current Dry	0.364	0.636	Dry is < 20.2092	Current Dry	0.273	0.727	Dry is < 23.1660
Current Wet	0.727	0.273	Wet is > 20.2093	Current Wet	0.818	0.182	Wet is > 23.1661
Difference	Dry	Wet		Difference	Dry	Wet	
Current Dry	-25.0%	14.3%		Current Dry	-66.7%	25.0%	
Current Wet	12.5%	-33.3%		Current Wet	22.2%	-100.0%	

Table 7: Compared Dry Period transition probabilities for BCCR3-D, BCCR5-D and CCSM-D to their respective Raw GCMs.

(a) Dry Period: CCSM-D_Plant & CCSM-Raw

CCSM-Raw	Dry	Wet	Units: $\times 10^{-2}$ m
Current Dry	0.500	0.500	Dry is < 28.5155
Current Wet	0.500	0.500	Wet is > 28.5156
CCSM-D_Plant	Dry	Wet	
Current Dry	0.500	0.500	Dry is < 18.6862
Current Wet	0.563	0.438	Wet is > 18.6863
Difference	Dry	Wet	
Current Dry	0.0%	0.0%	
Current Wet	11.1%	-14.3%	

(b) Dry Period: CCSM-D_Leo & CCSM-Raw

CCSM-Raw	Dry	Wet	Units: $\times 10^{-2}$ m
Current Dry	0.500	0.500	Dry is < 28.5155
Current Wet	0.500	0.500	Wet is > 28.5156
CCSM-D_Leo	Dry	Wet	
Current Dry	0.500	0.500	Dry is < 19.2735
Current Wet	0.563	0.438	Wet is > 19.2736
Difference	Dry	Wet	
Current Dry	0.0%	0.0%	
Current Wet	11.1%	-14.3%	

(c) Dry Period: BCCR3-D_Plant & BCCR3-RAW

BCCR3-RAW	Dry	Wet	Units: $\times 10^{-2}$ m
Current Dry	0.526	0.474	Dry is < 15.7429
Current Wet	0.529	0.471	Wet is > 15.743
BCCR3-D_Plant	Dry	Wet	
Current Dry	0.579	0.421	Dry is < 23.1155
Current Wet	0.412	0.588	Wet is > 23.1156
Difference	Dry	Wet	
Current Dry	9.1%	-12.5%	
Current Wet	-28.6%	20.0%	

(d) Dry Period: BCCR3-D_Leo & BCCR3-RAW

BCCR3-RAW	Dry	Wet	Units: $\times 10^{-2}$ m
Current Dry	0.526	0.474	Dry is < 15.7429
Current Wet	0.529	0.471	Wet is > 15.743
BCCR3-D_Leo	Dry	Wet	
Current Dry	0.421	0.579	Dry is < 20.1284
Current Wet	0.588	0.412	Wet is > 20.1285
Difference	Dry	Wet	
Current Dry	-25.0%	18.2%	
Current Wet	10.0%	-14.3%	

(e) Dry Period: BCCR5-D_Plant & BCCR5-Raw

BCCR5-Raw	Dry	Wet	Units: $\times 10^{-2}$ m
Current Dry	0.273	0.727	Dry is < 15.8422
Current Wet	0.818	0.182	Wet is > 15.8423
BCCR5-D_Plant	Dry	Wet	
Current Dry	0.364	0.636	Dry is < 20.2092
Current Wet	0.727	0.273	Wet is > 20.2093
Difference	Dry	Wet	
Current Dry	25.0%	-14.3%	
Current Wet	-12.5%	33.3%	

(f) Dry Period: BCCR5-D_Leo & BCCR5-Raw

BCCR5-Raw	Dry	Wet	Units: $\times 10^{-2}$ m
Current Dry	0.273	0.727	Dry is < 15.8422
Current Wet	0.818	0.182	Wet is > 15.8423
BCCR5-D_Leo	Dry	Wet	
Current Dry	0.273	0.727	Dry is < 23.1660
Current Wet	0.818	0.182	Wet is > 23.1661
Difference	Dry	Wet	
Current Dry	0.0%	0.0%	
Current Wet	0.0%	0.0%	

Table 8: Compared Wet Period transition probabilities BCCR3-Raw, BCCR5-Raw and CCSM-Raw

compared to gauges.

(a) Wet Period: CCSM-Raw & NOAA_Plant

NOAA_Plant	Dry	Wet	Units: $\times 10^{-2}$ m
Current Dry	0.471	0.529	Dry is < 52.2899
Current Wet	0.556	0.444	Wet is > 52.2900
<hr/>			
CCSM-Raw	Dry	Wet	
Current Dry	0.529	0.471	Dry is < 17.4929
Current Wet	0.500	0.500	Wet is > 17.4930
<hr/>			
Difference	Dry	Wet	
Current Dry	11.1%	-12.5%	
Current Wet	-11.1%	11.1%	

(b) Wet Period: BCCR3-RAW & NOAA_Leo

NOAA_Leo	Dry	Wet	Units: $\times 10^{-2}$ m
Current Dry	0.333	0.667	Dry is < 56.2249
Current Wet	0.632	0.368	Wet is > 56.2250
<hr/>			
BCCR3-RAW	Dry	Wet	
Current Dry	0.500	0.500	Dry is < 89.7145
Current Wet	0.526	0.474	Wet is > 89.7146
<hr/>			
Difference	Dry	Wet	
Current Dry	33.3%	-33.3%	
Current Wet	-20.0%	22.2%	

(c) Wet Period: BCCR5-Raw & NOAA_Plant

NOAA_Plant	Dry	Wet	Units: $\times 10^{-2}$ m
Current Dry	0.273	0.727	Dry is < 52.6900
Current Wet	0.667	0.333	Wet is > 52.6901
<hr/>			
BCCR5-Raw	Dry	Wet	
Current Dry	0.417	0.583	Dry is < 15.0802
Current Wet	0.636	0.364	Wet is > 15.0803
<hr/>			
Difference	Dry	Wet	
Current Dry	34.5%	-24.7%	
Current Wet	-4.8%	8.3%	

Table 9: Compared Wet Period transition probabilities for BCCR3-D, BCCR5-D and CCSM-D to gauges.

(a) Wet Period: CCSM-D_Plant & NOAA_Plant

NOAA_Plant	Dry	Wet	Units: $\times 10^{-2}$ m
Current Dry	0.471	0.529	Dry is < 52.2899
Current Wet	0.556	0.444	Wet is > 52.2900
CCSM-D_Plant	Dry	Wet	
Current Dry	0.556	0.444	Dry is < 53.8154
Current Wet	0.412	0.588	Wet is > 53.8155
Difference	Dry	Wet	
Current Dry	15.3%	-19.1%	
Current Wet	-34.9%	24.4%	

(b) Wet Period: CCSM-D_Leo & NOAA_Leo

NOAA_Leo	Dry	Wet	Units: $\times 10^{-2}$ m
Current Dry	0.333	0.667	Dry is < 56.2249
Current Wet	0.647	0.353	Wet is > 56.2250
CCSM-D_Leo	Dry	Wet	
Current Dry	0.444	0.556	Dry is < 55.9655
Current Wet	0.529	0.471	Wet is > 55.9656
Difference	Dry	Wet	
Current Dry	25.0%	-20.0%	
Current Wet	-22.2%	25.0%	

(c) Wet Period: BCCR3-D_Plant & NOAA_Plant

NOAA_Plant	Dry	Wet	Units: $\times 10^{-2}$ m
Current Dry	0.474	0.526	Dry is < 52.6900
Current Wet	0.556	0.444	Wet is > 52.6901
BCCR3-D_Plant	Dry	Wet	
Current Dry	0.444	0.556	Dry is < 55.7651
Current Wet	0.526	0.474	Wet is > 55.7652
Difference	Dry	Wet	
Current Dry	-6.6%	5.3%	
Current Wet	-5.6%	6.2%	

(d) Wet Period: BCCR3-D_Leo & NOAA_Leo

NOAA_Leo	Dry	Wet	Units: $\times 10^{-2}$ m
Current Dry	0.333	0.667	Dry is < 56.2249
Current Wet	0.632	0.368	Wet is > 56.2250
BCCR3-D_Leo	Dry	Wet	
Current Dry	0.500	0.500	Dry is < 56.8119
Current Wet	0.474	0.526	Wet is > 56.8120
Difference	Dry	Wet	
Current Dry	33.3%	-33.3%	
Current Wet	-33.3%	30.0%	

(e) Wet Period: BCCR5-D_Plant & NOAA_Plant

NOAA_Plant	Dry	Wet	Units: $\times 10^{-2}$ m
Current Dry	0.273	0.727	Dry is < 52.6900
Current Wet	0.667	0.333	Wet is > 52.6901
BCCR5-D_Plant	Dry	Wet	
Current Dry	0.583	0.417	Dry is < 57.5614
Current Wet	0.455	0.545	Wet is > 57.5615
Difference	Dry	Wet	
Current Dry	53.2%	-74.5%	
Current Wet	-46.7%	38.9%	

(f) Wet Period: BCCR5-D_Leo & NOAA_Leo

NOAA_Leo	Dry	Wet	Units: $\times 10^{-2}$ m
Current Dry	0.545	0.455	Dry is < 58.9000
Current Wet	0.500	0.500	Wet is > 58.9001
BCCR5-D_Leo	Dry	Wet	
Current Dry	0.500	0.500	Dry is < 57.5876
Current Wet	0.545	0.455	Wet is > 57.5877
Difference	Dry	Wet	
Current Dry	-9.1%	9.1%	
Current Wet	8.3%	-10.0%	

Table 10: Compared Wet Period for BCCR3-D, BCCR5-D and CCSM-D to their respective Raw GCMs.

(a) Wet Period: CCSM-D_Leo & CCSM-Raw

CCSM-Raw	Dry	Wet	Units: $\times 10^{-2}$ m
Current Dry	0.529	0.471	Dry is < 17.4929
Current Wet	0.500	0.500	Wet is > 17.4930
CCSM-D_Leo	Dry	Wet	
Current Dry	0.444	0.556	Dry is < 55.9655
Current Wet	0.529	0.471	Wet is > 55.9656
Difference	Dry	Wet	
Current Dry	-19.1%	15.3%	
Current Wet	5.6%	-6.3%	

(b) Wet Period: BCCR5-D_Plant & BCCR5-Raw

BCCR5-Raw	Dry	Wet	Units: $\times 10^{-2}$ m
Current Dry	0.417	0.583	Dry is < 15.0802
Current Wet	0.636	0.364	Wet is > 15.0803
BCCR5-D_Plant	Dry	Wet	
Current Dry	0.583	0.417	Dry is < 57.5614
Current Wet	0.455	0.545	Wet is > 57.5615
Difference	Dry	Wet	
Current Dry	28.6%	-40.0%	
Current Wet	-40.0%	33.3%	

(c) Wet Period: BCCR5-D_Leo & BCCR5-Raw

BCCR5-Raw	Dry	Wet	Units: $\times 10^{-2}$ m
Current Dry	0.417	0.583	Dry is < 15.0802
Current Wet	0.636	0.364	Wet is > 15.0803
BCCR5-D_Leo	Dry	Wet	
Current Dry	0.500	0.500	Dry is < 57.5876
Current Wet	0.545	0.455	Wet is > 57.5877
Difference	Dry	Wet	
Current Dry	16.7%	-16.7%	
Current Wet	-16.7%	20.0%	

2.6 Figures



Figure 1: CMIP3 and CMIP5 GCM locations and rain gauge locations for Tampa Bay, FL region

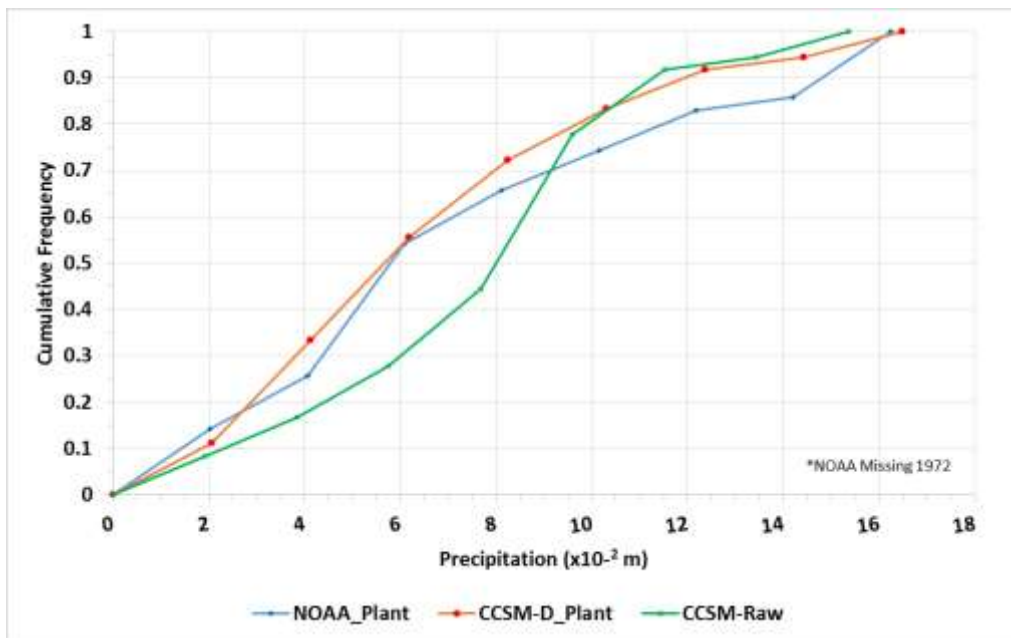


Figure 2: January PDF for NOAA_Plant, CCSM-Raw, and CCSM-D_Plant

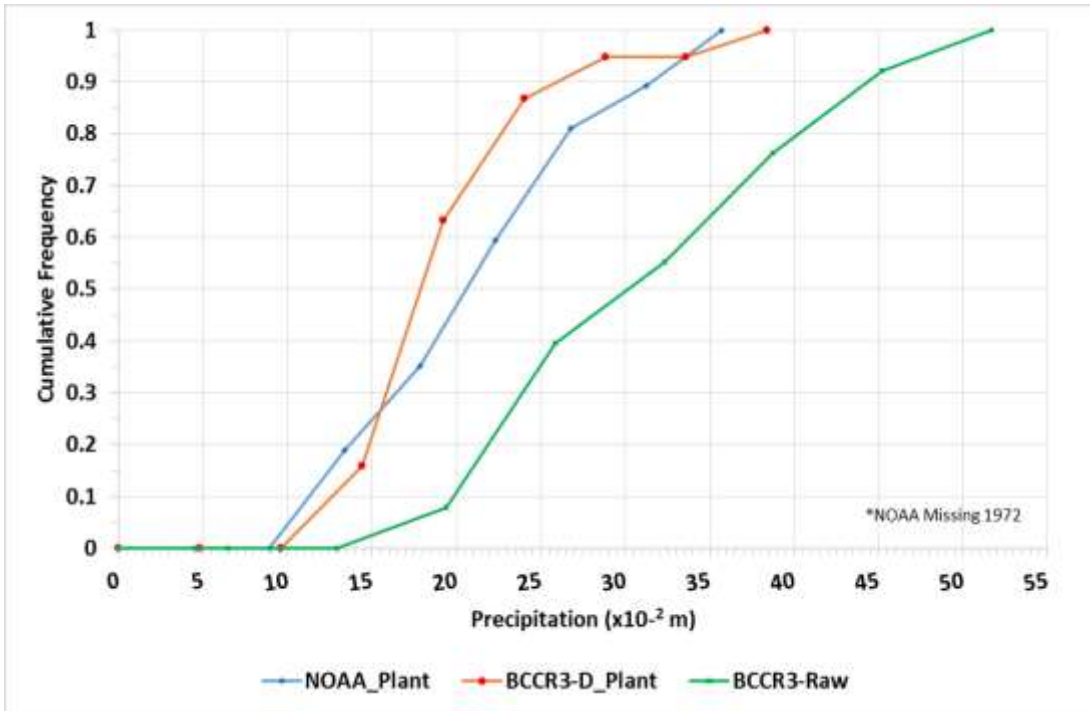


Figure 3: August PDF for NOAA_Plant, BCCR3-Raw, and BCCR3-D_Plant

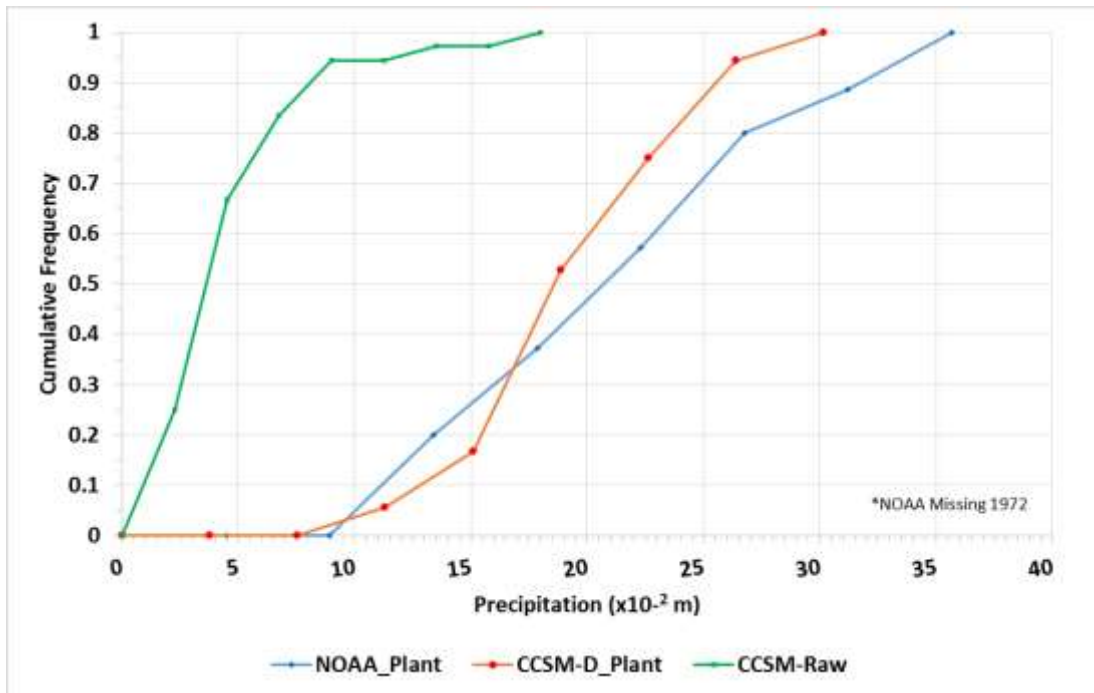


Figure 4: August PDF for NOAA_Plant, CCSM-Raw, and CCSM-D_Plant

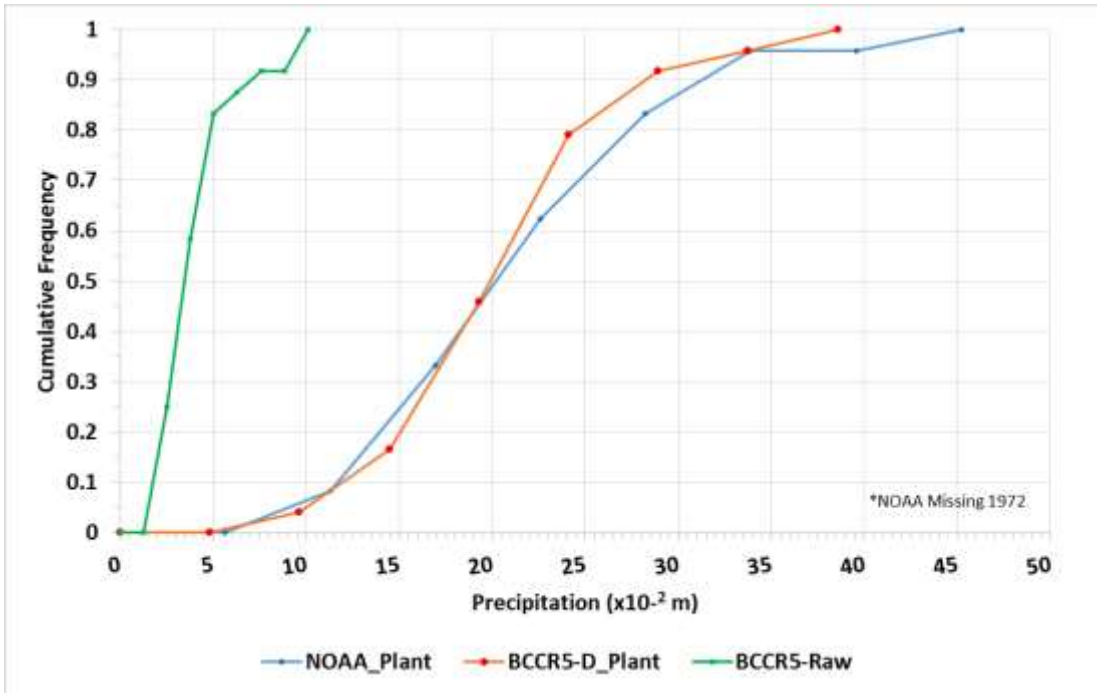


Figure 5: August PDF for NOAA_Plant, BCCR5-Raw, and BCCR5-D_Plant

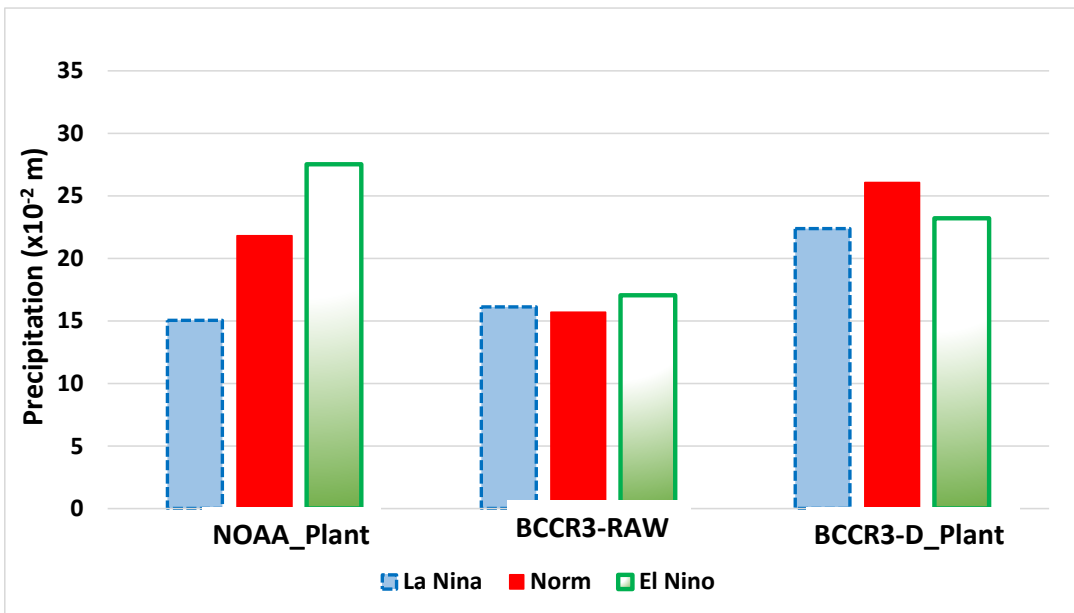


Figure 6: BCCR3-Plant City average precipitation for ENSO cycle

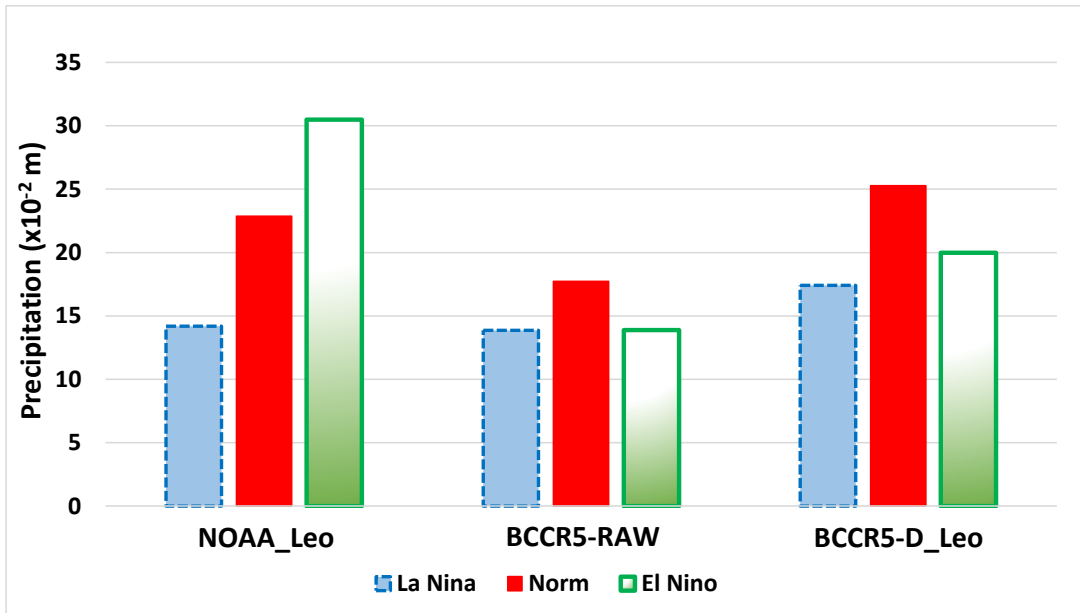


Figure 7: BCCR5-St. Leo average precipitation for ENSO cycle

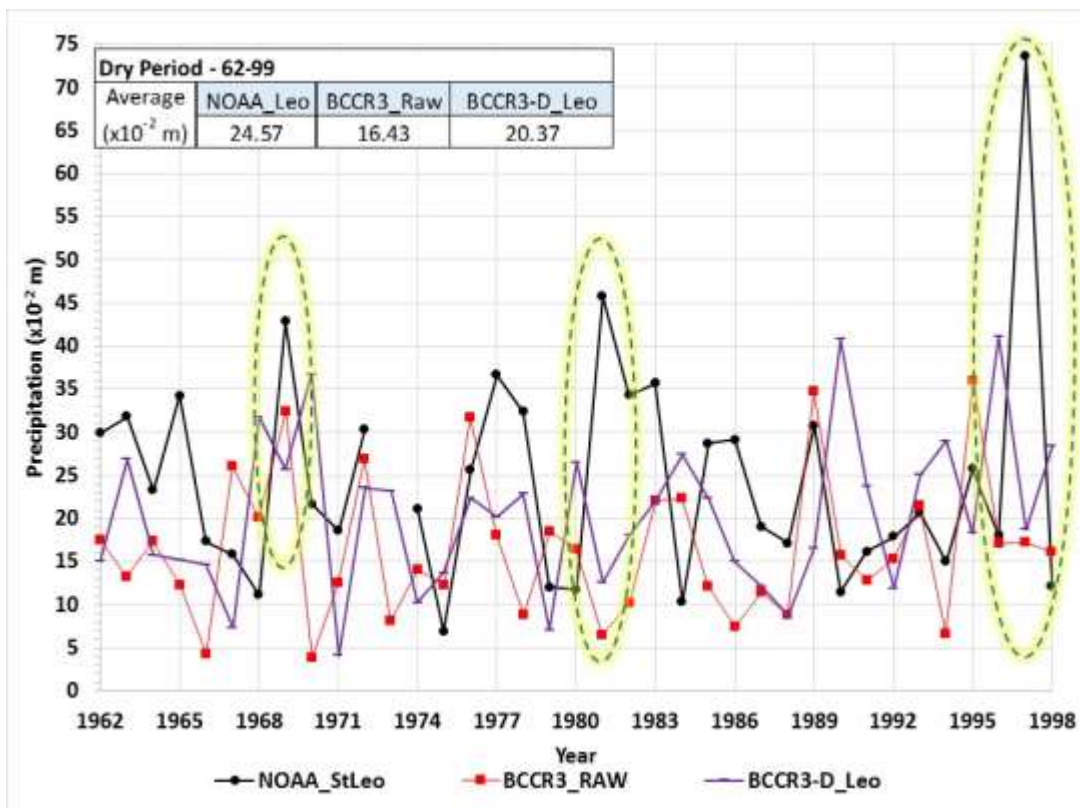


Figure 8: BCCR3-St. Leo - Dry Period (sum of December, January and February) showing ENSO cycles in Gauge, BCCR3-Raw and BCCR3-D_Leo

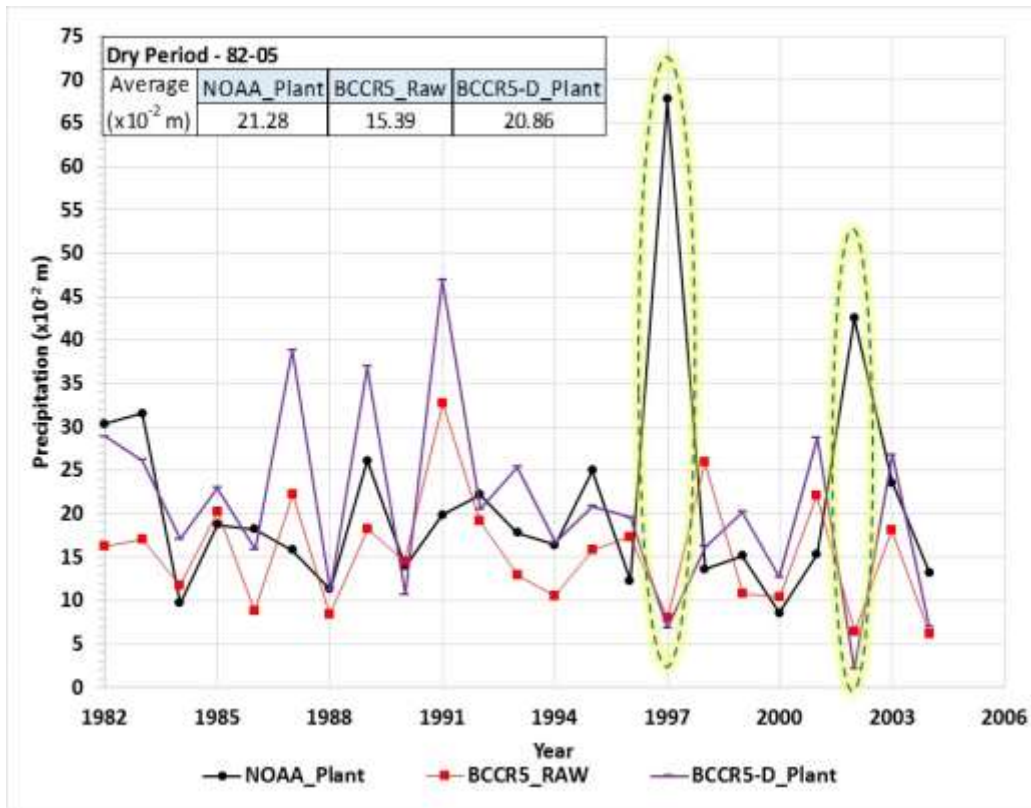


Figure 9: BCCR5-Plant City - Dry Period (sum of December, January and February) showing ENSO cycles in Gauge, BCCR5-Raw and BCCR5-D_Plant

CHAPTER 3: ASCERTAINING IF GENERAL CIRCULATION MODELS REPLICATE HISTORIC PERFORMANCE METRICS FOR HYDROLOGIC AND SYSTEMS SIMULATIONS

3.1 Introduction

Water managers are challenged to adapt supply sources and infrastructure systems to the reality of climate change. In 2017, the United Nations stated that by 2030 1.8 billion people will live in regions with extreme water scarcity (United Nations 2017). This concurred with the Intergovernmental Panel on Climate Change's (IPCC's) Fifth Assessment Report which estimated that many regions will suffer from reduced water supply by 2040. Inadequate water supply puts human lives at risk by creating food shortages and reducing potable drinking water, stressing the necessity for planning (IPCC 2014a).

To assess future water availability, hydrologists employ precipitation from general circulation models (GCMs) as inputs to drive streamflow and system simulation models. These GCMs incorporate various representative concentration pathways emission levels to model global climate response to greenhouse gas concentrations from air pollutant emissions and land use changes to capture a range of future scenarios (IPCC 2014b). The World Climate Research Programme's Coupled Model Intercomparison Project 5 (CMIP5 Lawrence Livermore National Laboratory of the U.S. Department of Energy, <http://www-pcmdi.llnl.gov/projects/pcmdi/>) provides access to data from several climate models such as BCC-CSM, CSIRO, GFDL-ESM2M and MIROC (see Table 11). Because GCMs are designed at a coarse scale, ~250 km to 600 km, they require downscaling to employ in regional and local hydrologic simulation models (IPCC 2013). Statistical downscaling techniques include bias-correction and constructed analog (BCCA), bias-correction and spatial disaggregation (BCSD), and bias-correction and stochastic analog method (BCSA) (Panaou et al. 2016; Gutmann et al. 2014; Hwang and Graham 2013a).

Due to spatial disparities, downscaled products result in residual biases and errors. For instance, Panaou et al. (2018) revealed that GCM and downscaled and bias-corrected data failed to capture historical climate cycles and the oscillations between wet and dry precipitation states or extremes associated with El Niño events. Further, when GCM precipitation was employed as inputs to hydrologic models, GCM errors propagated to simulated streamflow. Hwang et al. (2013b) showed how an integrated hydrologic model (IHM) streamflow outputs that were driven by GCMs differed from an IHM simulation produced with actual historical rainfall. However, it is unclear whether these mismatches would translate from the GCM precipitation to streamflow simulations, to the system model, and then ultimately the reservoir system. This research aimed to examine these impacts on reservoir operations via performance metrics because it is crucial to understand potential model simulation discrepancies for future water supply planning and adaptation.

To evaluate water supply systems, water managers have employed Reliability, Resilience and Vulnerability (RRV) performance metrics. In their popular forms, RRV was first introduced by Hashimoto, Loucks and Stedinger in 1982. Since then they have been used in a wide range of applications (e.g. Fowler et al. 2003, Asefa et al. 2014). Frequently, GCM precipitation feed in systems models providing streamflow outputs, enabling one to assess the performance of water supply systems in a changing climate. However, few studies have looked at all RRVs through the lens of GCM outputs (e.g. Soundharajan et al. 2016, Sandoval-Solis et al. 2011, Fowler et al. 2003, Yang et al. 2012, Seung Beom et al. 2015, Amarasinghe et al. 2016.). Soundharajan et al. (2016) assessed climate change's impact on the Pong reservoir in India. The authors utilized a rainfall–runoff model with delta perturbations to simulate future scenarios versus employing GCMs outputs directly into a hydrologic model. Sandoval-Solis et al. (2011) developed a sustainability Index to evaluate multiple water management policies by aggregating RRV indices. In contrast to this research, they compared scenarios of water management and policies, but did not consider climate change. Fowler et al. (2003) examined the influences of climate change on droughts in northern England via RRV. Although insightful, this study did not utilize CMIP5 GCMs but weather type frequency (Jenkinson and Collinson (1977)) using mean rainfall statistics and potential evapotranspiration. Yang et

al. (2012) investigated the impacts of climate change on water resources in Southern Taiwan using a weather generator to drive reservoir operation and hydrological simulation models using earlier GCMs, A1B emission scenario. They focused on identifying a drought risk index for their region by comparing three drought indexes, the sustainability index, modified sustainability index and drought risk index. Although insightful, it did not ascertain if GCMs could replicate each of the historic RRV metrics for a reservoir system. Seung Beom et al. (2015) employed GCMs to examine water supply for the Han River basin of Korea. This research examined both historical and future projections, but developed a conservative approach by assigning weights to IPCC's Fourth Assessment Report scenarios. Further, it refrained from using performance metrics to evaluate if GCMs were a suitable tool to downscale precipitation inputs to reservoir simulations. Amarasinghe et al. (2016) studied the impacts of reduced precipitation due to climate change on the resiliency of a water supply system. Resiliency was calculated for a water distribution network using pressure to evaluate the water grid system. The designed system was set to operate at a specific level of pressure and a drop in pressure reduced the level of service triggering a failure state.

Failure to estimate future water availability could result in water crisis, potentially leading to life threatening disasters. Furthermore, suppliers might implement different tactics and infrastructure development depending on a projected climate scenario. For instance, if models projected increased frequency of higher intensity storms that favors runoff, water resources managers might recommend increasing reservoir storage to capture larger fractions of streamflow. Conversely, if there is less annual precipitation, suppliers might opt for water reuse and water conservation strategies or other sources such as desalinated sea water. Therefore, it is critical to understand the nature of GCMs downscaled precipitation and whether it can accurately reproduce historical streamflow and, consequently, reservoir operations, before using GCMs to predict future climate scenario. This study aimed to determine if utilizing precipitation from GCMs as an input to a streamflow model is a feasible option, by providing an innovative assessment of both GCMs, hydrological reservoir tributaries and water supply systems. We are not aware of a study that considered a variety of performance metrics including reliability, resilience, vulnerability and sustainability, to evaluate the viability of employing GCMs downscaled precipitation into a streamflow

model to simulate a water supply and reservoir system. This research will increase the understanding of the GCMs capabilities and limitations prior to employment for water supply projections and mitigation.

3.2 Materials and Methods

For this research, the Greater Tampa Bay, Florida region was selected for the case study (Figure 10). Downscaling was performed via BCSA technique, which was found better suited for this area (e.g. Hwang and Graham 2013a). During downscaling, this stochastic process produced realizations of daily GCM precipitation that preserved the observed temporal frequency distribution of daily rainfall over space and spatial autocorrelation. The biases were then corrected by matching the GCM's cumulative distribution function (CDF) to historical rain gauge data observed at the local scale per respective month. Tampa Bay Water, the region's water supplier, developed a surface water modeling simulator, Flow Modeling System Version 2 (FMS2), to evaluate impacts of precipitation variability on water supply (Asefa et al. 2014). FMS2 is a stochastic model that simulates regional surface water supply source flows in the Hillsborough and Alafia rivers watersheds by utilizing monthly precipitation inputs at St. Leo, Plant City and Cypress Creek gauges (Figure 11). Employing a fully-exogenous, seasonal-multivariate linear regression model (SMLR), FMS2 generates stochastic time series ensembles for source flows to Tampa Bay regional surface water supply systems, specifically monthly flows at the Alafia River and entering the Hillsborough Reservoir/Tampa Bypass Canal (TBC) based on monthly precipitation. These flow locations include Alafia River at Bell Shoals, the Hillsborough River at Morris Bridge, and ungauged groundwater inflow and runoff into the TBC Lower and Middle Pools (Table 12). A multivariate, nonparametric disaggregation algorithm converts a simulated monthly flow time series to a corresponding daily flow time series. It then transforms flows to a daily time scale to match daily permit rules shown in Table 13 (Asefa et al. 2014).

3.2.1 Rainfall-Runoff Model

Precipitation from three gauges, St. Leo, Plant City and Cypress Creek (Figure 11), were used as inputs into SMLR rainfall-runoff model. This model is briefly explained below and details are in Asefa et al. (2014). Streamflow is estimated as:

$$y_t = \alpha_\tau + x_{\tau,t}\beta_\tau + \varepsilon_t, \quad \varepsilon_t \sim \mathbf{N}(\mathbf{0}, \Sigma_{\varepsilon,\tau}) \quad (5)$$

where \mathbf{y}_t represents the estimated streamflow; $\boldsymbol{\alpha}_\tau$ is a 1-by- n vector of model intercepts specific to season $\tau = \tau(\mathbf{t})$; and $\mathbf{X}_{\tau,t}$ is the predictor value for season $\tau = \tau(\mathbf{t})$ and time t .

$$\boldsymbol{\alpha}_t = [\alpha_{\tau,1}, \dots, \alpha_{\tau,n}] \quad \exists \tau \in \boldsymbol{\tau} \quad (1 \times n) \quad (6)$$

τ in $\mathbf{X}_{\tau,t}$ allows for different predictor values to be applied in different seasons. $\boldsymbol{\beta}_\tau$ is a p -by- n matrix of regression coefficients used only during season $\tau = \tau(\mathbf{t})$. For each unique seasonal value in $\boldsymbol{\tau}$, there are a total of $\|\boldsymbol{\tau}\|$ different $\boldsymbol{\beta}_\tau$ matrices.

$$\boldsymbol{\beta}_\tau = \begin{bmatrix} \beta_{\tau,11} & \dots & \beta_{\tau,1n} \\ \cdot & \cdot & \cdot \\ \cdot & \cdot & \cdot \\ \cdot & \cdot & \cdot \\ \beta_{\tau,p1} & \dots & \beta_{\tau,pn} \end{bmatrix} \quad \exists \tau \in \boldsymbol{\tau} \quad (p \times n) \quad (7)$$

The impact of the predictor x_j on predict and y_i during season τ is explained by each element $\beta_{\tau,ji}$, row $j \in [1 \dots p]$ and column $i \in [1 \dots n]$ of $\boldsymbol{\beta}_\tau$. Lastly, the residual $\boldsymbol{\varepsilon}_\tau$ is assumed to obey a multivariate normal distribution with stationary 1-by- n vector with 0 mean and n -by- n variance-covariance matrix $\boldsymbol{\Sigma}_{\boldsymbol{\varepsilon},\tau}$ specific to season $\tau = \tau(\mathbf{t})$. When estimates $\hat{\boldsymbol{\alpha}}_\tau$, $\hat{\boldsymbol{\beta}}_\tau$ and $\hat{\boldsymbol{\Sigma}}_{\boldsymbol{\varepsilon},\tau}$ are determined for $\boldsymbol{\alpha}_\tau$, $\boldsymbol{\beta}_\tau$ and $\boldsymbol{\Sigma}_{\boldsymbol{\varepsilon},\tau}$ in each season, an SMLR is specified. The SMLR parameters is computed by a least-square estimation; a separate analysis is performed for each season (Asefa et al. 2014).

3.2.2 Daily Flow Generations

While the precipitation in the rainfall-runoff model was at a monthly time step, operational models were simulated at a daily time scale to coincide with river flow daily withdrawal permits. To achieve this, a multi-variate nonparametric disaggregation procedure converted the models outputs using a family of K-Nearest Neighbor algorithms. Resampling from historical data for triplet streamflow traces was performed in a transformed space that was insensitive to the actual data size at a given stream flow location. This allowed for consideration of all three locations even though stream flow magnitudes varied, while the similarity measure was not overpowered by one stations values. This procedure preserved daily flow characteristic when transitioning from one month to the next month, which was vital for daily operational models. (For further details on the streamflow model see Asefa et al. 2014).

3.2.3 Performance Metrics

Reliability, Resilience, Vulnerability and Sustainability were adapted as metrics to evaluate the system's performance. Reliability evaluated how often the water supply system was in a satisfactory state and was calculated as the ratio of total number of satisfactory outcomes to total possible number of outcomes during the planning period (Equation 8). Satisfactory states are typically defined using system level variables such as target reservoir storage levels at time t , or meeting system demand at time t . In this case, performance metrics were calculated from simulated reservoir water level X_t series.

$$\text{Reliability: } \mathbf{Rel} = \frac{1}{n} \sum_{t=1}^n \mathbf{Z}_t \quad (8)$$

where Rel was the probability that a system was in satisfactory state, and $Z_t=1$ if $X_t \in S$ and $Z_t=0$ if $X_t \in F$; n was the total number of time steps which was 8766 days for these simulations; and S and F represented Success and Failure (unsatisfactory) states, respectively. In this study, an unsatisfactory state was triggered when the reservoir's elevation dropped below 26 meters (m). The system then remained in failure state until reservoir recovered to 30.5 m as shown in Figure 12. Reliability ranges from zero and one, with one being the most reliable and zero being least reliable (Asefa et al. 2014; Hashimoto et al. 1982; Loucks 1997).

Resilience measured the ability of a system to rebound from adversaries. It is typically defined as the ratio between the number of rebounds to the total time spent in an unsatisfactory state. Hashimoto et al. (1982) suggested that resilience reflected the expected length of time the system spent in an unsatisfactory state. However, since the system was forced to be in unsatisfactory state for prolonged period of time due to the 30.5 m recovery criteria, due to permits restricting unlimited water withdrawal, the resilience metric was examined at a monthly time step (30 days) (Equation 9). This provided an improved and better informed assessment of the system due to the constraints.

$$\text{Resilience: } \mathbf{Res} = \frac{\sum_{t=1}^n \mathbf{W}_t}{(n - \sum_{t=1}^n \mathbf{Z}_t)} \quad (9)$$

W_t indicated transition of the event from failure state to satisfactory state where $W_t=1$ if $X_t \in F$ and $X_{t+1} \in S$, and $W_t=0$ otherwise; $Z_t=1$ if $X_t \in S$ and $Z_t=0$ if $X_t \in F$; and n was the total number of time steps.

Resilience ranges from zero and one, with one being the most resilient and zero being least resilient (Chanda et al. 2014; Hashimoto et al. 1982; Loucks 1997).

Vulnerability described the severity of system once entering an unsatisfactory state. Severity could be represented in terms of quantity or loss of water production, and represented the average maximum deficit possible during failure event (Loucks 1997). For instance, Tampa Bay’s C.W. Bill Young Reservoir would be more vulnerable if the reservoir level dropped to an elevation of 23 m and rebounded in a week to an elevation of 30.6 m, versus if the reservoir level fell to 28 m and gradually recovered over several weeks. For this research, two forms of the equation were implemented, the maximum vulnerability (Vul Max) and the average vulnerability (Vul Avg) (Equations 10 and 11). The Vul Max examined only the most severe event over the entire period of record, whereas and the Vul Avg computed the vulnerability for each unsatisfactory event and then calculated the average. The Vul Max is traditionally examined, however, for water supply and planning it was deemed essential to extrapolate the average to improve system understanding. Since Vul Max would only occur one time, Vul Avg provided increased insight to typically elevation failures to allow for enhanced comparison of baseline and simulated GCM reservoir models by validation through multiple markers.

$$\text{Vulnerability: } \mathbf{Max Vul} = \mathbf{j = 1, m} \left\{ \frac{1}{n_j} \sum_{t=1}^{n_j} \left(\frac{C - Y_t}{C - Y_{\min}} \right) \right\} \quad (10)$$

$$\text{Vulnerability: } \mathbf{Avg Vul} = \frac{1}{m} \sum_{j=1}^m \left\{ \frac{1}{n_j} \sum_{t=1}^{n_j} \left(\frac{C - Y_t}{C - Y_{\min}} \right) \right\} \quad (11)$$

where $j = 1, \dots, m$ was running index for event failure with each event failure lasting n_j period in unsatisfactory states; and C was the Criterion to exit from an unsatisfactory state, in this case the reservoir level at 30.5 m; n was the number of time steps for the event period; m was the number of unsatisfactory events; Y_t was the elevation of the reservoir at that time step; and Y_{\min} was the minimum possible reservoir elevation at 22.8 m. Vul varies from zero to one, with zero being least vulnerable and one most vulnerable (Goharian 2016; Asefa et al. 2014).

Finally, calculating the geometric mean of reliability, resilience and vulnerability, the sustainability or the endurance of the system was assessed.

$$\text{Sustainability: } \mathbf{SI} = (\mathbf{Rel} * \mathbf{Res} * (\mathbf{1} - \mathbf{Vul}))^{1/3} \quad (12)$$

where SI is the Sustainability Index that ranges from zero to one, with one being the most sustainable and zero least sustainable. Rel is reliability, Res is resilience, and Vul is vulnerability which represents either Vul Max or Vul Avg (Linhoss and Ballweber 2015; Sandoval-Solis et al. 2011, Jain 2010).

3.3 Results and Discussion

3.3.1 Reliability, Resilience, Vulnerability and Sustainability Metrics

Figure 13 presents performance metrics for the reservoir system from simulations that utilized precipitation inputs from eight retrospective GCMs (GCMs-Sim) compared to a model driven by observed historical gauge data (Historical) for the same period of record. All GCMs-Sim predicted slightly more reliable reservoir (~0.88 to ~0.91) versus the model driven by historical rainfall (~0.87) (Figure 13a). This was an average increase of 3.55% in reliability, suggesting the system had fewer unsatisfactory days. Since all reliability metrics were close to one, this indicated that the reservoir was in a satisfactory state majority of the time.

The majority of GCMs-Sim predicted more resilient system than a model driven by historical rainfall whereas two GCMs-Sim, namely BCCR and GFDL-ESM2G, predicted less resilient system. Historical resiliency was 0.21, whereas GCMs-Sim data ranged from 0.12 to 0.24 (Figure 13b). The largest deviations were NorESM1 and GFDL-ESM2G with a -75.79% and -55.36% difference, respectively, whereas GFDL-CM only differed by 0.92%. These metrics translated into the length of time the system remained in an unsatisfactory state. Using historical precipitation, the reservoir remained in an unsatisfactory state for an average of 146 days per failure event, whereas the GCMs-Sim varied from 124 days (BNU) to 256 days (NorESM1) as shown in Table 14. Although all GCM driven simulations showed higher reliability, entry and exit to an event period were widely different among GCMs-Sim. For instance, GFDL-ESM2G remained in an unsatisfactory state for 577 days (2/12/2000-9/10/2001) and NorESM1 578 days (2/9/2000-9/8/2001), whereas Historical entered 1/15/2000 and recovered after summer precipitation on 8/31/2000 (229 days), and then returned to an unsatisfactory state in the dry season and remained in that state for 310 days (11/18/2000-9/23/2001) (Table 15). This period coincided with a La Niña cycle, which

typically reduces precipitation in the dry season for this region; however, some GCMs-Sim over predicted the reduction and the reservoir level struggled to recover during the wet season. There were no large differences in precipitation during this time frame; however, slight differences over multiple months and also how precipitation changed over time affected reservoir levels. These differences propagated to the sensitivity of the system to precipitation and water withdrawal limitations due to permit. Furthermore, requiring the system to rebound back to 30.6 m to emerge from an unsatisfactory event reduced the resiliency metrics. This definition limited oscillation between satisfactory and unsatisfactory states and lengthened the number of days to rebound, resulting in prolonging the recovery from the failure event. In water supply, it is important to maintain stability and not constantly alarm consumers. Therefore, it was imperative to ensure that once the system recovered from an unsatisfactory event it remained satisfactory for an extended period, hence the 30.6 m criteria was adopted by Tampa Bay Water.

Maximum vulnerability (Max Vul) metric examined the gravity of the most severe unsatisfactory event. None of the GCMs-Sim outputs replicated Historical's 0.87, with values ranging from 0.82 to 0.89 (Figure 13c). BCCR had the largest disparity with a -4.53% difference, followed by GFDL-ESM with -3.98%. Five of the GCMs-Sim were below Historical, indicating the system was not as vulnerable, an under prediction. Compared to Max Vul, the Avg Vul metric was even more under estimated. The Avg Vul incorporated the lowest and highest vulnerability values and described the average magnitude of a failure event over the entire period of record. Differences in Avg Vul were even larger at -7.77% (BCCR), -7.41% (GFDL-ESM2G), and -7.13% (CSIRO), although Historical Avg Vul decreased to 0.74 compared to Max Vul at 0.87. GCMs-Sim metrics fluctuated from 0.69 to 0.75 for Avg Vul, with seven of the GCMs-Sim displaying improved performance compared to Historical (Figure 14a). Further, when comparing Max Vul to Avg Vul, BNU, CSIRO and GFDL-CM were higher than Historical, i.e. more vulnerable (Figure 13c); however, for Avg Vul they were less vulnerable (Figure 14a). All vulnerability metrics were closer to one, indicating that on average when the system dropped below 30.6 m and got into an unsatisfactory state, the magnitude of the unsatisfactory state (how far the reservoir elevation dropped) was severe. All GCMs except MPI (0.75) underpredicted Historical's vulnerability (0.74) with values ranging from 0.69 to 0.72.

Finally, sustainability was a composite performance metric. Since two vulnerability metrics were determined, two sustainability values were also derived, Maximum Sustainability (Max Sus) and Average Sustainability (Avg Sus) (Figure 13d and Figure 14b). For Max Sus, the GCMs-Sim and Historical ranged from 0.27 to 0.34, indicating that the system was not very sustainable. Both the low resiliency values and high vulnerability results affected these values (Figure 13b). Most of the GCMs-Sim fluctuated from baseline with the largest deviations occurring in NorESM1 (16.99%), BCCR (16.40%), GFDL-ESM2G (13.30%) and MIROC (13.02%), and the smallest in GFDL-CM (-3.45%). The Avg Sus metrics (Figure 14b) improved compared to Max Sus with GCMs-Sim values ranging from 0.37 to 0.42, over predicting baseline (0.36). Compared to Historical, the largest deviations occurred in NorESM1 (14.05%), MIROC (13.43%) and BCCR (12.61%). MPI had the smallest divergence with 2.80% difference. Since both Max Sus and Avg Sus metrics were closer to zero, it further emphasized the system's inability to supply water for a prolonged period of time during unsatisfactory events. Therefore, diversifying sources of water supply is preferable since an unsatisfactory state persisted for over a year for some events. Although sustainability numbers were low, it is important to remember that the system was in a satisfactory state for most of the record. For instance, Historical was in an unsatisfactory state 13.3% of time, and therefore the system was able to meet water supply demand around 86.7% of the time. Diversifying supply sources, however, can help the system during the long failure events.

Performance metrics are an important tool for understanding whether streamflow simulated for retrospective runs reproduced key indicators that water resources managers rely upon. Differences among GCMs could be attributed to rainfall persistence in either wet or dry states over several seasons that was not quite captured by these models, which in turn impacted streamflow. Had streamflow and reservoir simulations only been compared via statistics, results would have shown negligible variations in GCMs-Sim statistics for the reservoir elevation (Table 16). This would not have provided information on how things changed on a daily time scale and if the system fell below a satisfactory state. Further, statistics were conflicting as it showed differences in the mean, minimum flow, and maximum flow values for Alafia, but Morris Bridge had minimal divergences (Table 17).

3.3.2 Statistical Analytics

Because basic statistics were inconclusive for the retrospective GCM precipitation and simulated streamflow compared to historical runs, the streamflow CDFs were evaluated to explain the discrepancies in the metrics (Figure 15 and Figure 16). Table 18 and Table 19 displayed experimental CDF at values above the permit level where water withdrawal was feasible. Although biases in GCM precipitation were corrected using the CDF match method (example shown in Figure 17), there were variances in the streamflow CDFs. For instance, at the minimum threshold of 65 mgd to allow withdrawal from Morris Bridge, Historical CDF was 0.385 whereas BNU, BCCR, GFDL-CM, GFDL-ESM3G, MIROC and MPI were significantly lower (Table 18). This potentially propagated into the GCMs-Sim generating more opportunities to withdraw water than Historical, which could have resulted in dissimilarities in reservoir water levels. Similarly, for Alafia, at 83 mgd Historical CDF was 0.253 but BCCR, GFDL-CM, GFDL-ESM2G and MPI had lower generated CDF values (Table 19). The precipitation inputs to the streamflow model attributed to the differences seen in the metrics. Figure 17 portrayed how below 0.30 CDF, the downscaled GCM's precipitation was consistently higher than gauge observation at Plant City station. For instance at CDF of 0.15, CCSM_Plant (GCM downscaled to the Plant City gauge location) precipitation was 15 mm whereas actual NOAA gauge data (NOAA_Plant) was 12 mm. Furthermore, the CDF revealed a smoothing of GCM precipitation data (Figure 17). The Plant City NOAA rain gauge data ranged between 9 mm and 36 mm with a narrow spread between the data points, whereas the GCM ranged between 7.5 mm and 30 mm exhibiting a wider range of variability. These discrepancies translated into the streamflow simulations, resulting in variations in the performance metrics which generally increased the reliability and sustainability indices generated by GCMs retrospective runs compared to Historical.

Box-and-whisker plots provided a clear visual statistical summary. The box-and-whisker plots for Morris Bridge (Figure 18a-1) and Alafia (Figure 19a-1) used a logarithmic scale. Although there were differences during the winter months, the plots displayed more inconsistency in streamflow during the summer between July and September, when this region received two-thirds of its precipitation. For instance, Morris Bridge July plot revealed that Historical (baseline) had a median close to 100 mgd with a wide range

in the 25th percentile versus 75th percentile (Figure 18g). Conversely, the median was higher for all GCMs-Sim except GFDL-CM. Furthermore, BNU, BCCR, CSIRO, GFDL-ESM2G and NorESM1 were less skewed compared to Historical. Similarly, there were also deviations in the Alafia plots (Figure 19a-1), with varied representations in the median, 25th percentile versus 75th percentile versus baseline.

3.3.3 Autocorrelation

Figure 20(a-i) and Figure 21(a-i) displayed the serial correlation for Morris Bridge and Alafia daily flows for the summer months (June through September). The time lag at which autocorrelation approaches zero, represented the memory of the system as seen in Figure 20 and Figure 21. For Morris Bridge, historical data had a memory of 18 days (Figure 20a) whereas the GCMs-Sim ranged from 14 to 25 days. For Alafia, Historical had a memory of 15 days (Figure 21a) whereas the GCMs-Sim estimated memory fluctuated from 8 to 22 days. None of the GCMs-Sim captured Historical's autocorrelation for either location. The differences in the memory influenced resilience, vulnerability and sustainability system metrics. For instance, GFDL-CM had the longest memory for Morris Bridge and highest maximum vulnerability value. This related to the sluggishness of the system and that once in unsatisfactory state the system tended to remain there for an extended period, i.e. daily values were highly correlated. This in turn affected the length and magnitude of the unsatisfactory event. Contrary, for Morris Bridge BCCR had the shortest memory and smallest Max Vul metric. Shorter serial correlation memory allowed quicker recovery to satisfactory levels.

3.4 Conclusion

This research presented an evaluation of the effects of retrospective GCMs runs on streamflow modeling and reservoir operation via performance metrics. These metrics included reliability, resilience, vulnerability and sustainability. Each metric evaluated different aspects of reservoir water resource supply system to determine if downscaled GCMs inputs could replicate historical system performance. Results showed that GCMs driven results generally captured Historical's resilience metric but none replicated reliability, vulnerability, and sustainability. Discrepancies occurred due to multiple factors, including variability in precipitation inputs due to smoothing and altered streamflow autocorrelation. The inconsistent results highlighted differences between utilizing precipitation from GCMs versus actual gauge data to

simulate streamflow and reservoir operations, further expressing the limitation of GCM data for water supply planning. This research further supported the importance of reproducing precipitation characteristics such as transition probabilities and persistence of climate states by GCMs, and streamflow autocorrelation. Further, bias-correction and downscaling of GCM precipitation aims at matching historical frequency distribution but may not adequately reproduce persistence over time for certain climate states such as those associated with La Niña. Although the retrospective GCMs did not perfectly mimic historical performance metrics, overall they performed reasonably well when aggregating statistics. Understanding the limitations of GCMs should provide insight when employing projected GCMs for streamflow and reservoir level simulations. Ultimately, for future climate change predictions, utilizing all the GCMs-Sim to create an ensemble might be a more reliable tool for water supply planning and management to deliver a spectrum of possible climate change and reservoir scenarios. Further, the historical GCM-Sim metric results can be used as a baseline for comparison for future GCM-Sim simulations for this region, which could then depict degrees of deviation that can be attributed to future climate change. Furthermore, this research provided valuable insights on mismatches that propagated from employing GCMs to simulate streamflow to aid in future model improvements.

3.5 Tables

Table 11: GCM models

Model Name	Model	Center
GCESS	BNU-ESM	College of Global Change and Earth System Science, Beijing Normal University
BCC	BCC-CSM	Beijing Climate Center, China Meteorological Administration
CSIRO-BOM	CSIRO-mk3.6.0	CSIRO (Commonwealth Scientific and Industrial Research Organization, Australia), and BOM (Bureau of Meteorology, Australia)
NOAA GFDL	GFDL-ESM2M; GFDL-ESM2G	Geophysical Fluid Dynamics Laboratory
MIROC	MIROC-ESM	Japan Agency for Marine-Earth Science and Technology, Atmosphere and Ocean Research Institute (The University of Tokyo), and National Institute for Environmental Studies
MPI-M	MPI-ESM-LR	Max Planck Institute for Meteorology
NCC	NorESM1-M	Norwegian Climate Centre

Table 12: Surface water source flows targets

Target	Historical Data Source
Alafia-Bell Shoals flow	Alafia-Bell Shoals flow is calculated over the historical record and then modeled as if a real gauged flow.
Cypress Creek flow	USGS daily flow data (02303800)
Hillsborough River flow @ Morris Bridge	USGS daily flow data (02303330)
Hillsborough River @ Zephyrhills	USGS daily flow data (02303000)
Trout Creek Flow	USGS daily flow data (02303350)
Ungauged Hillsborough Reservoir inflow	Using measured flow, elevation and operation data, three ungauged inflows are calculated as missing inflow/ outflow contributions in historical Hillsborough River and Tampa Bypass Canal volume balances
Ungauged Lower and Middle Pool inflow	

Table 13: Tampa Bay Water permits

Location	Permit										
S161 Diversion/Middle Pool (MP) Withdrawal	<ul style="list-style-type: none"> Criterion flow: total of measured previous-day flow over/through Hillsborough River Dam (HRD) and previous-day Control Structure S161 diversion: <table border="1" data-bbox="516 863 1365 1037"> <thead> <tr> <th>HRD flow (mgd)</th> <th>Permitted S161 Diversion/MP Withdrawal (mgd)</th> </tr> </thead> <tbody> <tr> <td>0 – 65</td> <td>0</td> </tr> <tr> <td>65 - 108.3</td> <td>0 - 43.3</td> </tr> <tr> <td>108.3 – 485</td> <td>43.3 - 194</td> </tr> <tr> <td>> 485</td> <td>194</td> </tr> </tbody> </table> Also limited by current-day (instantaneous) HRD flow to disallow withdrawals that will take HRD flow below 65 mgd (lesser of permit based on previous-day total and instantaneous HRD flow minus 65 mgd). 	HRD flow (mgd)	Permitted S161 Diversion/MP Withdrawal (mgd)	0 – 65	0	65 - 108.3	0 - 43.3	108.3 – 485	43.3 - 194	> 485	194
HRD flow (mgd)	Permitted S161 Diversion/MP Withdrawal (mgd)										
0 – 65	0										
65 - 108.3	0 - 43.3										
108.3 – 485	43.3 - 194										
> 485	194										
Lower Pool Permitted Withdrawal	<ul style="list-style-type: none"> 100% of any same-day measured Lower Pool volume over 2.74 m elevation No minimum flow requirement over S160 259 MGD maximum permitted withdrawal 										
Alafia Permitted Withdrawal	<p>Criterion flow:</p> <ul style="list-style-type: none"> Previous-day Alafia flow at Lithia Gauge x 1.117 + Historical daily average flows on day t of the year at Lithia Springs + Historical daily average flows on day t of the year at Buckhorn Springs + Historical daily average Mosaic withdrawal on day t of the year <table border="1" data-bbox="548 1436 1333 1608"> <thead> <tr> <th>Criterion flow (mgd)</th> <th>Permitted Alafia Withdrawal, (mgd)</th> </tr> </thead> <tbody> <tr> <td>0 – 82.73</td> <td>0</td> </tr> <tr> <td>82.73 – 92</td> <td>0 - 9.2</td> </tr> <tr> <td>92 – 600</td> <td>9.2 - 60</td> </tr> <tr> <td>> 600</td> <td>60</td> </tr> </tbody> </table>	Criterion flow (mgd)	Permitted Alafia Withdrawal, (mgd)	0 – 82.73	0	82.73 – 92	0 - 9.2	92 – 600	9.2 - 60	> 600	60
Criterion flow (mgd)	Permitted Alafia Withdrawal, (mgd)										
0 – 82.73	0										
82.73 – 92	0 - 9.2										
92 – 600	9.2 - 60										
> 600	60										

Table 14: Average number of days to rebound out of an unsatisfactory event (1982-2005)

1982-2005	Historical	BNU	BCCR	CSIRO	GFDL-CM	GFDL-ESM2G	MIROC	MPI	NorESM1
Avg number of days to rebound per event	146	124	168	125	144	226	150	152	256

Table 15: Reservoir unsatisfactory events (1982-2005)

1982-2005	Historical	BNU	BCCR	CSIRO	GFDL-CM	GFDL-ESM2G	MIROC	MPI	NorESM1
UnSat Dates				79 1/1/1982 - 3/20/1982					
UnSat Dates	127 4/13/1985 - 8/17/1985	112 4/27/1985 - 8/16/1985	126 4/24/1985 - 8/27/1985	167 3/13/1985 - 8/26/1985	144 3/20/1985 - 8/10/1985	133 4/10/1985 - 8/20/1985	123 4/24/1985 - 8/24/1985	102 5/10/1985 - 8/19/1985	110 4/29/1985 - 8/16/1985
UnSat Dates	66 6/15/1990 - 8/19/1990	18 7/9/1990 - 7/26/1990							
UnSat Dates	93 3/15/1991 - 6/12/1991	145 2/10/1991 - 7/4/1991	119 2/11/1991 - 6/9/1991		121 2/8/1991 - 6/8/1991	108 2/17/1991 - 6/4/1991			80 5/5/1991 - 7/23/1991
UnSat Dates			33 6/2/1992 - 7/4/1992	70 5/18/1992 - 7/26/1992	116 4/18/1992 - 8/11/1992			113 5/6/1992 - 8/26/1992	
UnSat Dates	160 3/10/1994 - 8/16/1994	154 2/28/1994 - 7/31/1994		85 4/26/1994 - 7/19/1994	120 4/22/1994 - 8/19/1994	87 5/21/1994 - 8/15/1994	98 5/6/1994 - 8/11/1994	228 12/25/1993 - 8/9/1994	
UnSat Dates	116 6/23/1997 - 10/16/1997	104 6/20/1997 - 10/1/1997	84 7/7/1997 - 9/28/1997	103 6/20/1997 - 9/30/1997	130 5/29/1997 - 10/5/1997		174 6/11/1997 - 12/1/1997	119 5/25/1997 - 9/20/1997	
UnSat Dates	229 1/15/2000 - 8/30/2000	100 4/26/2000 - 8/3/2000		195 1/12/2000 - 7/24/2000	155 4/4/2000 - 9/5/2000		113 4/10/2000 - 7/31/2000	92 4/30/2000 - 7/15/2000	
UnSat Dates	310 11/18/2000 - 9/23/2001	236 1/8/2001 - 9/27/2001	476 4/13/2000 - 8/1/2001	225 1/18/2001 - 8/30/2001	224 1/24/2001 - 9/4/2001	577 2/12/2000 - 9/10/2001	240 12/22/2000 - 8/18/2001	255 12/15/2000 - 8/26/2001	578 2/9/2000 - 9/8/2001
UnSat Dates	64 5/23/2002 - 7/25/2002			75 5/9/2002 - 7/2/2002					
Total # Days	8766	8766	8766	8766	8766	8766	8766	8766	8766
Total Sat	7601	7870	7928	7767	7756	7861	8018	7857	7998
Total UnSat	1165	896	838	999	1010	905	748	909	768
UnSat Count	8	7	5	8	7	4	5	6	3

*UnSat = Unsatisfactory; Sat = Satisfactory

Table 16: Daily reservoir elevation level (m) (1982-2005)

	Historical	BNU	BCCR	CSIRO	GFDL-CM	GFDL-ESM2G	MIROC	MPI	NorESM1
Median	39.1	39.5	39.8	38.3	39.5	39.8	39.5	39.4	39.7
Mean	36.4	36.8	37.1	36.3	36.9	37.0	37.2	36.9	37.2
STD	6.1	5.8	5.5	5.7	5.7	5.6	5.3	5.6	5.5
Min	22.7	22.8	22.7	22.8	22.7	22.8	22.8	22.7	22.8
Max	41.6	41.6	41.6	41.6	41.6	41.6	41.6	41.6	41.6

Table 17: Streamflow statistics for Alafia and Morris Bridge (mgd) (1982-2005)

	Historical	BNU	BCCR	CSIRO	GFDL-CM	GFDL-ESM2G	MIROC	MPI	NorESM1
Alafia Daily Flow									
Median	144.8	144.4	145.9	136.1	152.3	148.5	144.1	152.7	146.1
Mean	252.3	246.6	253.4	235.1	255.3	257.0	249.7	242.8	234.6
STD	393.4	399.9	380.4	348.7	366.0	407.4	398.4	372.0	317.6
Min	10.7	8.6	13.2	14.0	8.6	12.5	11.5	12.2	10.9
Max	6795.7	9872.4	6662.0	9276.0	7779.0	9872.4	9872.4	9872.4	4989.4
Morris Bridge Daily Flow									
Median	85.5	84.9	85.8	80.7	84.9	84.8	87.9	87.0	85.9
Mean	184.3	185.3	197.5	183.3	185.6	190.4	193.0	176.5	172.8
STD	344.1	339.5	391.0	333.9	350.0	383.1	359.4	289.7	284.2
Min	14.4	13.6	13.6	13.6	13.6	13.6	13.6	13.6	13.6
Max	5536.5	5536.5	5536.5	5536.5	5536.5	5536.5	5536.5	5536.5	5221.1

Table 18: Approximate CDF values of Morris Bridge daily flow (1982-2005)

Flow (mgd)	Historical	BNU	BCCR	CSIRO	GFDL-CM	GFDL-ESM2G	MIROC	MPI	NorESM1
65	0.385	0.375	0.370	0.405	0.375	0.378	0.362	0.373	0.392
108	0.582	0.591	0.585	0.597	0.592	0.579	0.585	0.587	0.594
200	0.773	0.770	0.772	0.771	0.776	0.762	0.770	0.780	0.783
300	0.853	0.854	0.852	0.850	0.862	0.849	0.853	0.858	0.854
400	0.884	0.882	0.881	0.881	0.888	0.882	0.882	0.888	0.895

*Closest values to Historical are bolded

Table 19: Approximate CDF values of Alafia daily flow (1982-2005)

Flow (mgd)	Historical	BNU	BCCR	CSIRO	GFDL-CM	GFDL-ESM2G	MIROC	MPI	NorESM1
83	0.253	0.259	0.245	0.276	0.248	0.232	0.253	0.237	0.256
92	0.297	0.299	0.283	0.318	0.286	0.273	0.297	0.276	0.286
200	0.630	0.640	0.634	0.655	0.670	0.623	0.629	0.618	0.653
400	0.835	0.854	0.844	0.862	0.846	0.841	0.849	0.850	0.840
600	0.903	0.912	0.905	0.918	0.899	0.904	0.910	0.918	0.927

*Closest values to Historical are bolded

3.6 Figures

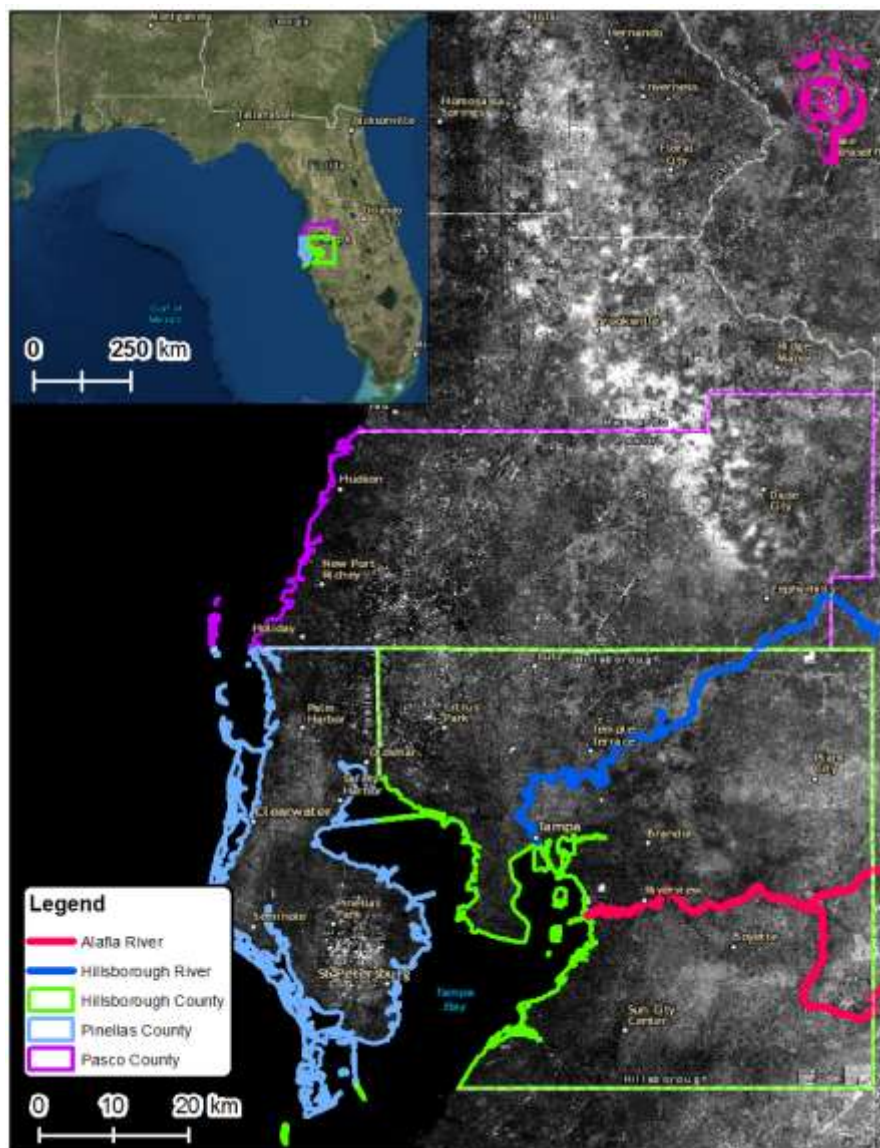


Figure 10: Site map of Greater Tampa Bay, Florida region

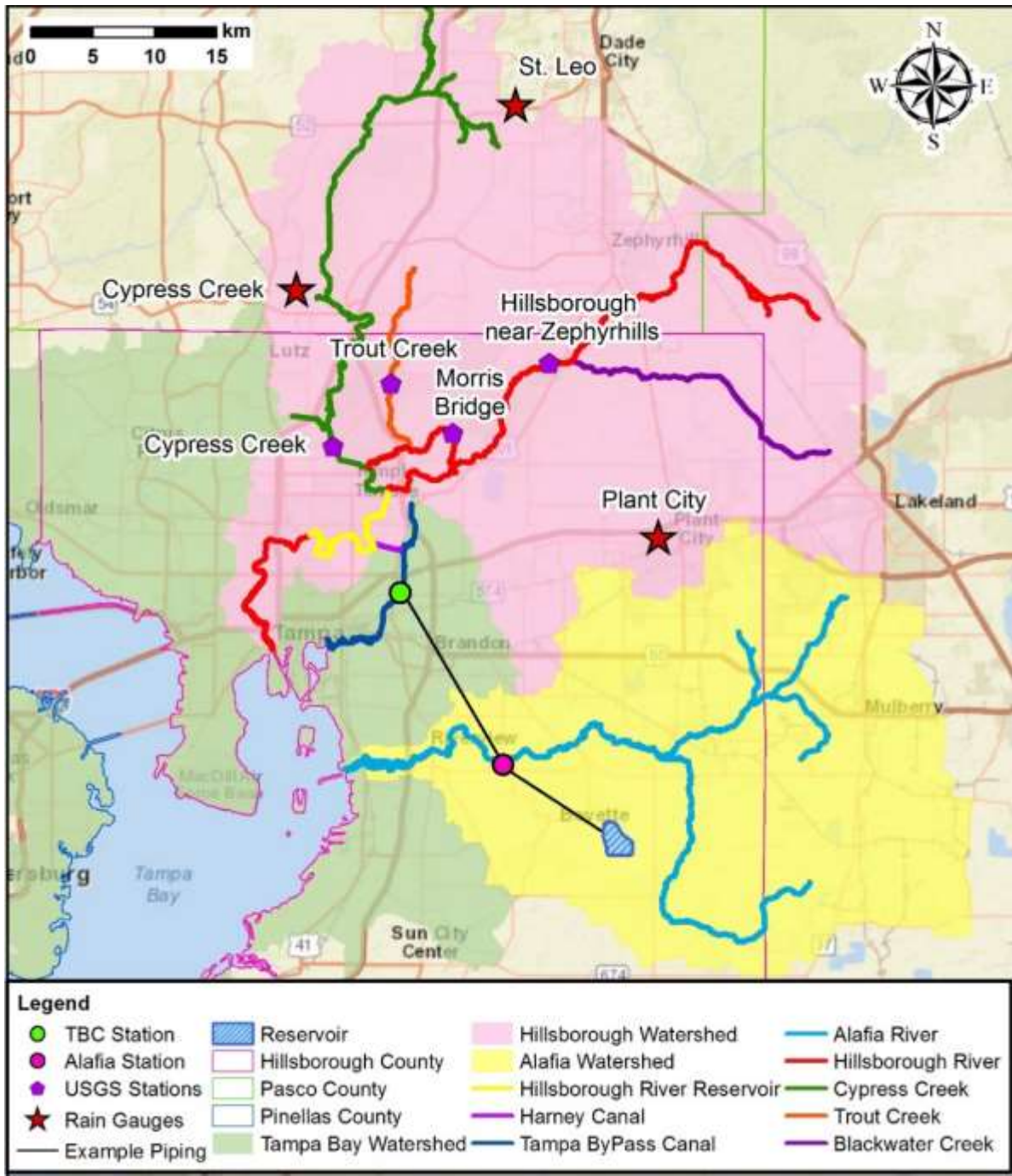


Figure 11: Water supply system including rain gauge and stream gauge locations, river tributaries and reservoir

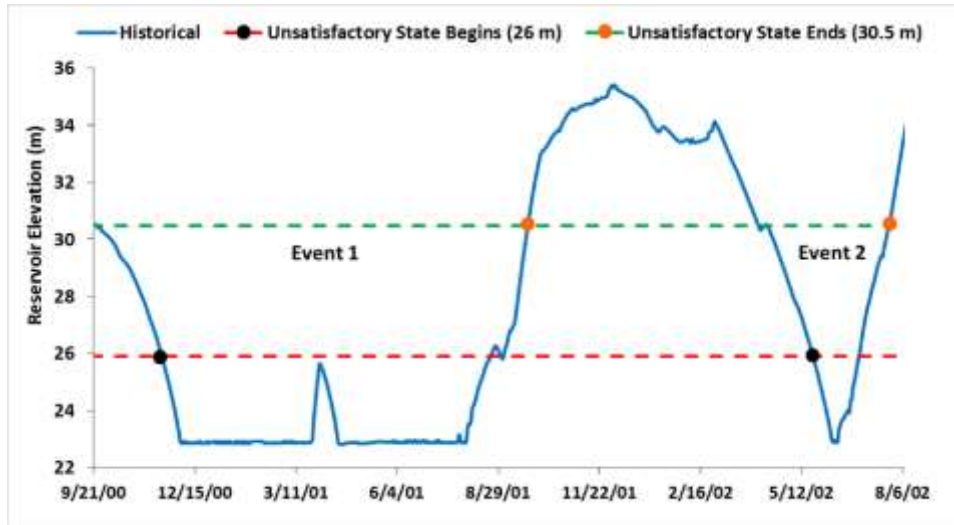


Figure 12: Reservoir system depicting failure events and unsatisfactory states

The system plunges into unsatisfactory states when reservoir level drops to 26 m, and exits the failure event when the water level recovers to 30.5 m

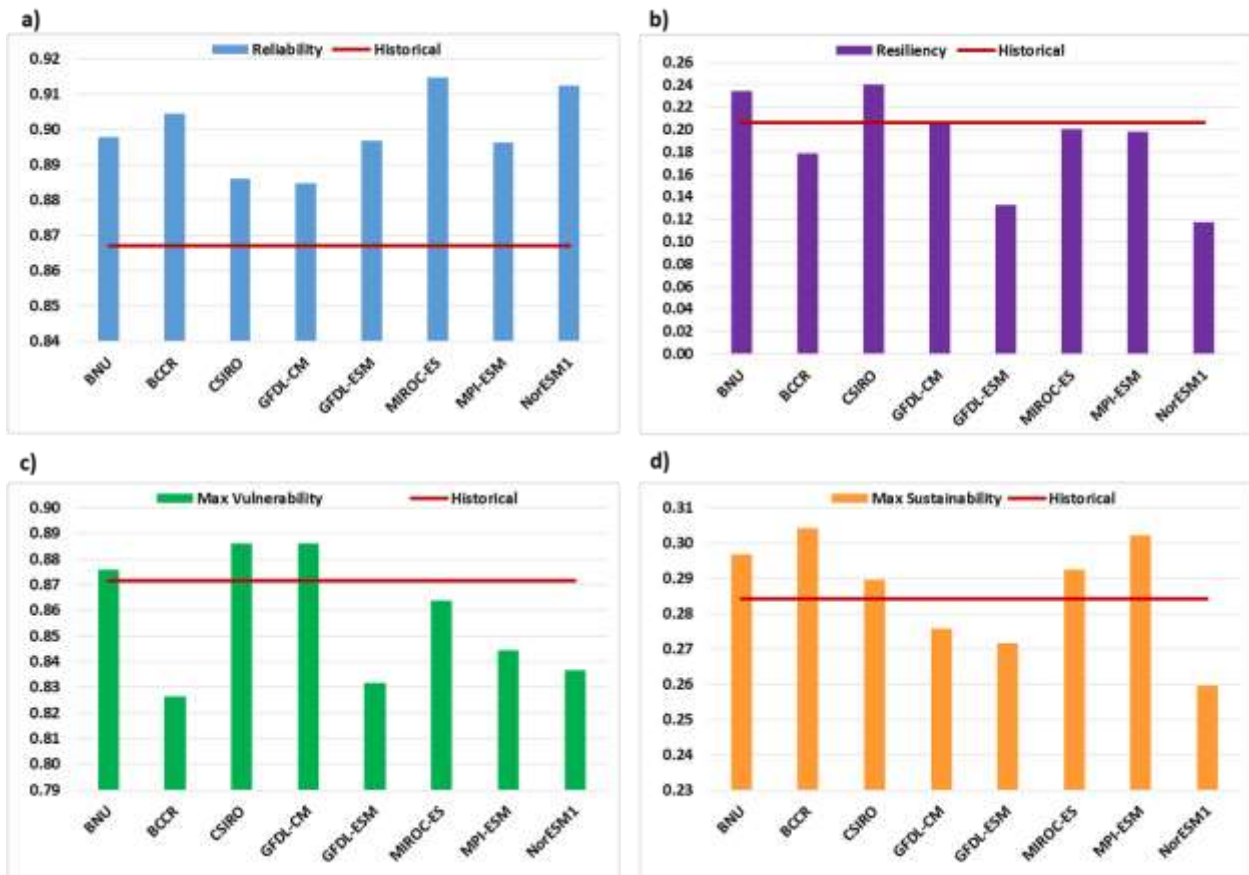


Figure 13: Historical reservoir performance metrics utilizing Maximum Vulnerability Metric

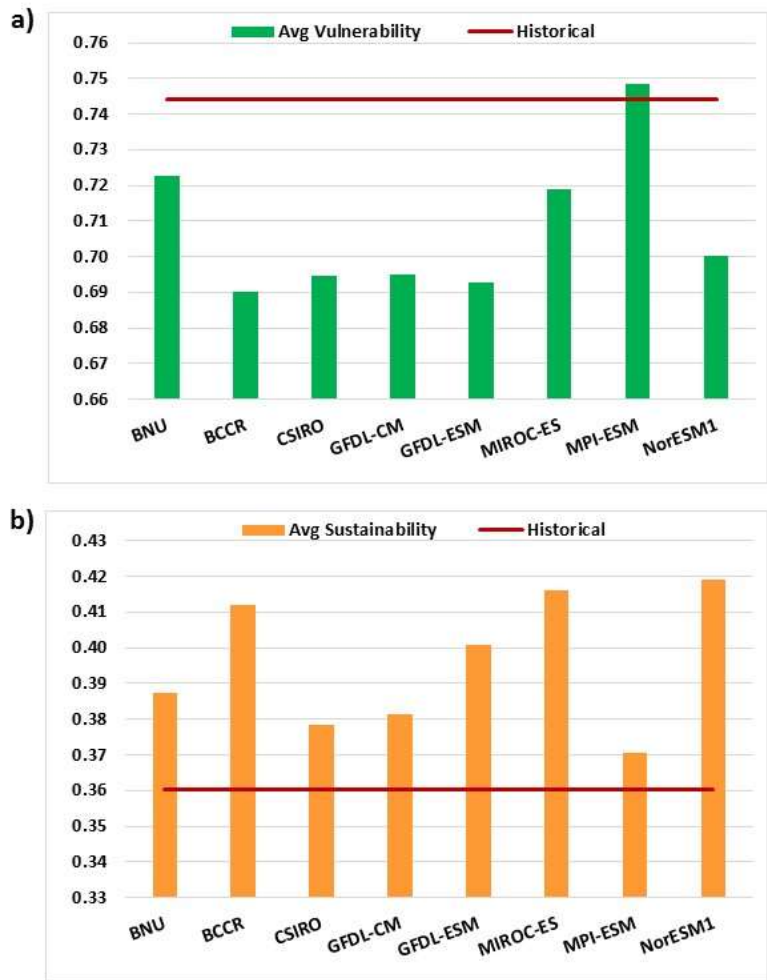


Figure 14: Historical reservoir performance metrics utilizing Average Vulnerability Metric

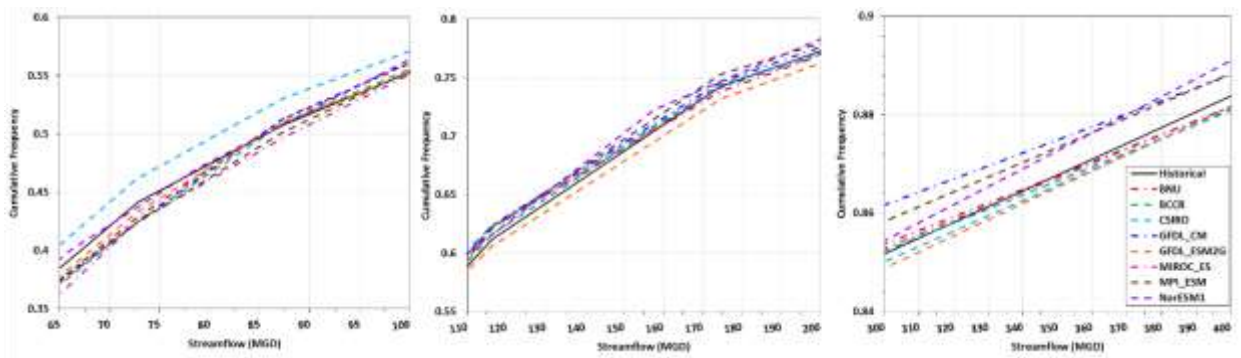


Figure 15: Historical CDF plots of Morris Bridge daily flow

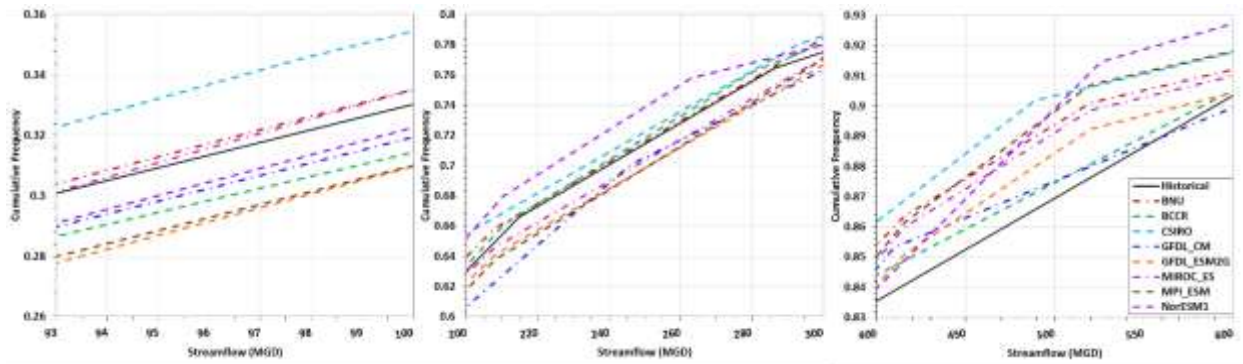


Figure 16: Historical CDF plots of Alafia daily flow

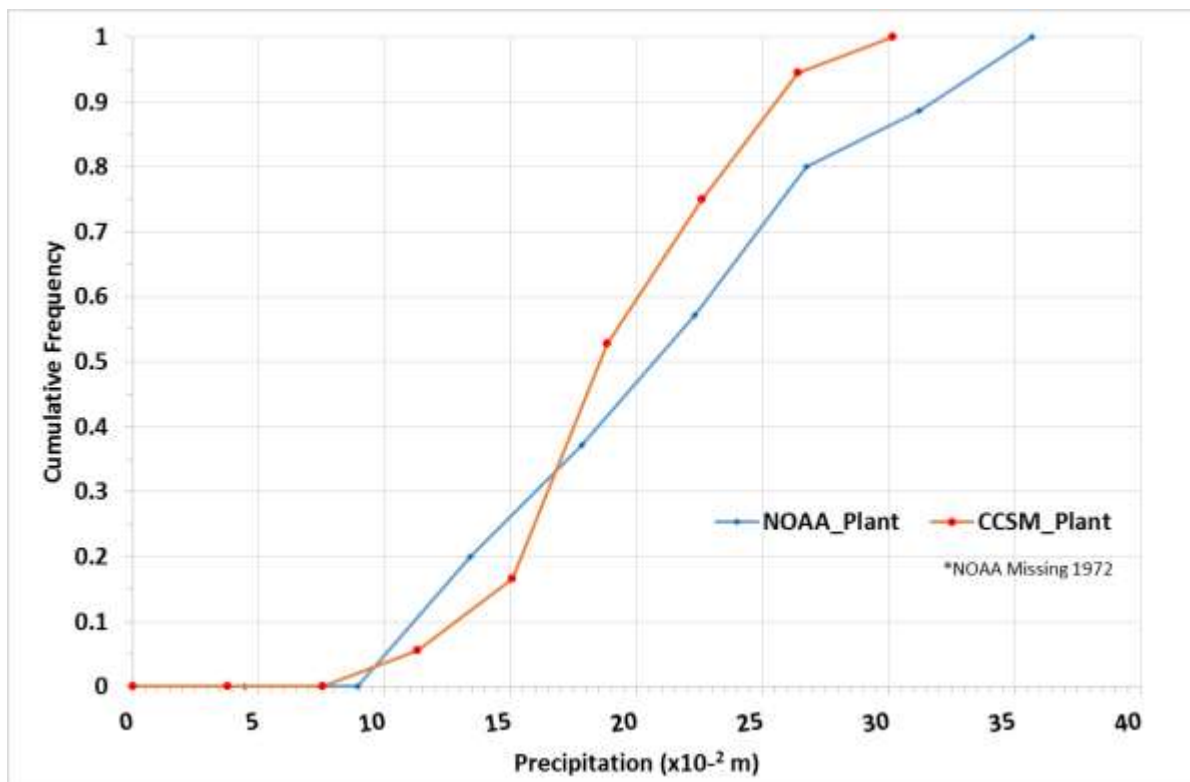


Figure 17: Historical August PDF for Plant City at gauge (NOAA_Plant) and GCM (CCSM-D_Plant)

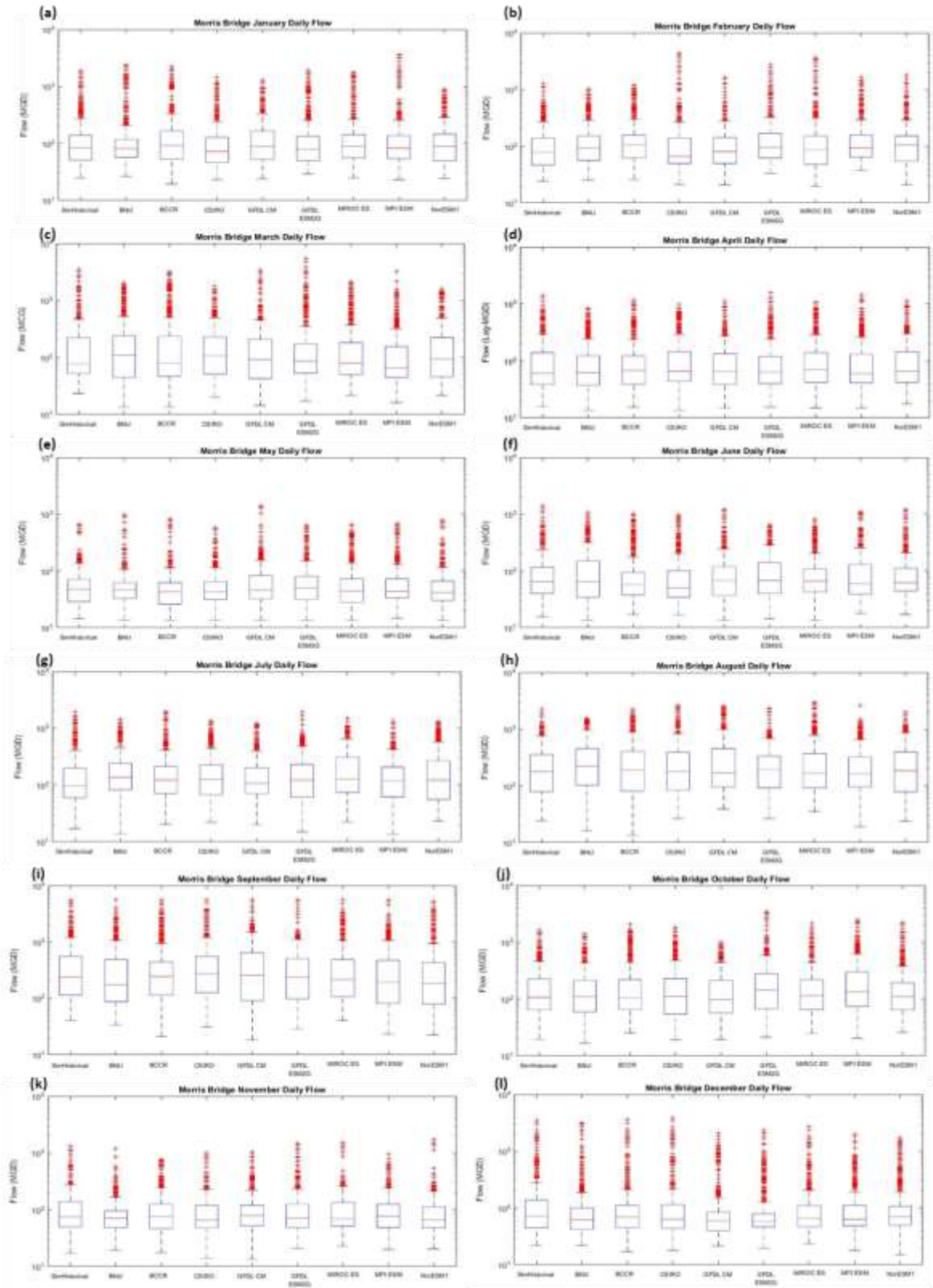


Figure 18: Historical monthly box-and-whisker plots for Morris Bridge daily flow

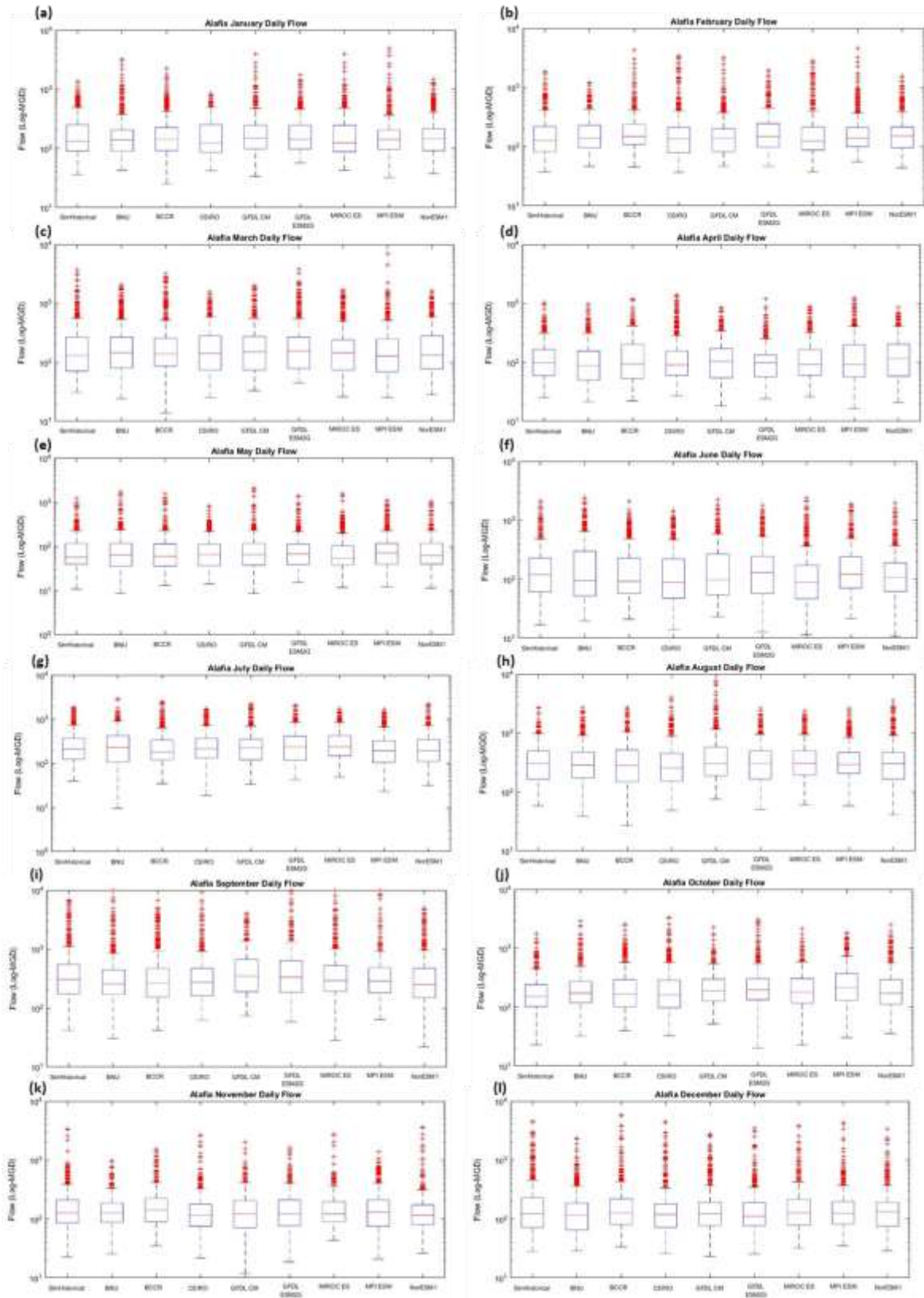


Figure 19: Historical monthly box-and-whisker plots for Alafia daily flow

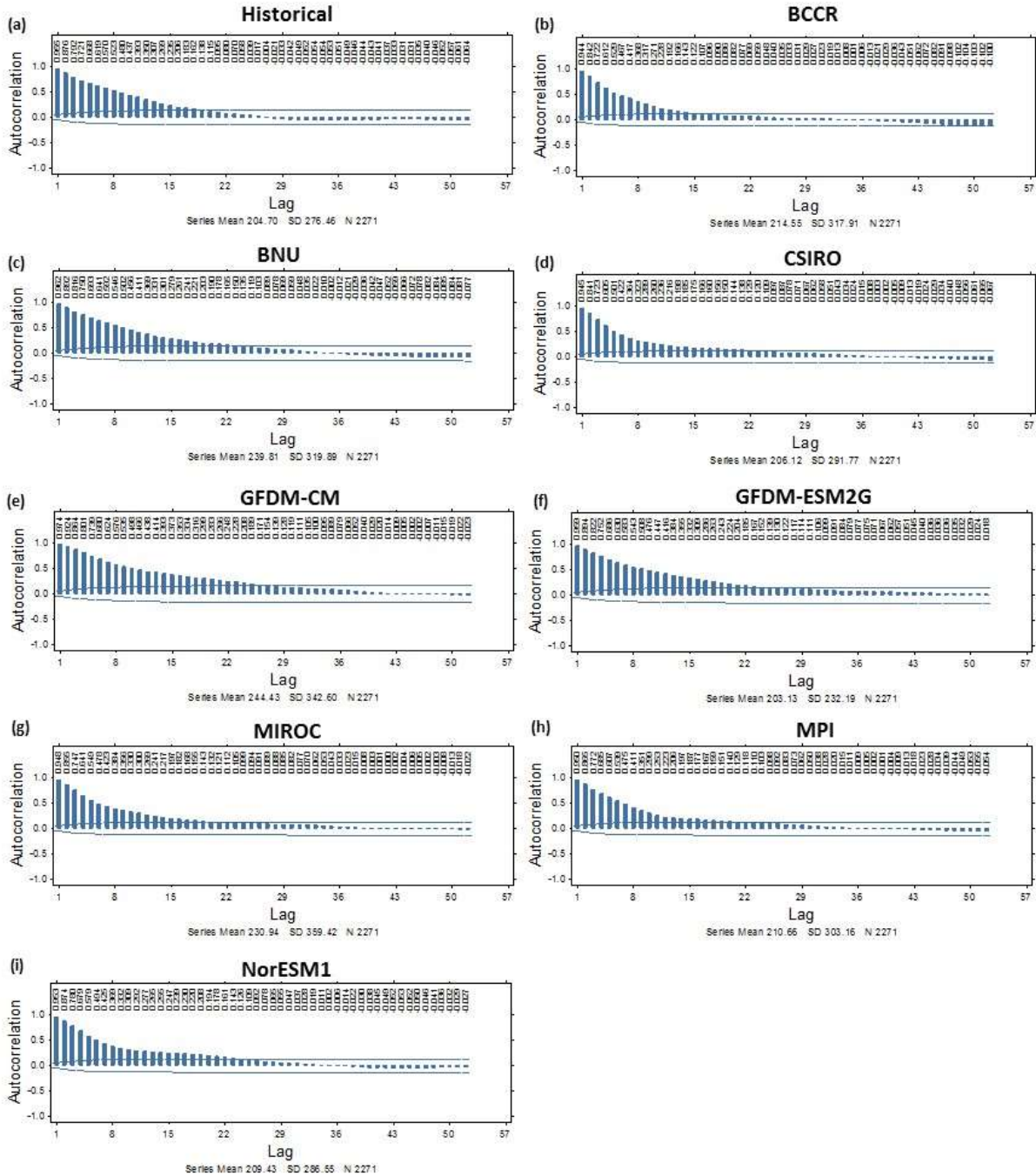


Figure 20: Daily auto correlation for simulated Historical and GCMs at Morris Bridge for summer months (June, July, Aug & Sept). Dashed lines indicate range of significance.

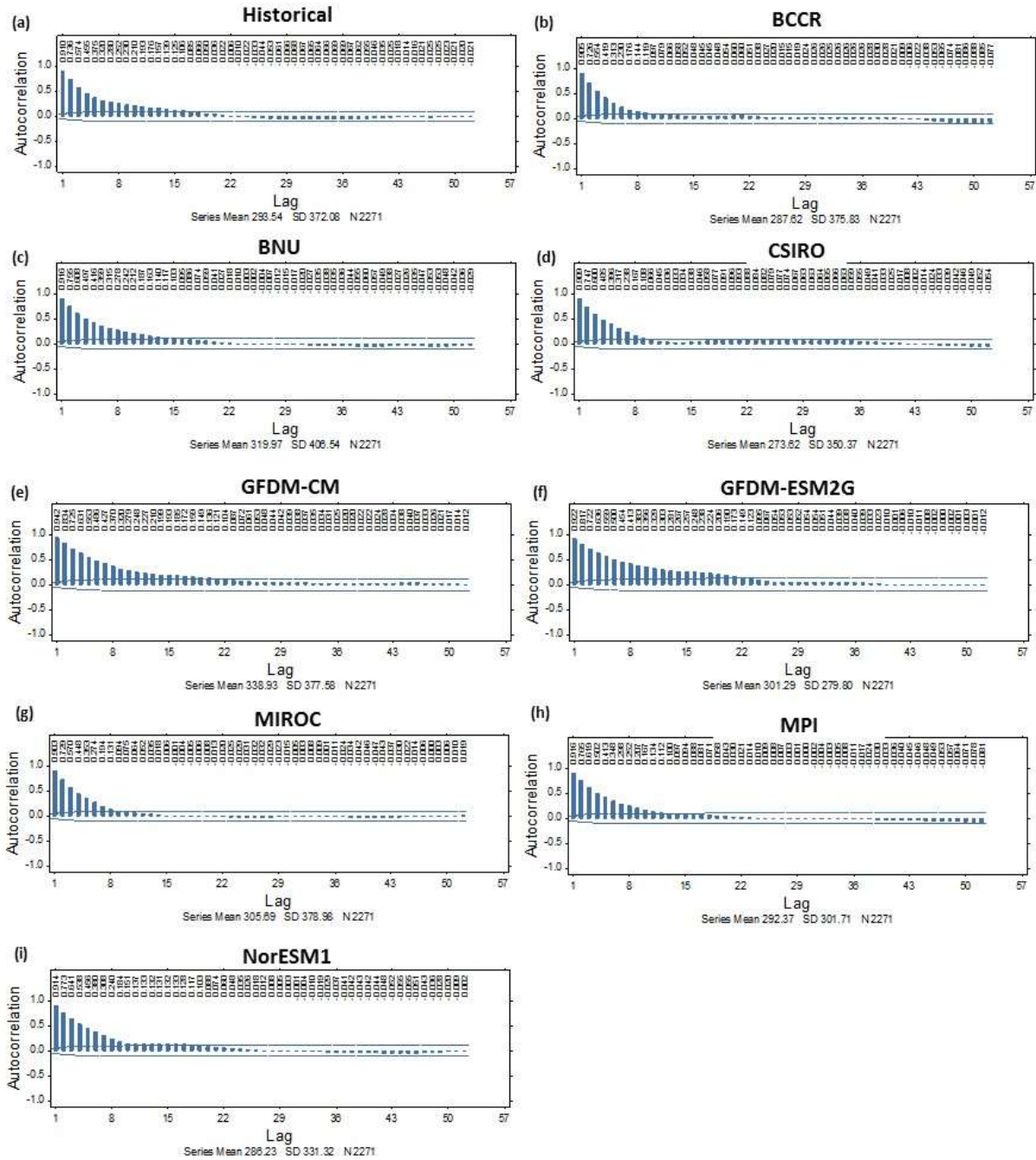


Figure 21: Daily auto correlation for simulated Historical and GCMs at Alafia for summer months (June, July, Aug & Sept). Dashed lines indicate range of significance

CHAPTER 4: PERFORMANCE EVALUATION OF A WATER SUPPLY SYSTEM UNDER A CHANGING CLIMATE

4.1 Introduction

Determining potential climate change impacts on streamflow is crucial for water suppliers as new infrastructure and technology cannot be developed and implemented over night. Changes in precipitation spatial and temporal inputs can strain sources of water supply, some with devastating effects (EPA 2016; Darren et al. 2015). For instance, beginning in 2012, Western United States (U.S.) faced low precipitation and high evapotranspiration, resulting in severe water shortages with lakes and rivers drying (NACSE 2017). California's dry conditions resulted in record-breaking drought conditions with the governor declaring a State of Emergency on January 17, 2014 (Williams 2015; Brown and Bowen 2014). On October 21, 2015, the New York Times posted an article depicting the severity of droughts in Ethiopia, the worst in a decade, with 15 million facing starvation due to water scarcity, causing crops and animals to die (NYT 2015). Around the same time, similar drought impacts were seen in other parts of Africa, including South Africa where their government declared the Free State and KwaZulu Natal provinces as disaster areas (South Africa 2015; Lyon 2014).

According to the Intergovernmental Panel on Climate Change (IPCC), the decadal average land temperature for 2002–2011 was $1.3^{\circ} \pm 0.11^{\circ}\text{C}$ above the 1850–1899 average for Northern Europe, and temperatures are expected to rise (Kovats et al. 2014). Increased temperature results in a rise in evaporation, which affects the hydrologic cycle and stresses water resources. IPCC's North America Fifth Assessment report indicated that in the future both the U.S. and Canada will experience diminished snowpacks due to increased evaporation, affecting the availability of fresh water. Furthermore, climate change is expected to put Mexico's water supply at risk (Romero-Lankao et al. 2014). Moreover, soil water content will decrease

in Southern Europe, making it rare to have saturation conditions. Further, there will likely be a change in snow accumulation and melting, especially in the mid-mountain areas (Kovats et al. 2014). Although forecast data is available for larger regions, limited information is available on how precipitation will effect water resources at regional or local levels. Since water supply planning occurs at smaller scales, such as cities or counties, understanding impacts of climate change are vital for sustainability of urban communities.

Although climatologists have found GCMs to be a suitable tool to for water supply planning, recommended common practice is to create an ensemble using multiple GCMs and Representative Concentration Pathways (RCPs) (i.e. emission scenarios see Figure 22) versus analyzing only one scenario to capture a range of options and detect consensus on future predictions (Panaou et al. 2018; Mani and Tsai 2017; Giorgi and Coppola 2010; Christensen and Lettenmaier 2007). For instance, Panaou et al. (2018) examined simulated streamflow using GCM precipitation as input drivers and determined using multiple GCMs provided improved evaluation of the reservoir system since no one GCM captured all historical performance metrics and key streamflow statistics such as frequency distribution function and serial correlation. Mani and Tsai (2017) used ensemble averaging methods to quantify climate change impacts on runoff for watersheds in North Louisiana and South Arkansas. They compared three projected ensemble average methods: the variance of future runoff for the hierarchical Bayesian model averaging, simple model averaging, and reliability ensemble averaging. Christensen and Lettenmaier (2007) employed an ensemble approach using 11 GCMs to drive water resource and hydrology models. Giorgi and Coppola (2010) examined precipitation and temperature from CMIP3 models and recommended at least four to obtain robust regional forecasts. The use of seven GCMs with multiple RCPs (17 scenarios) is demonstrated here (see Table 20). These were examined individually, but since all three RCPs emission scenarios were examined for GFDL-ESM2G, MIROC and NorESM, an Average GCM (Avg GCM) was also analyzed. Precipitation data were obtained from the World Climate Research Programme's Coupled Model Intercomparison Project 5 (CMIP5 Lawrence Livermore National Laboratory of the U.S. Department of Energy, <http://www-pcmdi.llnl.gov/projects/pcmdi/>).

In order to quantify future water supply changes, GCM precipitation was downscaled to a local scale then used to drive a hydrologic model to predict streamflow and evaluate water supply and reservoir performance metrics. Utilizing historical Reliability, Resilience, Vulnerability (RRV) and Sustainability metrics as a baseline, future predictions deviations were assessed. As introduced by Loucks et al. (1982), RRV metrics were used for performance of a water resource system. These metrics were aggregated using a Sustainability index (Sandoval-Solis et al. 2011) to evaluate a water resource system by accounting for both the water reservoir elevation and change in water demand. Yang et al. (2012) examined three drought indexes, the sustainability index, modified sustainability index and drought risk index, to determine potential impacts of climate change on a water resources system in Southern Taiwan using earlier GCMs, A1B emission scenarios. Singh et al. (2014) evaluated Lake Jordan, North Carolina reservoir system using stationary weather characteristics and climate change projections. They focused on a resilience index in order to establish strategies to ensure reliability under increased demands. In a recent study, Mateus and Tullos (2016) applied reliability and vulnerability metrics to examine reservoir operations under climate change, but did not consider resiliency and sustainability metrics. Additionally, they redefined vulnerability by contemplating the probability of operational failure and not the magnitude of the failure event. They also studied the effect of increasing temperatures and determined that although it impacted ground and surface water, it had minimal effects on surface reservoir. Amarasinghe et al. (2016) evaluated the impacts of climate change on a water supply system but only considered resiliency without addressing reliability, vulnerability and sustainability metrics. Further, resiliency was characterized by pressure recovery to evaluate performance water supply grid network. They set the design system to operate at a specific level of pressure and if the level of service was reduced to a pressure limit, it caused failure. Although all of these studies employed at least one of the performance metrics, none utilized all four to evaluate CMIP5 precipitation that drove streamflow and reservoir simulations.

Comparing reservoir performance with historical performance is critical to establish water resource operation strategies to mitigate climate change. For instance, if models predicted increased, higher intensity storms, additional reservoir storage might be needed to capture increased flows to meet demand.

Conversely, if annual precipitation was reduced suppliers might opt for strategies such as water reuse, desalinization and water conservation strategies. Therefore, this research examined future streamflow for time periods 2030-2053, 2054-2077 and 2077-2100, while using 1982-2005 as baseline to determine if the reservoir would meet operational targets. This research is novel as it provided an additional tactic to measure reservoir responses to climatic changes via performance metrics, as well as utilizing other statistical tools. These enabled future deviations to be calculated as well as determine periods when the reservoir system was at a critical level and unable to supply water. This method also assessed the degree of these unsatisfactory states, and the resiliency, vulnerability and sustainability of the surface water system. Multiple emission scenarios and an ensemble were analyzed since future emission trajectory is uncertain. Employing multiple GCMs and scenarios provided a range, enabling an enhanced and wider system understanding to allow suppliers to improve planning.

For Materials and Methods, refer to Chapter 3.2.

4.2 Results

4.2.1 Reliability, Resilience, Vulnerability and Sustainability Metrics

Employing performance metrics enabled a comprehensive analysis of the water resource system via evaluation of the reservoir elevation. Each metric was complimentary by investigating a different aspect to provide an enhanced understanding of how future reservoir supply changed from historical baseline. Figure 23 examined the reliability of the system by GCM and RCP. The bar in blue represented years 2030-2053, grey 2054-2077 and yellow 2077-2100. 1982-2005 was denoted by the red (GCM) and black lines (Historical), where Historical used rain gauge data to simulate the streamflow and reservoir. GCMs BNU, GFDL-ESM2G, BCCR, MIROC and NorESM, generally predicted the future reservoir to be less reliable. For instance, in 1982-2005 MIROC was 91% reliable but by 2100 MIROC 8.5 was only 44%. For all future periods, GFDL-CM and MPI 4.5 estimated a higher reliability, predicting less days when the elevation of the reservoir was in an unsatisfactory state. For instance, GFDL-CM was at 88% reliability for 1982-2005 but by 2100 GFDL-CM 6.0 increased to 99%. Further, there were zero unsatisfactory events for GFDL-CM 6.0 (2030-2053) and GFDL-CM 8.5 (2054-2100), and MPI 4.5 (2077-2100). Figure 24(a-d) examined

the average of GFDL-ESM2G, MIROC and NorESM for all four metrics. Figure 24a calculated the average reliability metrics by RCP for the reservoir. All future scenarios forecasted a less reliable system than historical. For example, the GCMs average reliability metric for 1982-2005 was 0.91 whereas for 2030-2053 RCP 6.5 declined to 0.82. RCP 8.5 exhibited a decreasing trend with being 85% reliable in 2030-2053 versus 56% in 2077-2100 periods. Avg GCM Reliability for RCP 4.5, the lowest emission scenario, depicted the system at first less reliable, 0.84 for 2030-2053, then dropped to 0.78 by 2077, but by 2100 improved to 0.87. This reflected the sluggishness of the system and that it would take time after reducing emissions to see an upward trend and atmospheric corrections.

Examining resiliency by individual GCMs by year and RCP revealed a range. Low resiliency metrics were prevalent with 71% above historical GCM benchmarks, and 29% below (Figure 25). Further, BNU, BCCR and MIROC (Figure 25a, c and e) were less resilient for all years and RCPs. This indicated the system remained in an unsatisfactory state for prolonged period of time, struggling to recover compared to the past. Conversely, GFDL-CM was more resilient for all years for RCP 8.5 as well as for 2054-2077 and 2077-2100 for RCP 6.0 (Figure 25d). In fact, there were zero unsatisfactory days during 2054-2077 period for both RCP 6.0 and RCP 8.5 and 2077-2100 timeframe for RCP 8.5. An ensemble of GFDL-ESM2G, MIROC and NorESM (Figure 24b) provided an average resiliency trajectory. RCP 4.5 first declined in 2054 but by 2100 recovered, although not to 1985-2005 GCM metric. As observed with reliability, once radiative forcing stabilized around 4.5 Watt per square meter (W/m^2) and the atmospheric system was allowed time to recuperate, the water resource system started improving. Contrary, RCP 8.5 resiliency was at first similar to 2030-2053GCM metric (0.14), but by 2100 decreased to 0.087, reflecting that higher emissions resulted in prolonged consecutive unsatisfactory days.

To explain future resiliency divergences, the average number of days the system remained in an unsatisfactory event period per RCP were examined. The average of GFDL-ESM2G, MIROC and NorESM is shown in Table 21. For 2030-2053 for all RCP's, average days in unsatisfactory state were higher than 1982-2005 period, indicating the system took longer to rebound. However, RCP 4.5 improved to 293 days by 2077, and then to 275 days by 2100. The worst case emission scenario, RCP 8.5, experienced the largest

average number of unsatisfactory days with a high of 464 days (2054-2077), double that of historical. Furthermore, assessment of individual GCMs revealed significant range. For instance, BNU (RCP 8.5) (Table 22) and MIROC (RCP 8.5) (Table 23) remained in an unsatisfactory state for 1,447 days (9/29/2032-9/14/2036) and 1,510 days (2/14/2093-4/3/2097) respectively, stating the system would not be able to supply water for around 4 years. This was an extremely long time for the reservoir to be below optimal levels, which, if an accurate prediction, could lead to a major water shortage crisis if there is inadequate planning. This persistence was reflected by the low resiliency numbers. Furthermore, MIROC recovered in April 2097 heading into the wet season but then in November 2097 became unsatisfactory again for another 859 days. Combining these consecutive events, the reservoir struggled to supply water for 7 years. It is important to note that this was just one of the GCM's predictions and they varied depending on the GCM and RCP, hence the need for the evaluation of an ensemble. For instance, MPI 8.5 was in an unsatisfactory state 6/10/92-10/14/92 (127 days), but did not reenter a failure state until a few years later (6/16/95).

Vul Max and Vul Avg were both examined for each GCM (Figure 26 and Figure 27). Vul Max measured the worst vulnerability event whereas Vul Avg provided a broader understanding of the system over all unsatisfactory events. Compared to GCMs baseline, 35 out of 51 future simulations had a more severe Vul Max metric, indicating that when the system was below satisfactory the average deficit was worse. For example, BCCR 8.5 historically had a metric of 0.83 but future exhibited a value of 0.88 (2030-2053), 0.95 (2054-2077), and 0.93 (2077-2100) (Figure 26). The highest possible number for vulnerability is one; therefore, after 2053 the system almost reached the maximum, experiencing the most extreme unsatisfactory events. Since simulated streamflow from the GCMs generally predicted less vulnerable reservoir than utilizing precipitation from the gauge (i.e. 1820-2005 for GFDL-ESM was 0.69 whereas the gauge was 0.74), it is feasible that these errors propagated to the future, resulting in a bleaker scenario than the simulated predicted. For vulnerability metric, GFDL-CM and MPI were outliers since there were no failures for some RCPs for 2054-2077 and 2077-2100 (Figure 26d and f). Taking the Vul Max metrics for GFDL-ESM2G, MIROC and NorESM and calculating the average by RCP (Figure 24c) indicated that the magnitude of the most severe failures steadily increased by 2100 with all years and RCPs being at or above

Historical GCM's metric. For all periods, RCP 4.5 was less vulnerable than RCP 6.0, while both were less than RCP 8.5. This indicated that higher emissions resulted in a more vulnerable surface water supply system. Vul Avg (Figure 27) also indicated that future water supply would be more vulnerable to water shortages. Vul Avg did not exhibit a trend, as in some instances 2030-2053 was more vulnerable than year 2100 (e.g. BCCR 8.5, MPI 8.5), whereas others it was reversed (e.g. GFDL-ESM2G 4.5, NorESM 8.5). There were 39 instances where this metric was greater than 1982-2005 GCM metric, and 12 times where it was less vulnerable. There were no unsatisfactory events for GFDL-CM3 8.5 from 2054 to 2100, and for period 2077-2100 for MPI 4.5.

Finally, evaluating the geometric mean of reliability, resiliency and vulnerability metrics sustainability of the system was explored. Since the system was examined during the most extreme failure as well as average unsatisfactory events, therefore the system was examined during both to determine how sustainable it was during the worst case scenarios, Sustainability Max (Figure 28), and how it typically behaved, Sustainability Avg (Figure 29). For Sustainability Max metrics, 40 scenarios predicted a less sustainable system compared to historical. These results were indicative that the system overall was likely to have more severe and prolonged unsatisfactory days. Outliers were all scenarios for GFDL-CM, 2030-2053 for MIROC 6.0, 2054-2100 for MPI 4.5, 2054-277 for MPI 8.5 and 2030-2053 for NorESM 4.5. Sustainability Avg metrics were only slightly improved with 39 scenarios predicting a less sustainable future. GFDL-ESM2G and MPI exhibited an increasing trend for RCP 4.5 and a decreasing trend for RCP 8.5 by 2100. On the other hand, BCCR and MIROC experienced a decline for all three RCPs by 2100. There was no consensus in the results among the GCMs in stating that lower emissions would result in a more sustainable water supply system. Utilizing Vul Max for GFDL-ESM2G, MIROC and NorESM and calculating the average Sustainability Max by RCP (Figure 24d), all scenarios demonstrated lower metrics than historical. RCP 6.0 sustainability slightly increased in 2054-2077 period (0.25) but then became less sustainable by 2100 (0.20). RCP 8.5 had similar sustainability metric to RCP 6.0 (0.24) for 2030-2053 but then plummeted to 0.16 by 2100. Employing an average, RCP 8.5 was always lower than RCP 4.5, which would be more indicative of lower versus higher emission scenarios.

4.2.2 Statistical Analytics

Table 24 expanded upon the streamflow statistics by GCM for RCP 8.5. Historically all GCMs flow averages were close to the baseline data (252 mgd at Alafia and 186 mgd at TBC), ranging from 234.6 mgd to 253.4 mgd for Alafia and 173 mgd to 198 mgd for TBC. By utilizing an ensemble and computing the average, the results almost matched for both flow and withdrawal. Interestingly, for RCP 8.5 the daily average flows were more extreme for future periods than historical. For instance, for 2030-2053 for Alafia flows ranged from 194 mgd (BNU) to 405 mgd (GFDL-CM), a difference of 211 mgd (109%). The highest value was more than double the lowest. Further, by 2100, GFDL-CM was at 589 mgd whereas MIROC was 147 MGC, producing a 442 mgd disparity (301% difference). Historically, the largest difference was significantly less at 22 mgd.

Furthermore, streamflow statistics exhibited a similar trend for both Morris Bridge and Alafia simulated streamflow. Figure 30a (Alafia) and Figure 30b (Morris Bridge) examined the average simulated streamflows of GFDL-ESM2G, MIROC and NorESM by RCP and period. RCP 4.5 mimicked historical through 2054, then increased. RCP 6.0 at first declined below Historical (Alafia 252 mgd and Morris Bridge 184 mgd) by 2053, then increased by 2077 to 271 mgd for Alafia and 202 mgd for Morris Bridge, then by 2100 matched Historical. RCP 8.5 slightly decreased by 2053 to 242 mgd for Alafia and 172 mgd for Morris Bridge; however, after 2054 there was a rapid decline dropping to 171 mgd for Alafia and 114 mgd for Morris Bridge. Withdrawal was limited by permits, therefore Alafia (Figure 30c) and TBC (Figure 30d) did not have similar withdrawal trends even though streamflow trends matched. For instance, for Alafia all future withdrawals are above Historical whereas for TBC all withdrawal amounts were reduced. There was also a greater difference in withdrawals for TBC by RCP (Figure 30d). For instance for 2030-2053, RCP 4.5 was at 70 mgd, then decreased slightly to 66 mgd, then by 2100 increased to 71mgd. Conversely, RCP 8.5 was initially at 69 mgd and continued to drop until it reached 56 mgd by 2100. On the other hand, for Alafia (Figure 30c) RCP 4.5 and RCP 6.0 almost flatlined for all time periods at around 16 mgd and 16.5 mgd, respectively. RCP 8.5 also had minimal variation with 17 mgd in 2030-2053 versus 16 mgd by 2100.

Variances in the reservoir elevation were also visible by RCP and period (Table 25). For example, RCP 4.5 declined in 2030-2053 and 2054-2077 with a median of 38.4 m and 36.9 m, respectively, but by 2100 increased to 39.3 m. This same trend was evident in TBC withdrawal, which provided greater amount of water (Figure 30d). RCP 4.5 once again reflected that the system recovered after the atmospheric time to recuperate. Contrary, RCP 8.5 median declined from 39.6 m to 35.1 m by 2100, replicating TBC withdrawal. Averages had the same tendencies.

These elevations trends could be translated to the number of unsatisfactory days (Table 26). For instance, RCP 4.5 exhibited a similar pattern by initially declining but then improving by 2100. It began with 1,332 unsatisfactory days in 2030-2053, decreased to 1,864 days in 2054-2077, and then improved to 1,182 unsatisfactory days. Although it improved, it never reach Historical's 807 unsatisfactory days. Furthermore, the average of these three GCMs under predicted Historical's number of unsatisfactory days by 358 days or 44%. If this underestimation error also propagated into the future, unsatisfactory days would increase. For instance, $1,864 * 1.44$ would translate to 2,684 days or 31% of the number of days in that period would be unsatisfactory. RCP 8.5 steadily increased in number of unsatisfactory days by 2100, painting a gloomy picture since 44% of the time the reservoir levels fell into a critical state. Further, RCP 8.5 also under predicted Historical (807 versus 1,165 days). Therefore, if the system estimated 3,841 unsatisfactory days, accounting for this error this would translate to 5,531 ($3,841 * 1.44$) unsatisfactory days or 63% of the time that period in a critical state.

Evaluation of CDFs expands upon divergents in the flows. Table 27 and Table 28 examined the average CDF for Morris Bridge and Alafia streamflow at a level where permits allowed for water withdrawal, 65 mgd and 83 mgd respectively. For both Morris Bridge and Alafia, Historical (0.38 and 0.25 respectively) was similar to the 1982-2005 gauge. For RCP 8.5 both CDF values steadily increased by the year 2100 with values of 0.55 for Morris Brides and 0.39 for Alafia. This translated into there being fewer opportunities to withdraw water. For instance, in 1982-2005 the system was able to withdraw water from Alafia 75% of the time whereas by 2100 was at 61%. For both simulated streamflows, RCP 4.5 CDF at first increased but by 2100 declined to a level similar to Historical, once again reflecting the systems recovery

after time. There were also variances amongst the individual simulations (Table 29). For example, GFDL-CM was at 0.15 CDF value whereas GFDL-ESM2G was at 0.61 for 2077-2100 for Morris Bridge. GFDL-ESM2G was double 1982-2005 value, and GFDL-CM was reduced by half. This was further reflected in the metrics where for this period GFDL-CM has no failures and GFDL-ESM2G reliability was one of the lowest (Figure 23d). All GCMs were similar for 1982-2005 period, but by 2100 ranged from 0.15 to 0.61 CDF value (Table 29). Some values increased with time such as GFDL-ESM2G, MIROC, NorESM. Others such as BCCR, BNU, MPI fluctuated. Higher CDF values resulted in fewer opportunities for water withdrawal since flows had to meet the permit minimum requirement, ultimately affecting the reservoir.

Evaluation of autocorrelation explained divergent flows by assessing how the memory of the system changed with RCP and timeframe. A short memory relates to less similar days in a state whereas a longer memory reflects persistence. Table 30 and Table 31 examined the average annual and summer autocorrelation examined flow for GFDL-ESM2G, MIROC and NorESM for streamflow, respectively. Compared to historical, the memory doubled in most instances. For example, 1982-2005 annual was at 30 days whereas by 2077-2100 RCP 4.5 and RCP 6.0 were at 62 and 61 days, respectively (Table 30). This was reflected both in the duration a system remains in an unsatisfactory state as well as in a satisfactory state. Historically none of the simulations had unsatisfactory event periods greater than 578 days and the memory was reduced; however, future scenarios depicted events reaching up to 1,510 days and annual autocorrelations were doubled for all RCPs. For summer (Table 31), serial correlation increased for RCP 4.5 for 2054-2077 but then declined by 2100. RCP 8.5 at first increased in 2030-2053, then decreased by 20177, then improved to a value of 31 by 2100. Results indicate that future periods' summer correlation, although not always on mark, was closer to historical than annual, revealing that the winter months had a greater variance. El Niño-Southern Oscillation (ENSO) affects this region primarily during the winter months with El Niño reducing precipitation and La Niña increasing prediction. It is possible that this is indicative of more intense events such as ENSO.

4.2.3 Precipitation

Precipitation is the driver for these streamflow simulations; therefore, understanding and capturing the hydrological cycle is extremely important. Water supply withdrawal is sensitive to stream's flowrate, which is affected by precipitation quantity, antecedent conditions, and persistence of a climate state (e.g. wet day follow by another wet day). Figure 31 displays precipitation at the Plant City gauge for the three time periods for each RCP. The average of the annual precipitation per time frame was computed. Figure 31a combined three GCMs, GFDM-ESM2G, MIROC and NorESM, to provide an average GCM value. Comparing this to the average streamflow (Figure 30), the relationship was evident. For instance, in both, RCP 4.5 increased after 2077, RCP 6.0 decreased by 2100 and RCP 8.5 declined after 2030. Since Streamflow was modeled from three gauges, they would be affected from all three trends although annual precipitation is not expected to drastically change by location. Figure 31b, c and d shows the precipitation for the individual GCMs by RCP. The GCMs varied for RCP 4.5 before 2077 but afterwards all three increased. Once again, seeing improvements once the atmosphere recovered. Both RCP 6.0 (Figure 31c) and RCP 8.5 (Figure 31d) had mixed results by 2100. Two out of the three GCMs declined in precipitation and one increased. There was also a larger spread in the values for RCP 8.5 and RCP 6.0. GFDL-ESM2G predicted the lowest precipitation at 111 m^2 , NorESM at 130 m^2 and MIROC at 142 m^2 , a difference of 31 m^2 . RCP 6.0 fluctuated from 129 m^2 to 154 m^2 , with a change of 25 m^2 . RCP 4.5 values were closer as they ranged from 134 m^2 to 142 m^2 (difference of 8 m^2). Since models have more of a consensus by RCP closer to the present, it is possible that there was more error the further out they project.

4.3 Discussion

There are a few ways to interpret these results. One could state that because a GCM better reproduced historical data (i.e. GFDL-CM has the closest Total Number of Unsatisfactory Days) that it is more likely to accurately predict the future. On the other hand, others could argue that with a changing climate the past is not like the future, therefore just because a GCM better represented the past does not automatically mean it will more precisely predict the future. Further, some GCMs such as GFDL-CM or MPI performance metrics were more optimistic than the other models, but just because they do not converge

with the general consensus does not mean they are not correct. We do not know how nations are going to manage all greenhouse gases and if there will be adequate technologies in place to curb emissions (e.g. non-reliant on fossil fuels for vehicles or other energy users), therefore it is really hard to determine the exact concentrations or path by the year 2100. Further, in order to plan for future water supply it might be challenging to find technologies that are less energy-intensive and will not admit greenhouse gases. For instance, desalination or reverse osmosis require a lot of energy to process the water. Therefore there is a need to find a balance between water supply and a reduction in emission. Finally, results revealed a consensus that serial correlation is significantly increasing in the future for all GCMs and RCPs. This can be reflected on the persistence of the system in turn potentially translating to more extreme events such as longer periods of drought or longer periods of precipitation.

4.4 Conclusion

This research evaluated potential climate change impacts on streamflow and water supply system for the Tampa, Florida region. After employing precipitation for streamflow modeling and reservoir operation, it evaluated each individual GCM and an average using reliability, resilience, vulnerability and sustainability performance metrics. Metrics enabled assessments of water resource reservoir system characteristics to determine future changes from the validation period. Three future periods were taken into consideration: an early-century period from 2030 to 2053, a mid-century period from 2054 to 2077, and a late-century period from 2077 to 2100, and these were compared to baseline (1982-2005). Key findings included the following: (1) As emissions increased, RCP 8.5 reliability declined whereas RCP 4.5 was on a recovering trajectory by 2100; (2) Resiliency depicted similar trend to Reliability for RCP 4.5 with an initial decline but slowing increasing by 2100. RCP 8.5 dropped by 2054 and then flatlined; (3) Vulnerability Max for all RCPs increased with time, however; RCP 4.5 was consistently less than RCP 6.0 and RCP 8.5 by 2100; (4) Once again, RCP 4.5 declined initially but improved with time for the overall sustainability of the system. The highest emission scenario, RCP 8.5, declined by year 2100; (5) GFDL-CM was an outlier typically reflecting the opposite of the other GCMs, or more extreme metric values compared to the past; (6) Low resiliency and high vulnerability had important implications on the reservoir

system, ultimately reducing the sustainability metrics; and (7) Autocorrelation increased with time reflected by the increasing reliability and persistence of an event.

To minimize impacts, a reduction of emissions would be imperative to decrease impacts to water supply. Since this would need to occur globally, it would require consensus and emission mitigation from all countries, which might prove extremely difficult. On a local level, diversifying of system (e.g. groundwater or desalination) or adding additional water storage would provide alternative water during reservoir failure events. Further, investigation of permits and adjustments to capture extreme flows might prove to be a useful tactic to combat climatic changes along with improvements in atmospheric emissions that exhibited beneficial system impacts over time.

Considerations of this research is important. Firstly, to our knowledge, utilizing all four performance metrics to evaluate future reservoir operations modeled from inputs of CMIP5 GCM precipitation has not been utilized. Metrics enable evaluation of change using key system attributes, reliability, resiliency, vulnerability and sustainability. The metrics gauge when the reservoir was below threshold or unable to supply water, and the degree of the magnitude of the failure compared to baseline. Secondly, employing ensemble averaging provided an alternate option for evaluation of climate change impact on the system, where the effect of variability of individual models (e.g., specific biases) were filtered via counterbalancing different models. A limitation in this research was that only three GCMs were averaged since not all data for all RCPs for other GCMs were readily available. Future studies might compare the addition of other GCMs in this average calculation comparison. Further, due to future uncertainty, it is unsure which model(s) are actually correct per time period; therefore, it should be noted that it is feasible the ensemble average might mask the actual scenario providing a more conservative estimate. Since it is uncertain, the future might result in a more extreme or deviated response or it could be more conservative. Unfortunately, there is no way to unambiguously ascertain which model projection is the most likely choice; therefore, both ensemble and individual outputs were examined to provide a range for enhanced understanding. Furthermore, due to biases within the GCM and downscaling process, it is also probable that none of these future predictions accurately captured 100% the system. Additionally, it is likely

this research is also impacted by uncertainties in the hydrological model since it does not incorporate groundwater or atmospheric conditions such as temperature and evaporation. Since the model selects streamflow based on precipitation at the three gauges, it is assumed that future streamflow would be similar to historical when precipitation matches. Future streamflow values might vary. Moreover, the metrics are sensitive to time scales, especially resiliency, and selecting a longer period or large time scale would alter the metric values. Although variable, this research is valuable in gauging a change or answering the ultimate question: “will the water supply system be drastically impacted by climate?” This will enable water resource authorities to determine mitigation strategies based on likely scenarios. Ultimately, utilization of results will be determined on the most practical and/or feasible action plan for an organization’s system and budget, whether it is based on the worst case scenario, middle of the road, or an ensemble.

4.5 Tables

Table 20: GCM models and RCPs of each utilized in the future scenario research

Model Name	Model	RCP
BNU	BNU-ESM	4.5; 8.5
BCCR	BCC-CSM	4.5; 8.5
NOAA GFDL	GFDL-CM3;	6.0; 8.5
	GFDL-ESM2G	4.5; 6.0; 8.5
MIROC	MIROC-ESM	4.5; 6.0; 8.5
MPI	MPI-ESM-LR	4.5; 8.5
NorESM	NorESM1-M	4.5; 6.0; 8.5

Table 21: Average number of days the system remained in an unsatisfactory state based on an average of GFDL-ESM2G, MIROC and NorESM

Average # Unsat Days	Avg RCP 4.5	Avg RCP 6.0	Avg RCP 8.5
1982-2005	211	211	211
2030-2053	323	269	234
2054-2077	293	223	464
2077-2100	275	297	379

Table 22: Unsatisfactory events for RCP 8.5 for timeframes 2030-2039

RCP 8.5	BCCR	BNU	GFDL-ESM2G	GFDL-CM	MIROC	MPI	NorESM
UnSat days		1,447		58		116	
Dates		9/29/32-9/14/36		5/7/32-7/3/32		4/4/32-7/28/32	
UnSat days	201						
Dates	1/4/33-7/23/33						
UnSat days	304		185	82			157
Dates	10/7/34-8/6/35		4/3/35-10/4/35	4/27/34-7/17/34			9/23/34-2/26/35
UnSat days	192		73			548	
Dates	1/14/36-7/23/36		11/27/36-2/7/37			4/16/36-10/15/37	
UnSat days					24		
Dates					6/30/37-7/23/37		
UnSat days	316						93
Dates	9/6/38-7/18/39						12/16/39-3/17/40

*UnSat = Unsatisfactory

Table 23: Unsatisfactory events for RCP 8.5 for timeframes 2090-2100

RCP 8.5	BCCR	BNU	GFDL- ESM2G	GFDL- CM	MIROC	MPI	NorESM
UnSat days Dates			797 11/26/90- 1/30/93				
UnSat days Dates	45 7/3/92- 8/16/92	609 2/13/92- 10/13/93			287 1/20/92- 11/1/92	127 6/10/92- 10/14/92	
UnSat days Dates			456 6/20/93- 9/18/94		1,510 2/14/93- 4/3/97		
UnSat days Dates	156 5/7/94- 10/9/94	28 6/7/94- 7/4/94					121 5/10/94- 9/7/94
UnSat days Dates	280 12/26/94- 10/1/95					79 6/16/95- 9/2/95	76 10/28/95- 1/11/96
UnSat days Dates			755 8/18/96- 9/11/98			501 10/28/95- 3/11/97	
UnSat days Dates							36 5/22/96- 6/26/96
UnSat days Dates	107 9/7/97- 12/22/97	668 3/19/98- 1/15/2100			859 11/7/97- 3/15/2100	91 7/17/98- 10/15/98	
UnSat days Dates							180 10/3/99- 3/31/2100
UnSat days Dates							33 5/16/2100- 6/17/2100
UnSat days Dates	257 4/19/2100- 12/31/2100		129 8/25/2100- 12/31/2100			395 7/27/99- 8/25/2100	14 12/18/2100- 12/31/2100

Table 24: Streamflow statistics for Alafia and Morris Bridge for RCP 8.5 by GCM simulation and average for all GCMs (mgd)

Daily Average (mgd)		Gauge	BCCR	BNU	GFDL-ESM2G	GFDL-CM	MIROC	MPI	NorESM	Avg ALL GCMs
1982-2005	ALA Flow	252.3	253.4	246.6	257.0	255.3	249.7	242.8	234.6	248.5
	ALA With	11.2	11.5	11.4	11.2	11.6	11.3	11.9	10.9	11.4
	MB Flow	184.3	197.5	185.3	190.4	185.6	193.0	176.5	172.8	185.9
	TBC With	70.8	70.9	71.3	71.2	71.1	73.3	70.5	72.2	71.5
2030-2053	ALA Flow		263.8	193.5	260.2	405.4	239.3	271.3	227.1	265.8
	ALA With		19.2	15.52	17.1	12.9	18.0	15.9	16.23	16.4
	MB Flow		195.7	136.6	186.9	322.3	169.6	206.9	160.9	197.0
	TBC With		68.3	61.8	65.9	77.9	69.3	71.5	69.9	69.2
2054-2077	ALA Flow		168.7	156.4	182.4	552.0	175.6	293.4	272.7	257.3
	ALA With		16.3	17.9	15.7	9.0	14.9	16.5	16.2	15.2
	MB Flow		112.2	101.9	134.9	468.8	116.5	208.5	179.1	188.8
	TBC With		59.5	55.9	63.7	81.9	56.7	72.0	65.2	65.0
2077-2100	ALA Flow		184.4	212.7	148.2	589.5	147.3	258.3	217.6	251.1
	ALA With		17.2	17.1	14.4	11.1	16.9	15.4	16.3	15.48
	MB Flow		123.5	150.1	105.4	475.1	91.3	192.6	146.4	183.5
	TBC With		59.1	65.4	51.9	80.5	51.9	70.3	63.8	63.3

*ALA = Alafia; MB = Morris Bridge; TBC = Tampa ByPass Canal; With = Withdrawal

Table 25: Daily reservoir level for gauge and average of GFDL-ESM2G, MIROC and NorESM

Daily Elevation (m)		Gauge	Avg RCP 4.5	Avg RCP 6.0	Avg RCP 8.5
1982-2005	Median	39.0	39.6	39.6	39.6
	Average	36.3	37.2	37.2	37.2
	Minimum	22.6	22.9	22.9	22.9
2030-2053	Median		38.4	37.5	39.6
	Average		36.3	35.4	37.5
	Minimum		22.9	22.9	22.9
2054-2077	Median		36.9	38.1	37.2
	Average		35.1	36.3	36.0
	Minimum		22.9	22.9	26.5
2077-2100	Median		39.3	38.1	35.1
	Average		36.6	35.7	34.7
	Minimum		22.9	22.9	25.9

Table 26: Unsatisfactory reservoir events for average of GFDL-ESM2G, MIROC and NorESM

		Gauge	Avg RCP 4.5	Avg RCP 6.0	Avg RCP 8.5
1982-2005	Total Days	8,766	8,766	8,766	8,766
	Total Unsat	1,165	807	807	807
	% Time Unsat	13.3%	9.2%	9.2%	9.2%
	Unsat Events	8	4	4	4
2030-2053	Total Days		8,766	8,766	8,766
	Total Unsat		1,332	1,629	1,305
	% Time Unsat		15.2%	18.6%	14.9%
	Unsat Events		4	6	6
2054-2077	Total Days		8,766	8,766	8,766
	Total Unsat		1,864	1,140	2,759
	% Time Unsat		21.3%	13.0%	31.5%
	Unsat Events		6	5	8
2077-2100	Total Days		8,765	8,765	8,765
	Total Unsat		1,182	1,507	3,841
	% Time Unsat		13.5%	17.2%	43.8%
	Unsat Events		4	6	10

Table 27: CDF values for Morris Bridge daily flow for average of GFDL-ESM2G, MIROC and NorESM

CDF Value at 65 mgd	Gauge	Avg RCP 4.5	Avg RCP 6.0	Avg RCP 8.5
1982-2005	0.39	0.38	0.38	0.38
2030-2053		0.39	0.43	0.41
2054-2077		0.44	0.39	0.50
2077-2100		0.36	0.43	0.55

Table 28: CDF values for Alafia daily flow for average of GFDL-ESM2G, MIROC and NorESM

CDF Value at 83 mgd	Gauge	Avg RCP 4.5	Avg RCP 6.0	Avg RCP 8.5
1982-2005	0.26	0.25	0.25	0.25
2030-2053		0.28	0.30	0.28
2054-2077		0.32	0.27	0.37
2077-2100		0.24	0.28	0.39

Table 29: CDF values for Morris Bridge daily flow for RCP 8.5 for individual GCM simulations

CDF Value at 65 mgd	BCCR	BNU	GFDL-ESM2G	GFDL-CM	MIROC	MPI	NorESM
1982-2005	0.37	0.38	0.38	0.38	0.36	0.37	0.39
2030-2053	0.46	0.51	0.48	0.25	0.36	0.38	0.38
2054-2077	0.56	0.56	0.54	0.15	0.54	0.35	0.41
2077-2100	0.55	0.49	0.61	0.15	0.59	0.38	0.45

Table 30: Annual autocorrelation in days by RCP for Morris Bridge daily flow for average of GFDL-ESM2G, MIROC and NorESM

Days	Historical	Avg RCP 4.5	Avg RCP 6.0	Avg RCP 8.5
1982-2005	24	30	30	30
2030-2053		54	51	64
2054-2077		63	70	50
2077-2100		62	61	69

Table 31: Summer (July-October) autocorrelation in days by RCP for Morris Bridge daily flow for average of GFDL-ESM2G, MIROC and NorESM

Days	Historical	Avg RCP 4.5	Avg RCP 6.0	Avg RCP 8.5
1982-2005	26	29	29	29
2030-2053		29	33	37
2054-2077		47	32	30
2077-2100		36	35	31

4.6 Figures

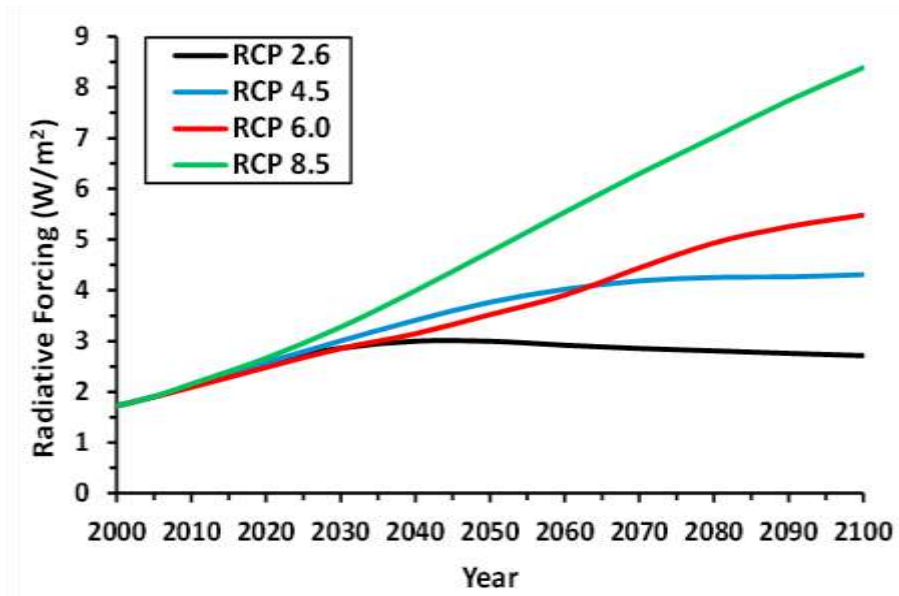


Figure 22: Emission scenarios with RCP 2.6 being the lowest and RCP 8.5 the highest (IPCC 2014c)

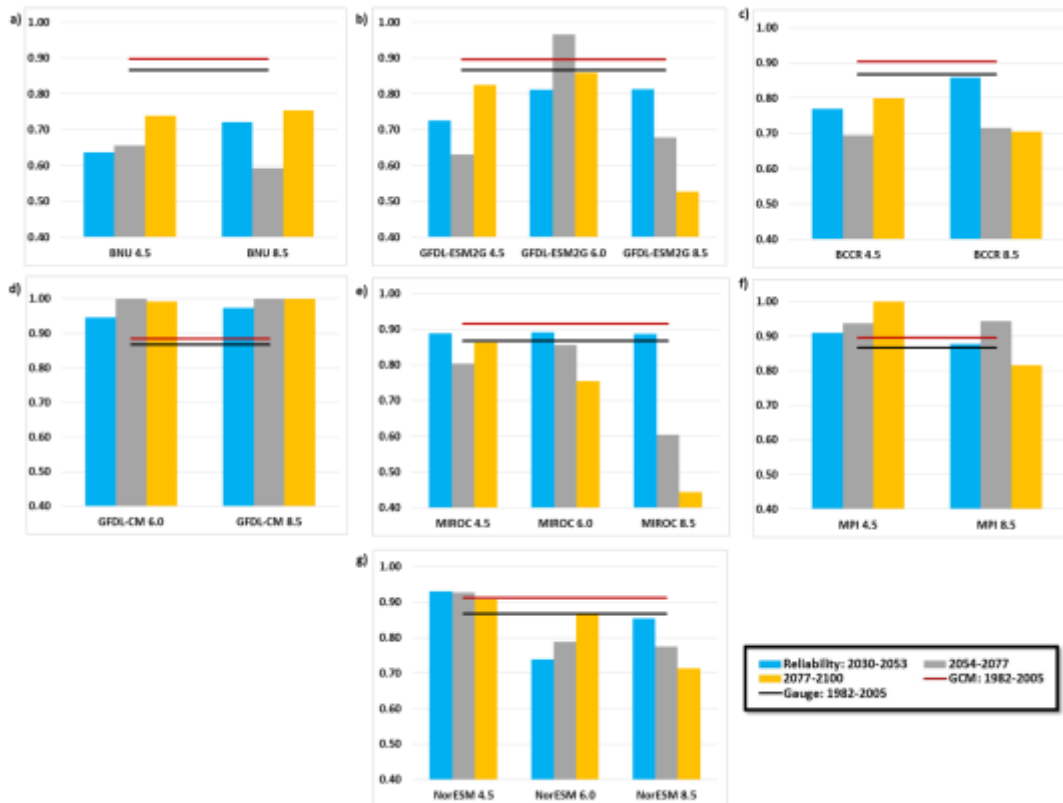


Figure 23: Reliability Metric by GCM

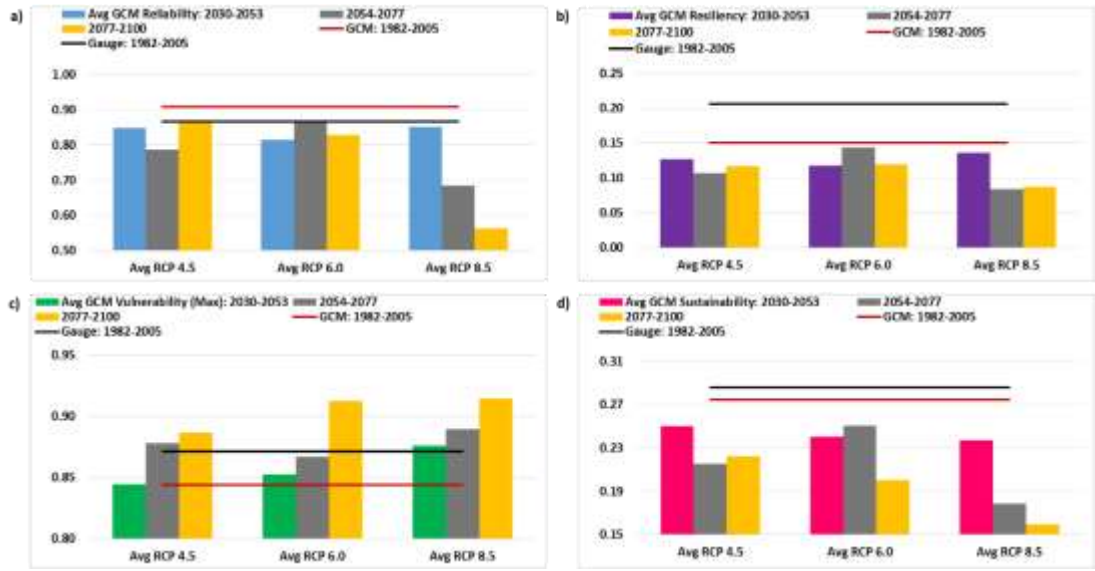


Figure 24: Metrics using the average of three GCMs Metrics (GFDL-ESM2G, MIROC and NorESM) by RCP and Max Vulnerability

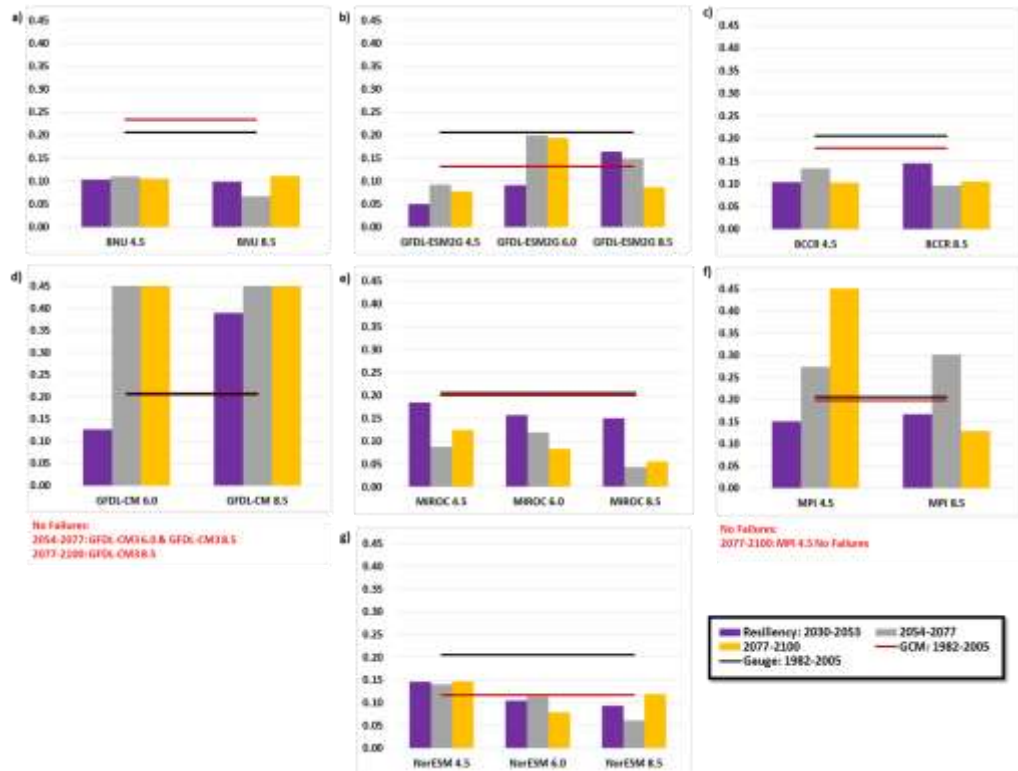


Figure 25: Resiliency Metric by GCM

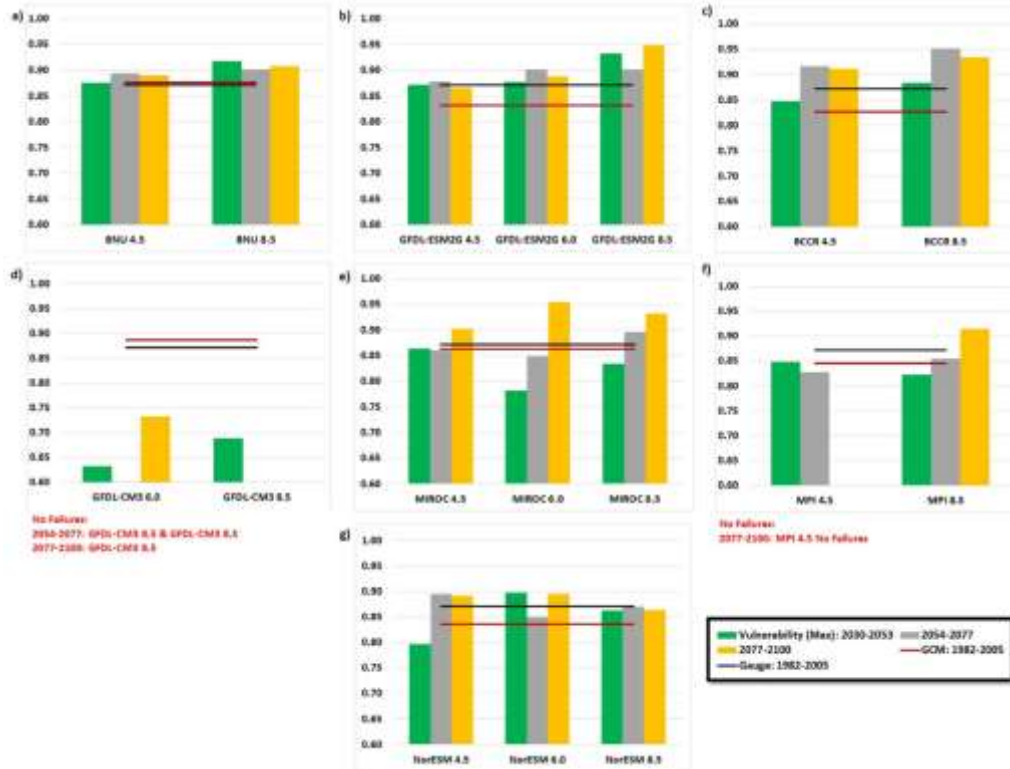


Figure 26: Examining Unsatisfactory Events with the Vulnerability Maximum Metric by GCM

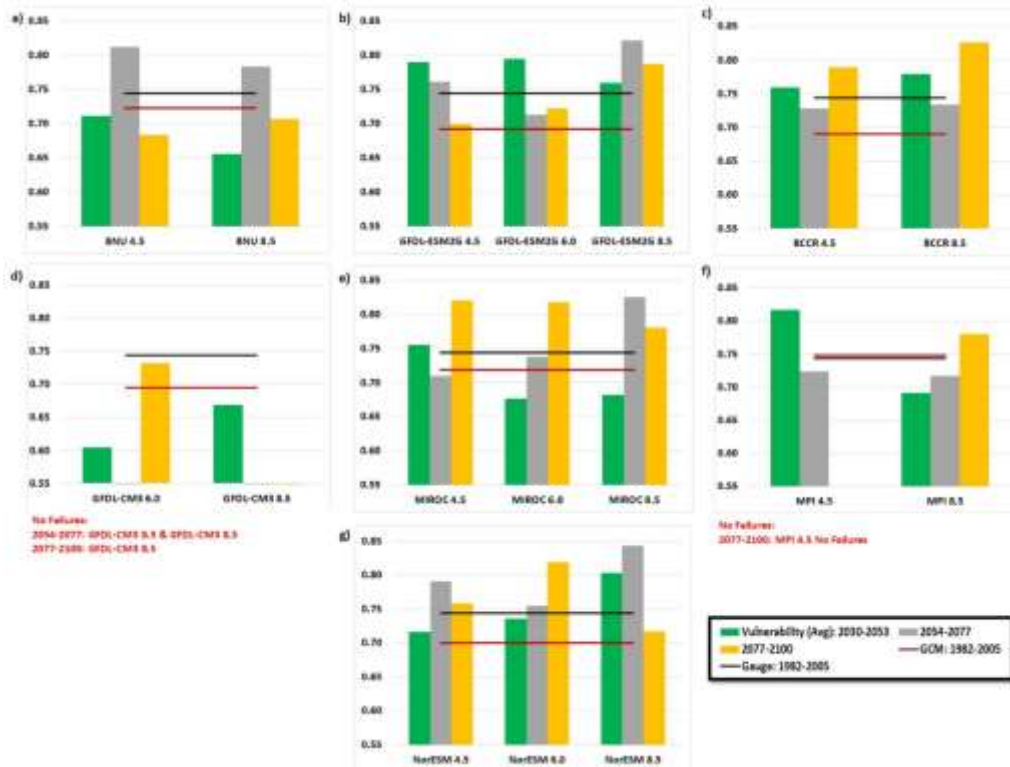


Figure 27: Examining all the Unsatisfactory Events to calculate the Vulnerability Average by GCM

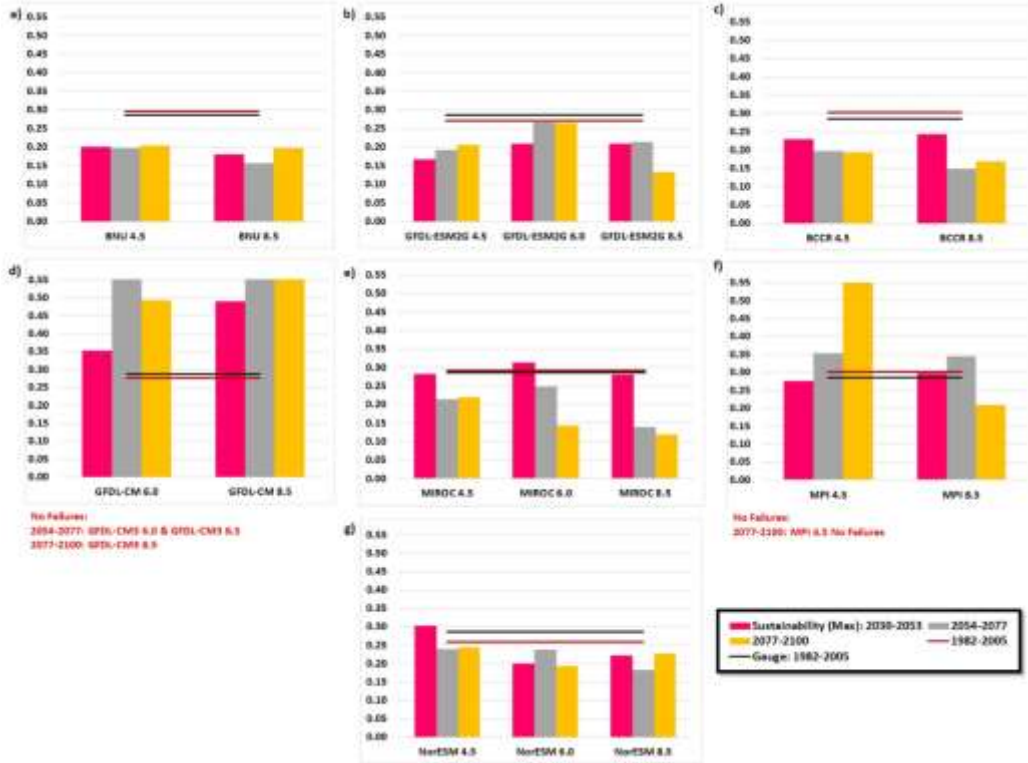


Figure 28: Sustainability Metric by GCM utilizing the Vulnerability Maximum Metric

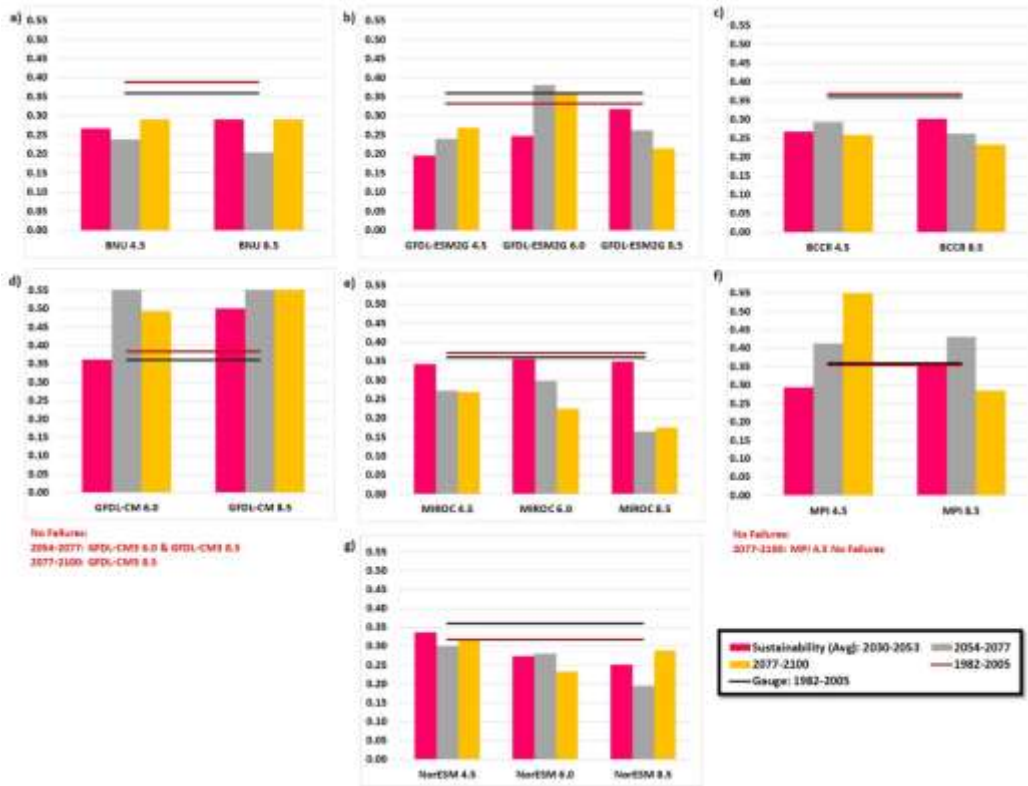


Figure 29: Sustainability Metric by GCM utilizing the Vulnerability Average Metric

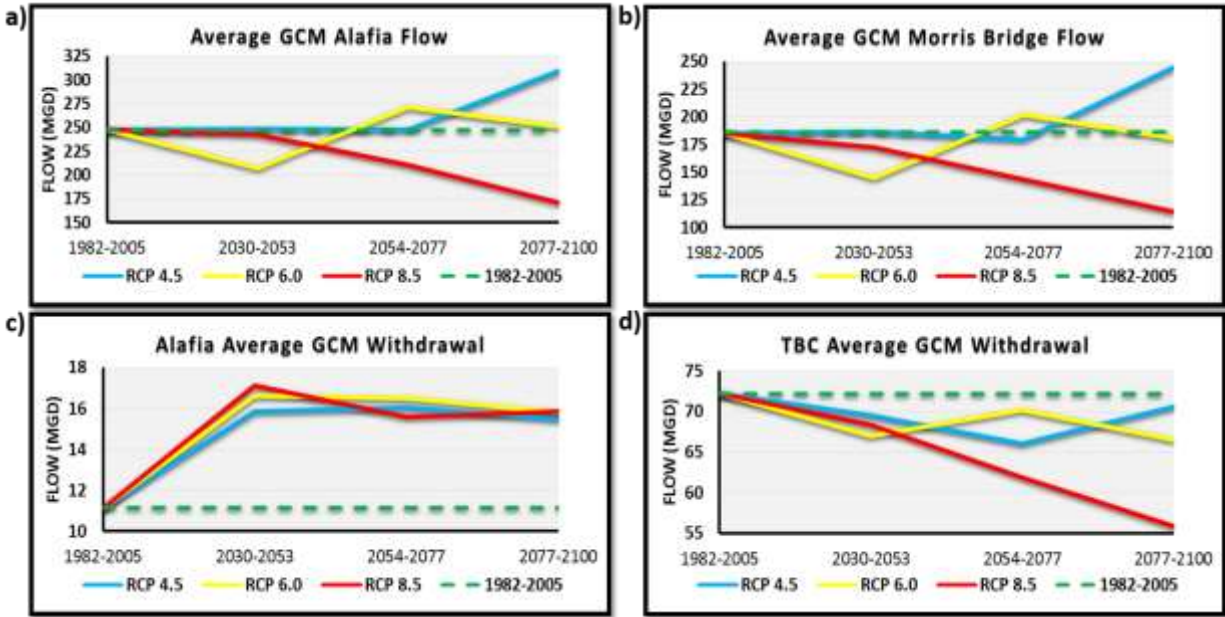


Figure 30: Alafia and Morris Bridge streamflow and water withdrawal at Alafia and TBC examined by RPC and time period

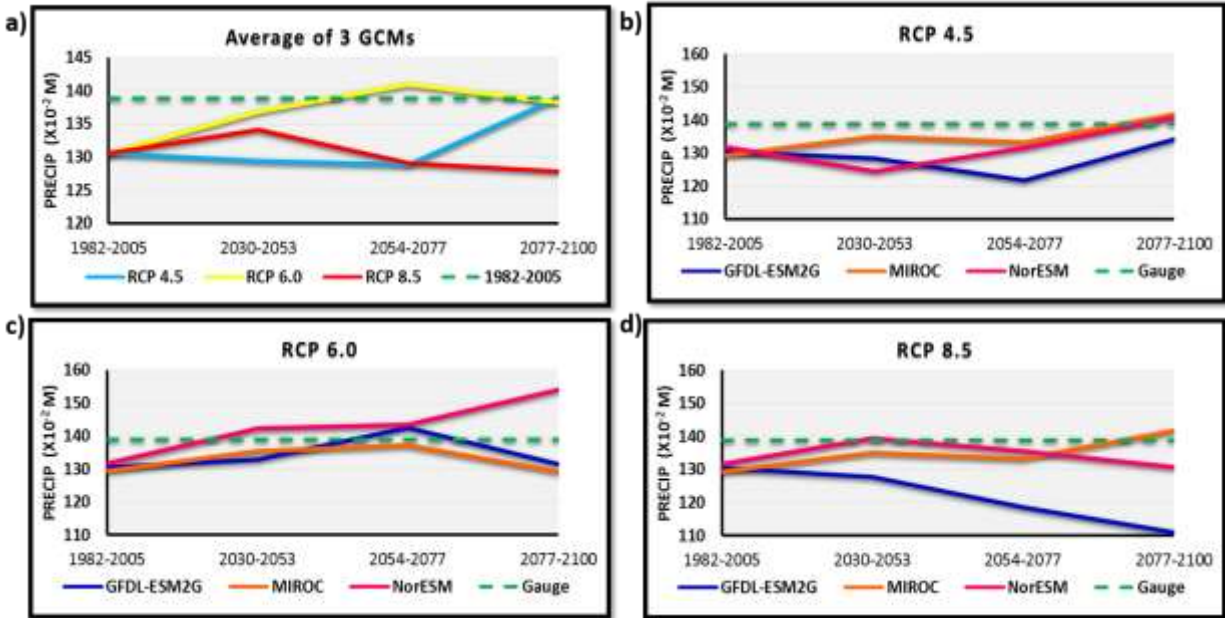


Figure 31: Average annual precipitation at Plant City gauge by time period and RCP for GFDL-ESM2G, MIROC, NorESM and average of all three

CHAPTER 5: CONCLUSION

This research first evaluated GCM precipitation to determine whether they captured important hydrologic characteristics. It utilized Markov Chain to determine whether climatic states were captured. Results indicated that GCM models and the downscaled and bias-corrected products did not replicate historical wet or dry season transition probabilities at the gauges. The second phase then employed GCM precipitation to simulate historical streamflow to see if these errors propagated to reservoir operations. Results were evaluated via performance metrics, reliability, resilience, vulnerability and sustainability, as well as using statistical tools such as serial correlation and PDF. On average, the simulations performed reasonably well, although they did not capture all markers. Finally, the last stage of the research ascertained whether future water supply would be susceptible to prolonged droughts. Depending on the emission scenario trajectory, lower or higher emissions, results varied. Overall consensus was that higher emissions would result in an increased strain on water supply resources, leading to multiple consecutive years when the reservoir would be unable to supply water. Lower emissions at first exhibited stresses on the system, but as time progressed and the atmosphere stabilized conditions improved. Therefore, it would be imperative for countries to have systems in place to reduce greenhouse gas emissions and have conservation and mitigation strategies. Additionally, water withdrawal permits could also be examined to determine if capturing additional water supply during extremely high flows might significantly increase the system's sustainability or if only minimal changes would be observed. Further, as GCM models are tweaked and enhanced, it would be beneficial to reevaluate the system to continue to understand future implications.

REFERENCES

- Acharya, A., and Ryu, J. H. (2014). "Simple Method for Streamflow Disaggregation." *Journal of Hydrologic Engineering*, 19(3), 509. doi:10.1061/(ASCE)HE.1943-5584.0000818
- Ahmed, K. F., Wang, G., Silander, J., Wilson, A. M., Allen, J. M., Horton, R., and Anyah, R. (2012). "Statistical downscaling and bias correction of climate model outputs for climate change impact assessment in the U.S. northeast." *Global and Planetary Change*, 100, 320–332.
- Akyuz, D. E., Bayazit, M., and Onoz, B. (2012). "Markov Chain Models for Hydrological Drought Characteristics." *Journal of Hydrometeorology*, 13 (1), 298–309. doi: 10.1175/JHM-D-11-019.1
- Amarasinghe, P., Liu, A., Egodawatta, P., Barnes, P., McGree, J., and Goonetilleke, A. (2016). "Research papers: Quantitative assessment of resilience of a water supply system under rainfall reduction due to climate change." *Journal of Hydrology*, 5401043-1052. doi:10.1016/j.jhydrol.2016.07.021
- Argüeso, D., Evans J. P., and Fita, L. (2013). "Precipitation bias correction of very high resolution regional climate models." *Hydrology and Earth System Sciences*, 17(11), 4379-4388. doi:10.5194/hessd-10-8145-2013
- Asefa, T., Clayton, J., Adams, A., and Anderson, D. (2014). "Performance evaluation of a water resources system under varying climatic conditions: Reliability, Resilience, Vulnerability and beyond." *Journal of Hydrology*, 508, 53–65. <http://dx.doi.org/10.1016/j.jhydrol.2013.10.043>
- Asefa, T., and Adams, A. (2013). "Reducing bias-corrected precipitation projection uncertainties: a Bayesian-based indicator-weighting approach." *Regional Environmental Change*, 13(1), 111-120. doi: 10.1007/s10113-013-0431-9
- Avilés, A., Célleri, R., Solera, A., and Paredes, J. (2016). "Probabilistic forecasting of drought events using Markov Chain- and Bayesian Network-Based models: A Case Study of an Andean Regulated River Basin." *Water*, 8(2), 37. doi:10.3390/w8020037
- Brown, E. G. and Bowen, D. (2014). "Governor brown declares drought state of emergency." <<https://www.gov.ca.gov/news.php?id=18368>> Retrieved 2-6-2017
- Bruyere, C. L., Done, J. M., Holland, G. J., and Fredrick, S. (2014). "Bias corrections of global models for regional climate simulations of high-impact weather." *Climate Dynamics*, 43 (7-8), 1847–1856.

Chanda, K., Maity, R., Sharma, A., and Mehrotra, R. (2014). "Spatiotemporal variation of long-term drought propensity through reliability-resilience-vulnerability based Drought Management Index." *Water Resources Research*, 50(10), 7662.

Christensen, N. S., and Lettenmaier, D. P. (2007). "A multimodel ensemble approach to assessment of climate change impacts on the hydrology and water resources of the Colorado River Basin." *Hydrology and Earth System Sciences*, 11(4), 1417-1434. doi:10.5194/hess-11-1417-2007

Clark, C., Nnaji, G. A., and Huang, W. (2014). "Effects of El-Niño and La-Niña Sea Surface Temperature Anomalies on Annual Precipitations and Streamflow Discharges in Southeastern United States." *Journal of Coastal Research*, 68113-120. doi:10.2112/SI68-015.1

Daniels, A. E., Morrison J. F., Joyce, L. A., Crookston, N. L., Chen, S. C., and McNulty, S. G. (2012). "Climate Projections FAQ." <http://www.fs.fed.us/rm/pubs/rmrs_gtr277.pdf> (Jan. 26, 2016)

Darren L, F., Justin T, M., Sally L, L., and Hamed, G. (2015). "A climatic deconstruction of recent drought trends in the United States." *Environmental Research Letters*, 10(4), 1. doi:10.1088/1748-9326/10/4/044009

Diallo, I., Sylla, M. B., Giorgi, F., Gaye, A. T., and Camara, M. (2012). "Multimodel GCM-RCM Ensemble-Based Projections of Temperature and Precipitation over West Africa for the Early 21st Century." *International Journal of Geophysics*, Vol 2012 (2012), doi:10.1155/2012/972896

Eden, J. M., and Widmann, M. (2013). "Downscaling of GCM-Simulated Precipitation Using Model Output Statistics." *Journal of Climate*, 27, 312-324. doi: 10.1175/JCLI-D-13-00063.1

Ehret, U., Zehe, E., Wulfmeyer, V., Warrach-Sagi, K., and Liebert, J. (2012). "Should we apply bias correction to global and regional climate model data?" *Hydrology and Earth System Sciences*, 16(9), 3391–3404. doi:10.5194/hess-16-3391-2012

EPA (2016). "Climate Impacts on Water Resources." <<https://www.epa.gov/climate-impacts/climate-impacts-water-resources>> (Retrieved 2-5-17)

Florida Climate Center (FCC) (2017). "Climate Variability." <<https://climatecenter.fsu.edu/topics/climate-variability>> (March 29, 2017)

Fowler, H. J., Kilsby, C. G., and O'Connell, P. E. (2003). "Modeling the impacts of climatic change and variability on the reliability, resilience, and vulnerability of a water resource system." *Water Resources Research*, 39(8), doi:10.1029/2002WR001778

Gergis, J. L., and Fowler, A. (2005). "Classification of synchronous oceanic and atmospheric El-Niño-Southern Oscillation (ENSO) events for palaeoclimate reconstruction." *International Journal of Climatology*, 25(12), 1541-1566. doi: 10.1002/joc.1202

Giorgi, F., and Mearns, L. O. (1999). "Introduction to special section: Regional Climate Modeling Revisited." *Journal of Geophysical Research. Atmospheres*, 104(D6), 6335 -6352. doi:10.1029/98JD02072

Goharian, E., Burian, S. J., Bardsley, T., and Strong, C. (2016). “Incorporating Potential Severity into Vulnerability Assessment of Water Supply Systems under Climate Change Conditions.” *Journal of Water Resources Planning & Management*, 142(2), doi: 10.1061/(ASCE)WR.1943-5452.0000579

Grillakis, M. G., Koutroulis, A. G., and Tsanis, I. K. (2013). “Multisegment statistical bias correction of daily GCM precipitation output.” *Journal of Geophysical Research*, Volume 118, Issue 8, Pages 3150–3162. doi:10.1002/jgrd.5032

Grinstead, C. M., and Snell, J. L. (1997). *Introduction to Probability*. 2nd Edition. American Mathematical Society; Chapter 11.

Gutmann, E., Pruitt, T., Clark, M. P., Brekke, L., Arnold, J. R., Raff, D. A., and Rasmussen, R. M. (2014). “An intercomparison of statistical downscaling methods used for water resource assessments in the United States.” *Water Resources Research*, 50(9), 7167-7186. doi:10.1002/2014WR015559.

Hashimoto, T., Loucks, D. P., and Stedinger, J. R. (1982). “Reliability, Resiliency, and Vulnerability Criteria for Water Resource System Performance Evaluation.” *Water Resources Research*, 18(1), 14.

Hempel, S., Frieler, K., Warszawski, L., Schewe, J., Piontek, F. (2013). “A Trend-preserving bias correction – the ISI-MIP approach.” *Earth System Dynamics Discussions*, 49, 219-236. doi:10.5194/esd-4-219-2013

Hwang, S., and Graham, W. D. (2013). “Development and comparative evaluation of a stochastic analog method to downscale daily GCM precipitation.” *Hydrology and Earth Systems*, 17(10), 2141–2181. doi:10.5194/hessd-10-2141-2013

Hwang, S., Graham, W. D., Adams, A. and Geurink, J. (2013b). “Assessment of the utility of dynamically-downscaled regional reanalysis data to predict streamflow in west central Florida using an integrated hydrologic model.” *Regional Environmental Change*, (13)1, 69-80. doi 10.1007/s10113-013-0406-x

Hwang, S. (2012). “Utility of Gridded Observations for Statistical Bias-Correction of Climate Model Outputs and its Hydrologic Implication over West Central Florida.” *Journal of the Korean Society of Agricultural Engineers*, 54(5), 91-102. doi: <http://dx.doi.org/10.5389/KSAE.2012.54.5.091>

IPCC (2013). “What is a GCM?” <http://www.ipcc-data.org/guidelines/pages/gcm_guide.html> (Nov. 6, 2015)

IPCC (2014a). “Climate Change 2014: Impacts, Adaptation, and Vulnerability. Part B: Regional Aspects. Contribution of Working Group II to the Fifth Assessment Report of the Intergovernmental Panel on Climate Change [Core Writing Team, Barros, V.R., C.B. Field, D.J. Dokken, M.D. Mastrandrea, K.J. Mach, T.E. Bilir, M. Chatterjee, K.L. Ebi, Y.O. Estrada, R.C. Genova, B. Girma, E.S. Kissel, A.N. Levy, S.]

IPCC (2014b). “Climate Change 2014: Synthesis Report. Contribution of Working Groups I, II and III to the Fifth Assessment Report of the Intergovernmental Panel on Climate Change.” [Core Writing Team, R.K. Pachauri and L.A. Meyer (eds.)]. IPCC, Geneva, Switzerland, 151 pp. <https://www.ipcc.ch/pdf/assessment-report/ar5/syr/SYR_AR5_FINAL_full_wcover.pdf> (February 11, 2017)

IPCC (2014c). “Scenario process for AR5.” <http://sedac.ipcc-data.org/ddc/ar5_scenario_process/RCPs.html> (June 4, 2016)

Jain, S. K. (2010). “Investigating the behavior of statistical indices for performance assessment of a reservoir.” *Journal of Hydrology*, 391, 90-96.

Jenkinson, A. F. and Collison, F. P. (1977). “An Initial Climatology of Gales Over the North Sea.” *Synoptic Climatology Branch Memorandum*, 62, 18 Pages, Meteorological Office, Bracknell

Kendon, E. J., Jones, R. G., Kjellström, E., and Murphy, J. M. (2010). “Using and Designing GCM--RCM Ensemble Regional Climate Projections.” *Journal of Climate*, 23(24), 6485-6503. doi:10.1175/2010JCLI3502.1

Kovats, R. S., Valentini, R., Bouwer, L. M., Georgopoulou, E., Jacob, D., Martin, E., Rounsevell, M. and Soussana, J. F. (2014). “Europe. In: Climate Change 2014: Impacts, Adaptation, and Vulnerability. Part B: Regional Aspects. Contribution of Working Group II to the Fifth Assessment Report of the Intergovernmental Panel on Climate Change.” Cambridge University Press, Cambridge, United Kingdom and New York, NY, USA, pp. 1267-1326. <https://www.ipcc.ch/pdf/assessment-report/ar5/wg2/WGIIAR5-Chap23_FINAL.pdf>

Lafon, T., Dadson, S., Buys, G., and Prudhomme, C. (2013). “Bias correction of daily precipitation simulated by a regional climate model: a comparison of methods.” *International Journal of Climatology*, 33(6), 1367–1381. doi: 10.1002/joc.3518

Li, H., Sheffield, J., and Wood, E. F. (2010). “Bias correction of monthly precipitation and temperature fields from Intergovernmental Panel on Climate Change AR4 models using equidistant quantile matching.” *Journal of Geophysical Research*, 115(D10), 115:D10101. doi:10.1029/2009JD012882

Linhoss, A. and Jeff Ballweber, J. D. (2015). "Incorporating Uncertainty and Decision Analysis into a Water-Sustainability Index." *Journal of Water Resource Planning Management*, 141, 10.1061/(ASCE)WR.1943-5452.0000554, A4015007

Loucks, D. P. (1997). “Quantifying trends in system sustainability.” *Hydrological Sciences Journal*, 42(4), 513-530.

Lyon, B. (2014). “Seasonal Drought in the Greater Horn of Africa and Its Recent Increase during the March-May Long Rains.” *Journal of Climate*, 27(21), 7953-7975. doi:10.1175/JCLI-D-13-00459.1

MacCracken, P. R. Mastrandrea, and L. L. White (eds.]. Cambridge University Press, Cambridge, United Kingdom and New York, NY, USA, pp. 688. <https://www.ipcc.ch/pdf/assessment-report/ar5/wg2/WGIIAR5-PartB_FINAL.pdf> (February 11, 2017)

Mani, A., and Tsai, F. T. (2017). “Ensemble Averaging Methods for Quantifying Uncertainty Sources in Modeling Climate Change Impact on Runoff Projection.” *Journal of Hydrologic Engineering*, 22(4), 1. doi:10.1061/(ASCE)HE.1943-5584.0001487

Maraun, D. (2016). “Bias Correcting Climate Change Simulations - a Critical Review. Current Climate Change Reports”, *Regional Environmental Change*, 2, 211–220. doi: 10.1007/s40641-016-0050-x

Mateus, M. C. and Tullos, D. (2016). “Reliability, Sensitivity, and Vulnerability of Reservoir Operations under Climate Change.” *Journal of Water Resource Planning Management*, doi: 10.1061/(ASCE)WR.1943-5452.0000742

Maurer, E. P., Wood, A. W., Adam, J. C., Lettenmaier, D. P., and Nijssen, B. (2002). “A Long-Term Hydrologically-Based Data Set of Land Surface Fluxes and States for the Conterminous United States.” *Journal of Climate*, 15, 3237-3251. doi: [http://dx.doi.org/10.1175/1520-0442\(2002\)015<3237:ALTHBD>2.0.CO;2](http://dx.doi.org/10.1175/1520-0442(2002)015<3237:ALTHBD>2.0.CO;2)

Mishra, A. K., Ines, A. V. M., Singh, V. P., and Hansen, J. W. (2013). “Extraction of information content from stochastic disaggregation and bias corrected downscaled precipitation variables for crop simulation.” *Stochastic Environmental Research and Risk Assessment*, 27(2), 449-457. doi 10.1007/s00477-012-0667-9

Moon, S. E., Ryoo, S. B., and Kwon, J. G. (2006). “A Markov Chain model for daily precipitation occurrence in South Korea.” *International Journal of Climatology*, 14, 1009-1016. doi: 10.1002/joc.3370140906

Ning, L., Riddle, E. E., and Bradley, R. S. (2015). “Projected Changes in Climate Extremes over the Northeastern United States.” *Journal of Climate*, 28(8), 3289-3310. doi: 10.1175/JCLI-D-14-00150.1

NOAA (2015). What are El Niño and La Niña? <<http://oceanservice.noaa.gov/facts/ninonina.html>> (Jan, 12, 2016)

NOAA National Weather Service Climate Prediction Center (NWSCPC) (2015). Cold & Warm Episodes by Season. <http://www.cpc.ncep.noaa.gov/products/analysis_monitoring/ensostuff/ensoyears.shtml> (Mar. 3, 2016)

Northwest Alliance for Computational Science & Engineering (NACSE) (2017). “Drought Indicator: Precipitation Deviation from Long-Term (30-Year) Averages.” Oregon State University. <<http://www.prism.oregonstate.edu/comparisons/drought.php>> Retrieved 2-6-2017.

Notaro, M., Bennington, V., and Lofgren, B. (2015). “Dynamical Downscaling-Based Projections of Great Lakes Water Levels.” *Journal of Climate*, 28(24), 9721-9745. doi: 10.1175/JCLI-D-14-00847.1

Null, J. (2016). El Niño and La Niña Years and Intensities Based on Oceanic Niño Index (ONI). <<http://ggweather.com/enso/oni.htm>> (May 26, 2016)

NWSCPC (2003). “ENSO Impacts on the U.S. Florida.” <http://www.cpc.ncep.noaa.gov/products/predictions/threats2/enso/el_nino/fl_bar.html> (Mar. 29, 2017)

- Panaou, T., Alao, S. and Jacob, B. (2016). "Hypothetically quantifying flood vulnerability in a reservoir tributary employing 3-dimensional geomorphological terrain related covariants, a stochastic iterative quantitative interpolator and a space-time global circulation model paradigm." *Journal of Remote Sensing & GIS*, 5(4); doi: 10.4182/2469-4134.1000183
- Panaou, T., Tirusew, A. and Nachabe, M. (2018). "Keeping Us honest: Examining climate states and transition probabilities of precipitation projections in General Circulation Models." *Journal of Water Resources Planning and Management*, doi: 10.1061/(ASCE)WR.1943-5452.0000910 (With permission from ASCE)
- Peña, A. J., Bermudez, L. N., Ramírez, C., and Riaño, N. M. (2015). "Oceanic Niño Index as a Tool to Determine the Effect of Weather on Coffee Plantation in Colombia." *American Journal of Experimental Agriculture*, 7(6): 395-404. doi: 10.9734/AJEA/2015/15876
- Rahman, M. S. (1999). "A stochastic simulated first-order Markov chain model for daily rainfall at Barind, Bangladesh." *Journal of Interdisciplinary Mathematics*, 2(1), 7-32. doi: 10.1080/09720502.1999.10700255
- Raskin, P., Gleick, P., Kirshen, P., Pontius, G., and Strzepek, K. (1997). "Comprehensive assessment of the freshwater resources of the world. Water futures: Assessment of long-range patterns and problems." *National Resources*, Forum, 81-90.
- Romero-Lankao, P., Smith, J. B., Davidson, D. J., Diffenbaugh, N. S., Kinney, P. L., Kirshen, P., Kovacs, P., and Villers Ruiz, L. (2014): "North America. In: Climate Change 2014: Impacts, Adaptation, and Vulnerability. Part B: Regional Aspects. Contribution of Working Group II to the Fifth Assessment Report of the Intergovernmental Panel on Climate Change." Cambridge University Press, Cambridge, United Kingdom and New York, NY, USA, pp. 1439-1498. <https://www.ipcc.ch/pdf/assessment-report/ar5/wg2/WGIIAR5-Chap26_FINAL.pdf>
- Sandoval-Solis, S., McKinney, D., and Loucks, D. (2011). "Sustainability Index for Water Resources Planning and Management." *Journal of Water Resource Planning Management*, 137(5), 381-390.
- Schmidt, N., Lipp, E., Rose, J., and Luther, M. (2001). "ENSO Influences on Seasonal Rainfall and River Discharge in Florida." *Journal of Climate*, 14(4), 615. doi: [http://dx.doi.org/10.1175/1520-0442\(2001\)014<0615:EIOSRA>2.0.CO;2](http://dx.doi.org/10.1175/1520-0442(2001)014<0615:EIOSRA>2.0.CO;2)
- Seung Beom, S., Young-Oh, K., and Cho-Rong, K. (2015). "A New Way for Incorporating GCM Information into Water Shortage Projections." *Water* (20734441), 7(5), 2435. doi:10.3390/w7052435
- Sharma, M., Coulibaly, P., and Dibike, Y. (2011). "Assessing the need for downscaling RCM data for hydrologic impact study." *Journal of Hydrologic Engineering*, 16(6), 534-539. doi: 10.1061/(ASCE)HE.1943-5584.0000349
- Singh, H., Sinha, T., and Sankarasubramanian, A. (2015). "Impacts of Near-Term Climate Change and Population Growth on Within-Year Reservoir Systems." *Journal of Water Resources Planning & Management*, 141(6), 1. doi:10.1061/(ASCE)WR.1943-5452.0000474

Smith, T. J., and Marshall, L. A. (2008). "Bayesian methods in hydrologic modeling: A study of recent advancements in Markov chain Monte Carlo techniques." *Water Resources Research*, 44(12) W00B05, doi: 10.1029/2007WR006705

Soundharajan, B., Adeloye, A. J., and Remesan, R. (2016). "Evaluating the variability in surface water reservoir planning characteristics during climate change impacts assessment." *Journal of Hydrology*, 538, 625–639. doi:10.1016/j.jhydrol.2016.04.051

South Africa: Worst Drought In Years. (2015). *Africa Research Bulletin: Economic, Financial & Technical Series*, 52(10), 21031A. doi:10.1111/j.1467-6346.2015.06726.x

Tebaldi, C., and Knutti, R. (2007). "The Use of the Multi-Model Ensemble in Probabilistic Climate Projections." *Philosophical Transactions: Mathematical, Physical and Engineering Sciences*, 365(1857), 2053 -2075..

The New York Times. (NYT) (2015) "El Niño Strikes Ethiopia." <https://www.nytimes.com/2015/10/22/opinion/el-nino-strikes-ethiopia.html> Retrieved 2-6-2017

Todorovic, P., and Woolhiser, D. A. (1975). "A stochastic model of n-Day precipitation." *Journal of Applied Meteorology and Climatology*, 14(1), 17-24. doi: [http://dx.doi.org/10.1175/1520-0450\(1975\)014<0017:ASMODP>2.0.CO;2](http://dx.doi.org/10.1175/1520-0450(1975)014<0017:ASMODP>2.0.CO;2)

Tryhorn, L., and DeGaetano, A. (2011). "A comparison of techniques for downscaling extreme precipitation over the Northeastern United States." *International Journal of Climatology*, 31, 975–1989. doi: 10.1002/joc.2208

United Nations (2017). "Leaders Taking Action Joint Statement of the High Level Panel on Water For World Water Day 2017." https://sustainabledevelopment.un.org/content/documents/13308HLPW_World_Water_Day_statement_21_March_2017.pdf (Retrieved March 25, 2017)

van Pelt, S.C., Kabat, P., ter Maat, H. W., van den Hurk, B. J. J. M., and Weerts, A. H. (2009). "Discharge simulations performed with a hydrological model using bias corrected regional climate model input." *Hydrology and Earth System Sciences*, 3(2), 2387-2397. doi:10.5194/hess-13-2387-2009

Wang, H., and Kumar, A. (2015). "Assessing the impact of ENSO on drought in the U.S. Southwest with NCEP climate model simulations." *Journal of Hydrology*, 526, 30-41. <http://dx.doi.org/10.1016/j.jhydrol.2014.12.012>

Watanabe, S., Kanae, S., Seto, S., Yeh, P. J., Hirabayashi, Y., and Oki, T. (2012). "Intercomparison of bias-correction methods for monthly temperature and precipitation simulated by multiple climate models." *Journal of Geophysical Research – All Series*, 117(D23):D23114. doi:10.1029/2012JD018192

Watson, J. S., and Colucci, S. J. (2002). "Evaluation of Ensemble Predictions of Blocking in the NCEP Global Spectral Model." *Monthly Weather Review*, 130(12), 3008-3021

- Weiss, L. L. (1964). "Sequences of wet or dry days described by a Markov chain probability model." *Monthly Weather Review*, 92(4), 169–176. doi: [http://dx.doi.org/10.1175/1520-0493\(1964\)092<0169:SOWODD>2.3.CO;2](http://dx.doi.org/10.1175/1520-0493(1964)092<0169:SOWODD>2.3.CO;2)
- Wetterhall, F., Pappenberger, F., He, Y., Freer, J., and Cloke, H. L. (2012). "Conditioning model output statistics of regional climate model precipitation on circulation patterns." *Nonlinear Processes in Geophysics*, 19(6), 623–633. doi:10.5194/npg-19-623-2012
- Williams, A. P., Seager, R., Abatzoglou, J. T., Cook, B. I., Smerdon, J. E., and Cook, E. R. (2015). "Contribution of anthropogenic warming to California drought during 2012-2014." *Geophysical Research Letters*, 42(16), 6819-6828. doi:10.1002/2015GL064924
- Wood, A. W., Leung, L. R., Sridhar, V., and Lettenmaier, D. P. (2004). "Hydrologic implications of dynamical and statistical approaches to downscaling climate model outputs." *Climate Change*, 62(1), 189–216. doi: 10.1023/B:CLIM.0000013685.99609.9e.
- Yang, T. C., Chen, C., Kuo, C. M., Tseng, H. W., and Yu, P. S. (2012). "Drought risk assessments of water resources systems under climate change: a case study in Southern Taiwan." *Hydrology & Earth System Sciences Discussions*, 9(11), 12395. doi:10.5194/hessd-9-12395-2012
- Yin, Y., Ma, D., Wu, S., and Pan, T. (2015). "Projections of aridity and its regional variability over China in the mid-21st century." *International Journal of Climatology*, 35(14), 4387–4398. doi: 10.1002/joc.4295
- Zorn, M. R., and Waylen, P. R. (1997). "Seasonal response of mean monthly streamflow to El Niño/Southern Oscillation in North Central Florida." *The Professional Geographer*, (1), 51. doi: 10.1111/0033-0124.00055

APPENDIX A: LIST OF ACRONYMS

AR5	Fifth Assessment Report
Avg GCM	Average GCM
Avg Sus	Average Sustainability
BCCA	Bias-Correction and Constructed Analog
BCCR	Bjerknes Centre for Climate Research
BCCR3	BCCR3-BCM2.0
BCCR5	BCC-CSM1-1
BCSA	Bias-Correction and Stochastic Analog
BCSD	Bias-Correction and Spatial Disaggregation
BNU	Beijing Normal University
BOM	Bureau of Meteorology
CCSM	Community Climate System Model
CDF	Cumulative distribution function
cm	Centimeters
CMIP	Coupled Model Intercomparison Projects
CSIRO	Commonwealth Scientific and Industrial Research Organization
CWBYR	C.W. Bill Young Reservoir
DJF	December January February
ENSO	El Niño Southern Oscillation
FL	Florida
FMS2	Flow Modeling System Version 2
GCM	General Circulation Model
GCMs-Sim	Retrospective GCMs
GFDL	Geophysical Fluid Dynamics Laboratory
HRD	Hillsborough River Dam
IHM	Integrated Hydrologic Model
IPCC	Intergovernmental Panel on Climate Change
ISI-MIP	Inter-Sectoral Impact Model Intercomparison Project
km	kilometers
km	Kilometers
m	Meters
Max Sus	Maximum Sustainability
mgd	Million Gallons Per Day
MND	Multivariate, Nonparametric Disaggregation
MPI	Max Planck Institute
NCC	Norwegian Climate Centre

NOAA	National Oceanic and Atmospheric Administration
ONI	Oceanic Niño
PDF	Probability Distribution Function
RCP	Representative concentration pathway
RRV	Reliability, Resilience and Vulnerability
SMLR	Seasonal-Multivariate Linear Regression
SST	Sea Surface Temperature
TBC	Tampa Bypass Canal
U.S.	United States
Vul Avg	Average Vulnerability
Vul Max	Maximum Vulnerability
W/m ²	Watt per square meter

APPENDIX B: COPYRIGHT PERMISSIONS

Below is permission for the use of material in Chapter 2.



Antonia Panaou <apanaou@mail.usf.edu>

Decision on Manuscript MS WRENG-2997R2 - [EMID:6a5c7a2bf8f6969b]

PERMISSIONS <permissions@asce.org>
To: "apanaou@mail.usf.edu" <apanaou@mail.usf.edu>
Cc: ASCE Journal-Submissions1 <journal-submissions1@asce.org>

Thu, Oct 5, 2017 at 8:55 AM

Dear Toni,

Thank you for your permissions inquiry. You have permission to reuse your paper in your dissertation provided it does not account for more than 25% of the new work. Please use the final draft of your work (which as an original author) you can post on open, unrestricted Internet sites or deposit it in an institutional repository when the draft contains a link to the bibliographic record of the published version in the [ASCE Library](#) or [Civil Engineering Database](#). "Final draft" means the version submitted to ASCE after peer review and prior to copyediting or other ASCE production activities; it does not include the copyedited version, the page proof, or a PDF of the published version.

Also, please note that ASCE retains the copyright for the article "Keeping Us honest: Examining climate states and transition probabilities of precipitation projections in General Circulation Models". A **full credit line** must be added to the material being reprinted. For reuse in non-ASCE publications, add the words "With permission from ASCE" to your source citation. For intranet posting, add the following additional notice: "This material may be downloaded for personal use only. Any other use requires prior permission of the American Society of Civil Engineers."

Sincerely,

Leslie Connelly
Senior Marketing Coordinator
American Society of Civil Engineers
1801 Alexander Bell Drive
Reston, VA 20191

PERMISSIONS@asce.org

703-295-6169

Internet: www.asce.org/pubs | www.ascelibrary.org | <http://ascelibrary.org/page/rightsrequests>

A full credit line must be added to the material being reprinted. For reuse in non-ASCE publications, add the words "With permission from ASCE" to your source citation. For intranet posting, add the following additional notice: "This material may be downloaded for personal use only. Any other use requires prior permission of the American Society of Civil Engineers."

To view ASCE Terms and Conditions for Permissions Requests: <http://ascelibrary.org/page/ascetermsandconditionsforpermissionsrequests>

Each license is unique, covering only the terms and conditions specified in it. Even if you have obtained a license for certain ASCE copyrighted content, you will need to obtain another license if you plan to reuse that content outside the terms of the existing license. For example: if you already have a license to reuse a figure in a journal, you still need a new license to use the same figure in a magazine. You need separate license for each edition.

Authors may post the final draft of their work on open, unrestricted Internet sites or deposit it in an institutional repository when the draft contains a link to the bibliographic record of the published version in the ASCE Library or Civil Engineering Database. "Final draft" means the version submitted to ASCE after peer review and prior to copyediting or other ASCE production activities; it does not include the copyedited version, the page proof, or

a PDF of the published version.